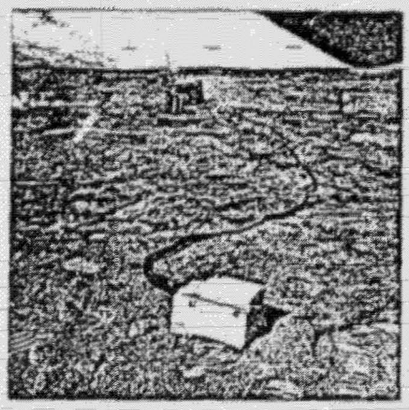

NASA CR-
150946

APOLLO 17

LUNAR ATMOSPHERIC COMPOSITION EXPERIMENT

FINAL REPORT

(NASA-CR-150946) LUNAR ATMOSPHERIC COMPOSITION EXPERIMENT Final Report, 1 Jun. 1971 - 30 Sep. 1975 (Texas Univ. at Dallas, Richardson.) 132 p HC $6.00 CSCL 03B

N76-32089

Unclas

G3/91 02474

SEP 1976
RECEIVED
NASA STI FACILITY
INPUT BRANCH

UTD

THE UNIVERSITY OF TEXAS AT DALLAS

DALLAS, TEXAS

LUNAR ATMOSPHERIC COMPOSITION EXPERIMENT

FINAL REPORT

NAS 9-12074

June 1, 1971 thru September 30, 1975

John H. Hoffman

Principal Investigator

THE UNIVERSITY OF TEXAS AT DALLAS

P. O. Box 688

Richardson, Texas 75080

INTRODUCTION

Apollo 17 carried a miniature mass spectrometer, called the Lunar Atmospheric Composition Experiment (LACE), to the moon as part of the Apollo Lunar Surface Experiments Package (ALSEP) to study the composition and variations in the lunar atmosphere. The instrument was successfully deployed in the Taurus-Littrow Valley with its entrance aperture oriented upward to intercept and measure the downward flux of gases at the lunar surface (Figure 1).

Initial turn-on of the LACE instrument occurred on December 27, approximately 50 hours after sunset and operation continued throughout the first lunar night. The advent of sunrise brought a high background gas level and necessitated discontinuing operation during lunar daytime except for a brief check near noon. Near sunset, operation was resumed and continued throughout the night. This sequence was repeated for the second through ninth lunations. During the tenth lunation the electron multiplier high voltage power supply developed a problem which ultimately spelled the demise of the instrument. The symptoms indicate that corona developed in the high voltage section of the power supply which acted like a variable load on the supply reducing its output voltage to several hundred volts instead of 2900 volts.

Numerous attempts were made to overcome the problem by alternately heating and cooling the electronics to ever increasing levels. A typical example of such an attempt is given below, quoted from the ALSEP Performance Summary Report of 26 October 1973:

> "The Lunar Atmospheric Composition Experiment is currently ON and configured to discriminator level, LOW; filament, OFF; high voltage power supply, OFF: and back-up heater, ON. The LACE data of 17 October was played back during real-time support

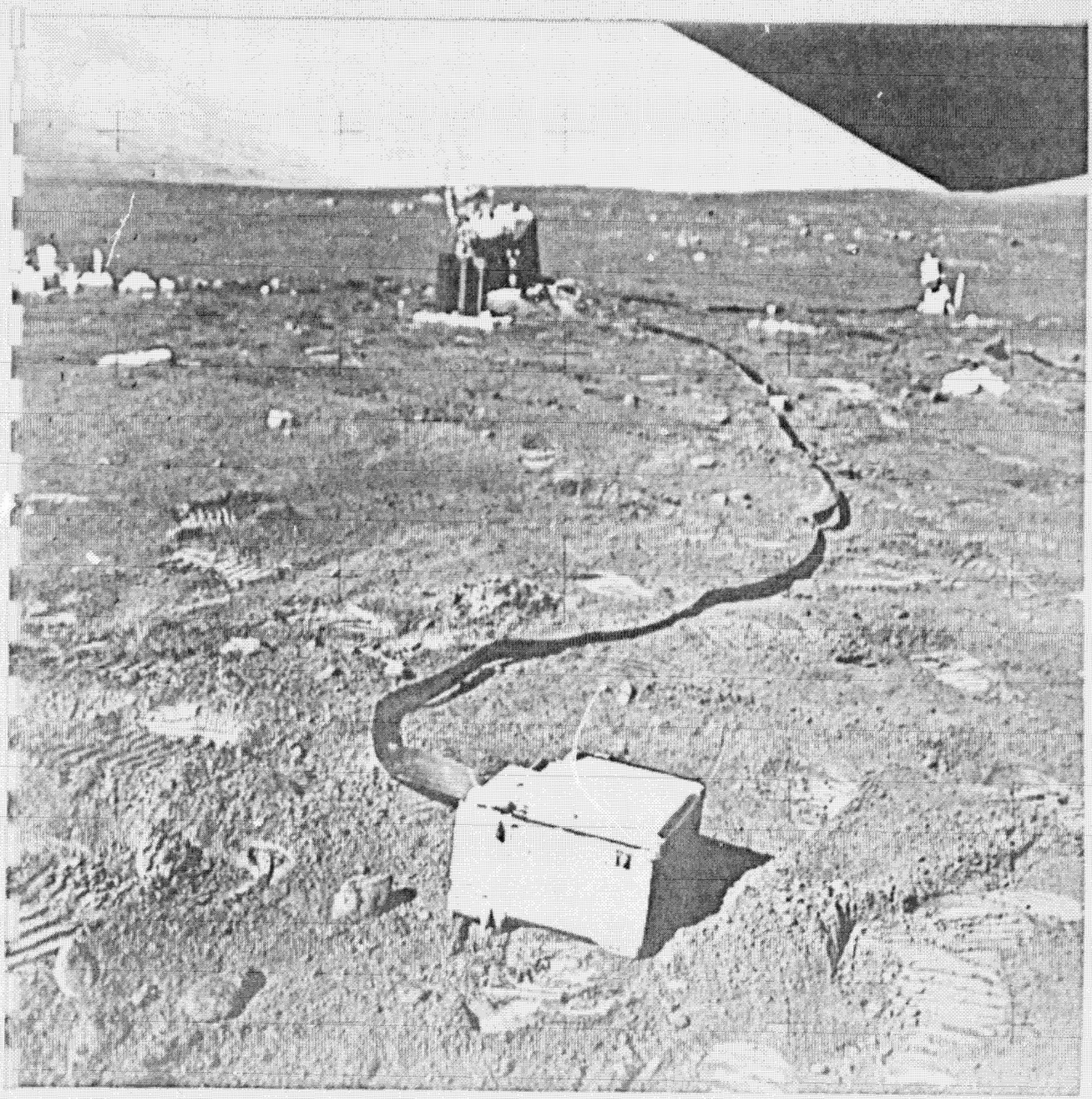

Figure 1

REPRODUCIBILITY OF THE
ORIGINAL PAGE IS POOR

on 19 October by the Canarvon tracking station. The playback indicated that at 1732 G.m.t., 17 October, the sweep high voltage (AM-44) dropped to zero. The electronics noise data ramp also disappeared from all three data channel outputs and the anomaly locked all three data channels into the continuous calibration mode (data offscale HIGH). This failure was preceded by a series of noise spikes on the low and mid mass range data channels which appeared at 1723 G.m.t., 17 October.

A series of high voltage and filament commands were executed during the real-time support period in an attempt to correct the anomaly. Cursory real-time analysis concluded that the multiplier high voltage supply had apparently failed. This common high voltage power supply also affected the sweep high voltage (AM-44), and cross coupled into the data channel outputs (DM-03, DM-04, and DM-05).

The LACE was allowed to cool down (i.e., back-up heater OFF) by a temperature Δ of 15°F. Attempts to correct the anomaly by ground command were made again on 22 October without success.

It is further planned to allow the LACE to cool down (i.e., STANDBY or OFF) for five hours later today. Attempts will again be made by ground commanding to correct this anomaly. Analysis of the anomaly is continuing."

The instrument never recovered from the anomaly. The high voltage supply in question was potted. Apparently, within the potting material or between it and the printed circuit board, a void developed in which outgassing supplied sufficient gas to support a corona. From this experience it would seem inadvisable to pot high voltage circuits that

are to be exposed to high vacuums for extended periods, especially if this involves large temperature excursions.

During the ten lunations that the LACE operated it produced a large base of data on the lunar atmosphere, mainly collected at night time. Prior to its flight on Apollo 17 a number of papers had addressed the subject of the lunar atmosphere. These predicted that the most likely sources of the lunar atmosphere are the solar wind, lunar volcanism and meteoritic impact (Johnson, 1971). Of these, the only one amenable to prediction of the composition of the lunar atmosphere is the solar wind. Thermal escape is the most rapid loss mechanism for light gases (H and He). For heavier gases, photoionization followed by acceleration by the solar wind electric field accounts for most of the loss. A more detailed description of the formation and loss mechanisms of the lunar atmosphere is given by Johnson (1971), Johnson et al. (1972), Hoffman et al. (1972a), and Siscoe and Mukherjee (1972).

The Apollo 14 and 15 cold cathode gauge experiments have determined an upper bound on the gas concentrations at the lunar surface of about 10^7 cm^{-3} in the daytime and 2×10^5 cm^{-3} at night (Johnson et al., 1972). This large daytime increase suggests most of the moon's gases are readily adsorbed on the cold nighttime surface. Hodges and Johnson (1968) have shown that gases which are not likely to be adsorbed at night, such as neon and nitrogen, should be distributed in concentration as $T^{-5/2}$ and thus have nighttime maxima. Contaminant gases originating from the Lunar Module (LM), other ALSEP experiments or adsorbed on surfaces in the site area could be influencing the daytime cold cathode gauge readings, although such outgassing would have to exhibit very stable long term rates due to the repeatability of the data from day

to day. If the daytime maximum is a natural feature of the atmosphere, then it is probably a result of condensible gases, some of which may be of volcanic origin, while the nighttime level represents the non-condensible gases. The present experiment is designed to identify the various gases in the lunar atmosphere and determine the concentration of each species.

The dominant gases on the moon are argon and helium, rather than neon which was predicted earlier. The most significant results from the LACE are the helium and argon distributions and models which are described in detail in the attached papers. Helium originates from the solar wind, whereas, argon results from the decay of radioactive potassium in the interior of the moon. Production and loss rates have been calculated by fitting the model to the diurnal variations of ^{40}Ar. A variability in argon content has been correlated with high-frequency lunar teleseismic events. The only apparent region of the moon which could possibly supply the amount of argon needed for escape via a plausible temporal mechanism is a semimolten asthenosphere which may be entirely primitive unfractionated lunar material, or an Fe-FeS core that is enriched in potassium. A core that is devoid of potassium is not compatible with the atmospheric argon measurements.

Most of the helium in the lunar atmosphere is of solar wind origin, although about 10% may be due to effusion of radiogenic helium from the lunar interior. The atmospheric helium abundance changes in response to solar wind fluctuations, suggesting surface weathering by the solar wind as a release mechanism for trapped helium. Atmospheric escape accounts for the radiogenic helium and about 60% of the solar wind α particle influx. The mode of loss of the remaining solar wind helium

is probably nonthermal sputtering from soil grain surfaces.

There is also good evidence for the existence of very small amounts of methane, ammonia and carbon dioxide in the very tenuous lunar atmosphere. All of these gases originate from solar wind particles which impinge on the lunar surface and are imbedded in the surface material. Here they may form molecules before being released into the atmosphere or may be released directly, as is the case for rare gases. Evidence for the existence of the molecular gas species is based on the pre-dawn enhancement of the mass peaks attributable to these compounds in the data from the Apollo 17 Lunar Mass Spectrometer. Methane is the most abundant molecular gas but its concentration is exceedingly low, 1×10^3 mol cm^{-3}, slightly less than ^{36}Ar, whereas the solar wind flux of carbon is approximately 2000 times that of ^{36}Ar.

The Lunar Atmospheric Composition program has led into the Lunar Synthesis program from which additional funding has been obtained to continue the modelling of the lunar atmosphere. The first report from that program is attached.

The remainder of this report consists of copies of publications resulting from this program which detail the results outlined above.

REFERENCES

Hodges, R. R., Jr. and F. S. Johnson, "Lateral transport in planetary exosphere," J. Geophys. Res., 73, 7307-7317, 1968

Hoffman, J. H., R. R. Hodges, Jr., and D. E. Evans, "Lunar orbital mass spectrometer experiment," Geochimica et Cosmochimica Acta, Supplement 3, 3, 2205-2216, 1972a

Johnson, F. S., "Lunar atmosphere," Rev. of Geophysics and Space Physics, 9, 813-823, 1971

Johnson, F. S., J. M. Carroll and D. E. Evans, "Lunar atmosphere measurements, Geochimica et Cosmochimica Acta, Supplement 3, 3, 2231-2242, 1972

Siscoe, G. L. and N. R. Mukherjee, "Upper limits on the lunar atmosphere determined from solar wind measurements," J. Geophys. Res. 77, 6042-6051, 1972

PUBLISHED PAPERS

1. "Lunar Atmospheric Composition Experiment," J. H. Hoffman, R. R. Hodges, Jr., F. S. Johnson, and D. E. Evans
2. "Absolute Calibration of Apollo Lunar Orbital Mass Spetrometer," P. R. Yeager, A. Smith, J. J. Jackson and J. H. Hoffman
3. "Composition and Dynamics of Lunar Atmosphere," R. R. Hodges, Jr., J. H. Hoffman, and F. S. Johnson
4. "Composition and Physics of the Lunar Atmosphere," J. H. Hoffman, R. R. Hodges, Jr., F. S. Johnson, D. E. Evans
5. "Helium and Hydrogen in the Lunar Atmosphere," R. R. Hodges, Jr.
6. "The Lunar Atmosphere," R. R. Hodges, Jr., J. H. Hoffman, and F. S. Johnson
7. "Episodic Release of ^{40}Ar from the Interior of the Moon," R. R. Hodges, Jr. and J. H. Hoffman
8. "Measurements of Solar Wind Helium in the Lunar Atmosphere," R. R. Hodges, Jr. and J. H. Hoffman
9. "Model Atmospheres for Mercury Based on a Lunar Analogy," R. R. Hodges, Jr.
10. "Implications of Atmospheric ^{40}Ar Escape on the Interior Structure of the Moon," R. R. Hodges, Jr. and J. H. Hoffman
11. "Molecular Gas Species in the Lunar Atmosphere," J. H. Hoffman and R. R. Hodges, Jr.
12. "Formation of the Lunar Atmosphere," R. R. Hodges, Jr.
13. Semi-Annual Status Report for Investigation of the Daytime Lunar Atmosphere for Lunar Synthesis Program 4-1-74 thru 9-30-74, R. R. Hodges, Jr.

17. Lunar Atmospheric Composition Experiment

J. H. Hoffman,[a†] *R. R. Hodges, Jr.,*[a] *F. S. Johnson,*[a] *and D. E. Evans*[b]

On the Apollo 17 mission, a miniature mass spectrometer, called the lunar atmospheric composition experiment (LACE), was carried to the Moon as part of the Apollo lunar surface experiments package (ALSEP) to study the composition of and variation in the lunar atmosphere. The instrument was successfully deployed in the Taurus-Littrow valley with its entrance aperture oriented upward to intercept and measure the downward flux of gases at the lunar surface (fig. 17-1).

Initial activation of the LACE instrument occurred on December 27, 1972, approximately 50 hr after sunset, and operation continued throughout the first lunar night. Sunrise brought a high background gas level and necessitated discontinuing operation during lunar daytime except for a brief check near noon. Near sunset, operation was resumed and continued throughout the night. This sequence was repeated for the second and third lunations.

The atmosphere of the Moon is very tenuous. Gas molecules do not collide with each other but, instead, travel in ballistic trajectories between collisions with the lunar surface, forming a nearly classical exosphere.

Possible sources of the lunar atmosphere are the solar wind, lunar volcanism, and meteoroid impact (ref. 17-1). Of these sources, the only one amenable to prediction of the composition of the lunar atmosphere is the solar wind. Thermal escape is the most rapid loss mechanism for light gases (hydrogen and helium). For heavier gases, photoionization followed by acceleration by the solar wind electric field accounts for most of the loss. More detailed descriptions of the formation and loss mechanisms of the lunar atmosphere are given in references 17-1 to 17-4.

The Apollo 14 and 15 cold cathode gage experiments have determined an upper bound on the gas concentrations at the lunar surface of approximately 1×10^7 molecules/cm^3 in the daytime and 2×10^5 molecules/cm^3 at night (ref. 17-2). This large daytime increase suggests that most of the lunar gases are readily adsorbed on the cold nighttime surface. Hodges and Johnson (ref. 17-5) have shown that gases that are not likely to be adsorbed at night, such as neon and nitrogen, should be distributed in concentration as a function of temperature ($T^{-5/2}$) and thus have nighttime maximums. Contaminant gases originating from the lunar module (LM) or from other ALSEP experiments, or being adsorbed on surfaces in the site area could be influencing the daytime cold cathode gage readings, although such outgassing would have to exhibit very stable long-term rates because of the repeatability of the data from day to day. If the daytime maximum is a natural feature of the atmosphere, then it is probably a result of condensable gases, some of which may be of volcanic origin, while the nighttime level represents the noncondensable gases. The LACE was designed to identify the various gases in the lunar atmosphere and to determine the concentration of each species. A brief description of the instrument and a discussion of the results obtained during the first three lunations after deployment of the instrument are given in this section.

INSTRUMENTATION

Identification of gas molecules in the lunar atmosphere by species and determination of concentrations are accomplished by a miniature magnetic-deflection mass spectrometer. Gas molecules entering the instrument aperture are ionized by an electron bombardment ion source, collimated into a beam, and sent through a magnetic analyzer to the detector system.

The ion source contains two tungsten (with 1 percent rhenium) filaments, selectable by command,

[a]The University of Texas at Dallas.
[b]NASA Lyndon B. Johnson Space Center.
[†]Principal Investigator.

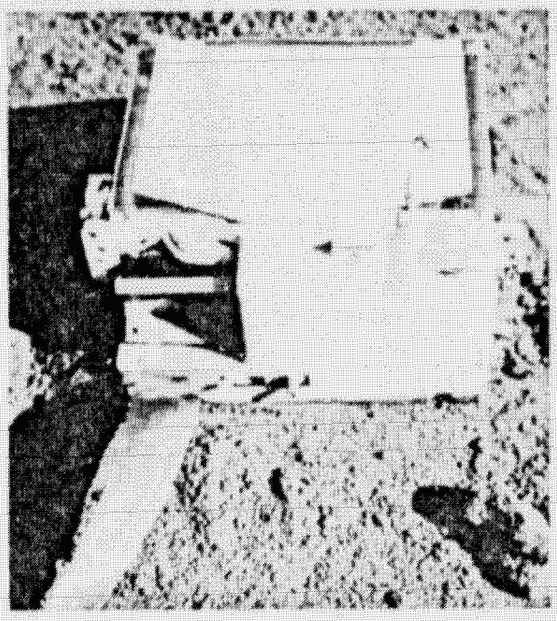

FIGURE 17-1.—The LACE deployed on the Moon. The entrance aperture covered by a nylon dust screen is at the lower right corner of the instrument. The mass analyzer is mounted behind the front cover with the electronics in a box to the rear. The white dust cover on top protects the mirrored surface during mission activities and LSPE explosive package detonations. The instrument package measures 34 by 32 by 17 cm and weighs 9.1 kg. The cable connecting the spectrometer to the central station is at the bottom of the photograph (AS17-134-20498).

as electron emitters. In the normal mode of operation, the fixed mode, the electron bombardment energy is fixed at 70 eV with the electron emission current regulated at 250 μA. This produces a sensitivity to nitrogen of 5×10^{-5} A/torr, sufficient to measure concentrations of gas species in the 1×10^{-15}-torr range. An alternate mode, the cyclic mode, provides four different electron energies (70, 27, 20, and 18 eV) that are cycled by successive sweeps of the mass spectrum. Identification of gases in a complex mass spectrum is greatly aided when the spectra are taken at several different electron ionization energies because the cracking patterns of complex molecules are strongly dependent on the bombardment electron energy. Also, at low energy, many gas species are eliminated from the spectrum, thus greatly simplifying the task of identifying parent molecules.

Two small heaters, consisting of ceramic blocks with embedded resistors, are mounted in the ion source, enabling its temperature to be raised to 520 K for in situ outgassing. The gas entrance is pointed upward and has a dust trap around the source region that precludes the possibility of dust falling into the source itself.

Voltage scan of the mass spectrum is accomplished by a high-voltage stepping power supply. The ion-accelerating voltage (sweep voltage) is varied in a stepwise manner through 1330 steps from 320 to 1420 V with a dwell time of 0.6 sec/step. Each step is synchronized to a main frame of the telemetry format. Ten steps of background counts (zero sweep voltage) and 10 steps of an internal calibration frequency are inserted between sweeps, making a total of 1350 steps/spectrum. The sweep time is 13.5 min.

In an alternate mode, the sweep voltage may be commanded to lock on to any of the 1350 steps, enabling the instrument to monitor continuously any given mass number peak in the spectrum with a time resolution of 0.6 sec/sample. A one-step advance command is also available. The lock mode permits high time resolution monitoring of mass peaks that may be suspected to be of volcanic origin.

The sweep step number, being a function of the ion-accelerating voltage, is directly related to ion mass number. Each sweep step number, in turn, is uniquely related to a main frame telemetry word. Therefore, word position in the telemetry format serves as the identifier of atomic mass number in the spectrum.

Ions accelerated from the source region by the sweep voltage are collimated into a beam and directed through a magnetic field of 0.43 T. Three allowed trajectories (of radii 1.21, 4.20, and 6.35 cm) through the magnetic field region define the locations of three collector slits. Figure 17-2 is a schematic drawing of the analyzer showing the major parts and the three ion beam trajectories. Thus, three mass ranges are scanned simultaneously, namely 1 to 4, 12 to 48, and 27.4 to 110 amu, termed low-, mid-, and high-mass ranges, respectively. The advantage of a triple-channel analyzer is that a wide mass range may be scanned by a relatively narrow voltage excursion. Also, the mid- and high-mass ranges are so related that mass 28 and 64 peaks are detected simultaneously. Therefore, in the lock mode, carbon monoxide (CO) and sulfur dioxide (SO_2), which may be candidates for volcanic gases, can be monitored simultaneously.

Resolution of the analyzer is set at approximately

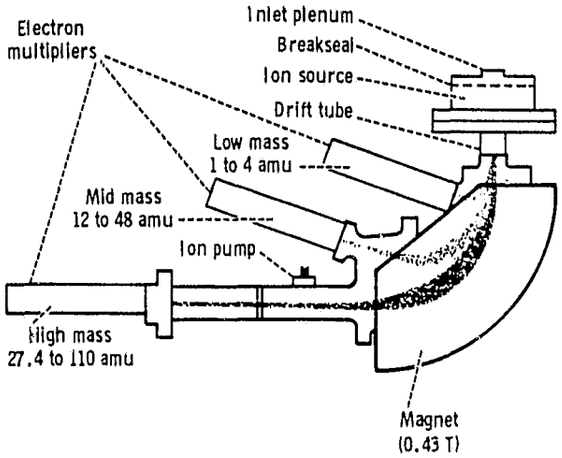

FIGURE 17-2.–Schematic diagram of mass analyzer. An ion beam is formed in the ion source from gas molecules entering the inlet plenum aperture. Three ion trajectories are shown through the magnet. Electron multipliers serve as charge amplifiers. An ion pump is used to check the internal analyzer pressure before application of high voltage to the ion source or the electron multiplier electrodes.

100 for the high-mass channel at mass 82. This is defined as less than a 1-percent valley between peaks of equal amplitude at mass 82 and 83. Krypton is used to verify the resolution.

Standard ion-counting techniques employing electron multipliers, pulse amplifiers, discriminators, and counters are used, one system for each mass range. The number of counts accumulated per voltage step (0.6 sec) for each channel is stored in 21-bit accumulators until sampled by the telemetry system. Just before interrogation, the 21-bit word is converted to a floating point number in base 2, reducing the data to a 10-bit word, consisting of a 6-bit number and a 4-bit multiplier. This scheme maintains 7-bit accuracy (1 percent) throughout the 21-bit (2×10^6) range of data counts.

Electron multiplier gains may be adjusted by command to a high or low value, differing by an order of magnitude. Likewise, the discriminator threshold level may be set at high or low (6-dB change) by command. The high level is used most of the time because it tends to minimize a spurious background noise that occurs toward the high-voltage end of the mass ranges. The internal calibration frequency read between each spectral scan verifies the operation of the counter system, the discrimination level, and the data compression circuits.

Housekeeping circuits monitor 15 functions within the instrument (supply voltages, filament current, emission current, sweep voltage, and several temperatures). One temperature sensor monitors the ion source temperature; this value is used in data reduction. Housekeeping words are subcommutated, one each 90 main frames, thus requiring a full spectral scan time to read each monitor once.

The mass spectrometer analyzer, magnet, ion source, and detectors are mounted on a baseplate that bisects the instrument package and are covered by a housing as shown in figure 17-1. The entrance aperture, which was sealed by a ceramic cap until it was opened by the crewman, points upward, enabling the downward flux of gas molecules to be measured. Behind the baseplate is a thermally controlled box containing the electronics. The top of the box has a mirrored surface covered by a dust cover that was commanded open after the last lunar seismic profiling experiment (LSPE) explosive package was detonated, 6 days after deployment. An arrow and bubble level on top of the package aided in proper deployment of the instrument.

Calibration of the instrument was performed at the NASA Langley Research Center (LRC) in a manner similar to that of the lunar orbital mass spectrometers flown on the Apollo 15 and 16 missions (ref. 17-6). A molecular beam apparatus produces a beam of known flux in a liquid helium cryochamber. The instrument entrance aperture intercepts the beam at one end of the chamber. With known beam flux and ion source temperature, instrument calibration coefficients are determined. Variation of gas pressure in the molecular beam source chamber behind a porous silicate glass plug varies the beam flux and provides a test of the linearity of the instrument response. Good linearity was achieved to as high as 5×10^5 counts/sec, where the onset of counter saturation occurs.

Calibrations were done with a number of gases that may be candidates for ambient lunar gases; for example, argon, carbon dioxide (CO_2), CO, krypton, neon, nitrogen, and hydrogen. Because helium is not cryopumped at the wall temperature, no helium beam can be formed in the chamber; therefore, helium calibrations are not possible with this system. Sensitivity to helium was determined in the ultrahigh vacuum chamber at the University of Texas at Dallas using the LRC absolute argon calibration of the instrument as a standard for calibrating an ionization

pressure gage. The gage calibration for helium was subsequently inferred from the ratio of ionization cross sections for helium and argon (ref. 17-7). The resulting helium sensitivity is the ratio of the calibrated gage pressure to the helium counting rate.

RESULTS

Operation of the instrument commenced approximately 50 hr after the first sunset after deployment (16 days). Performance was very good in general. All housekeeping monitors were nominal, and data were recorded on all three mass channels. Figure 17-3 is an example of a typical "quick look" nighttime spectrum recorded on a strip chart recorder in real time near the antisolar point during the third lunar night. Time, which is equivalent to voltage step number and related to atomic mass number, is plotted against the counting rate. Principal peaks are identified by mass number. The large-amplitude square pulse at the beginning and end of the spectrum in each channel is the internal calibration pulse; it is preceded by a zero level segment indicating the background count in each channel. All the data presented in this section have been obtained from quick-look charts such as figure 17-3 and are considered preliminary at this time.

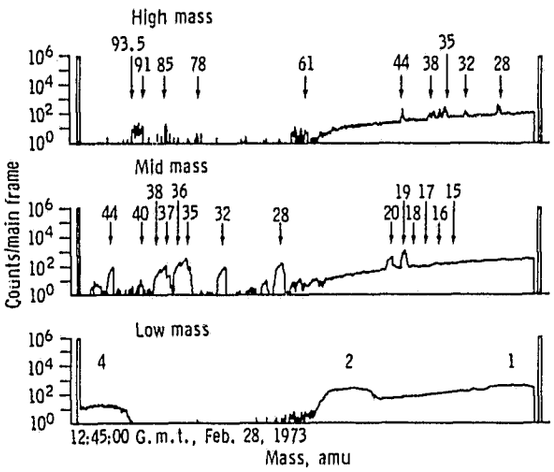

FIGURE 17-3.–Quick-look data recorded on a strip chart recorder. These mass spectral data were taken near the antisolar point during the third lunar night. Three output channels are identified as high-, mid-, and low-mass ranges. The ordinate is a logarithmic scale of ion counts from 10^0 to 10^6 counts per telemetry main frame (0.6 sec). Mass scale is plotted on the abscissa. Principal peaks are identified by mass number. The large pulses at the beginning and end of each spectrum are internal calibration frequencies to check operation of detector circuit. The solar zenith angle is 160°.

Each of the major peaks in the spectrum in figure 17-3 will be discussed in turn and will be given a tentative identification, which is essential in trying to determine its origin (native or artifact). Although many of the mass peaks observed undoubtedly arise from outgassing of the instrument or other materials at the landing site, three gases have been identified that are believed native to the Moon–helium, neon, and argon.

Peaks at mass 1, 2, and 4 are identifiable in the low-mass channel. Mass 1, atomic hydrogen, is almost certainly due to dissociation of artifact hydrocarbon molecules and other hydrogen compounds, including molecular hydrogen, in the ion source. Mass 2, molecular hydrogen, results largely from outgassing of the ion source, as it is steadily decreasing with time. Eventually, a stable hydrogen peak may appear that will then probably be truly lunar hydrogen. During the third lunation, the minimum hydrogen concentration observed was 1×10^5 molecules/cm^3, which is approximately a factor of 5 greater than the theoretical value of Hodges et al. (ref. 17-8). In the daytime, when the mass 2 peak is somewhat larger, a mass 3 peak appears that is 0.03 percent of the hydrogen peak (close to the isotopic ratio for HD of terrestrial origin), which supports the hypothesis of the hydrogen source as artifact. The helium at mass 4 is certainly native and will be discussed in more detail.

The ramp commencing near the mass 2 peak is probably due to an electronic coupling of spurious counts into the detector. The amplitude of the ramp is somewhat temperature sensitive and its onset position is variable. Although it appears to be large on a logarithmic scale, the amplitude of the ramp has a maximum value of 300 counts/main frame, which is not seriously detrimental to reduction of the data; it requires, for example, a correction of 10 to 20 percent or less for most peaks except in the 12- to 18-amu range where it is somewhat larger.

Identifiable peaks in the mid-mass range, beginning at the right with mass 15 and 16, may be methane with some contribution at mass 16 from atomic oxygen. Mass 17 and 18 are primarily due to water vapor and are relatively small, implying that the instrument is surprisingly well degassed of water

REPRODUCIBILITY OF THE ORIGINAL PAGE IS POOR

vapor. Even in the daytime, the mass 18 peak is not large relative to other peaks. An upper limit of 2×10^7 water molecules/cm^3 has been established for the second lunar day, which indicates that little water vapor is present at the site.

Mass 19 being a dominant peak is a puzzle. The H_3O^+ ion is precluded because of the small H_2O peak. Fluorine is the only other possibility. This implies that much of the mass 20 peak may be hydrogen fluoride (HF) instead of neon. The mass 20 peak is smaller than the mass 19 peak by a factor of 3 at night and larger by the same factor in the daytime. The origin of the fluorine is unknown, but possibilities are the outgassing of solvents used in cleaning the instrument before flight, the outgassing of other warm areas of the site (e.g., instruments, the central station, or the radioisotope thermoelectric generator), or the natural degassing of the lunar materials. To study the neon question further, the temperature of the ion source was reduced from 270 K several times during the lunar night by turning off the filament for periods of approximately 30 min. Reactivation of the filament just before scanning the mass 20 to 22 range revealed stable, net mass 20 and 22 peaks with an amplitude ratio of approximately 13, in close agreement with the solar wind isotopic ratio of neon determined by Geiss et al. (ref. 17-9). The mass 44 peak was not large enough at the time to contribute significantly to the mass 22 peak as a doubly ionized species. A neon concentration of 7×10^4 molecules/cm^3 results, which is a factor of 20 less than that predicted by Johnson et al. (ref. 17-2).

The mass 28 peak is probably nitrogen or possibly CO, and mass 32 corresponds to oxygen. These will be discussed subsequently. Peaks at mass 35, 36, 37, and 38 fall into the same category as mass 19 and 20, most likely being chlorine and hydrogen chloride (HCl). The mass 35 to 37 ratio corresponds to the terrestrial chlorine isotopic ratio. As with fluorine, the origin of the chlorine is undetermined but is likely the same as that of fluorine. The ion source temperature reduction test was conducted for the mass 36 and 40 range also. The mass 36 and 38 peaks decreased to essentially zero; the mass 40 peak also was essentially zero, indicating a late night upper limit for any of the argon isotopes less than 200 molecules/cm^3. These tests indicate that the formation of HF and HCl is strongly temperature dependent and may arise from a reaction with hydrogen in the ion source $H_2 + F_2 = 2HF$ or $H_2 + Cl_2 = 2HCl$. Hydrocarbon peaks at this time are all near zero amplitude. Native argon-40 (^{40}Ar) has been identified at other times and its diurnal behavior will be discussed later. Mass 44 is CO_2, thought to originate primarily from outgassing of the instrument. The remaining mid-mass peaks are mainly hydrocarbons principally from outgassing of the ion source.

The high-mass range spectrum duplicates the mid range below mass 44. Additional peaks of significant amplitude are the group near mass 61 and peaks at mass 78 and 85 that, as yet, are unidentified. The latter two are continuing to decrease in amplitude with time and are not considered significant. The unresolved set of peaks from 91 to 93.5 amu is probably doubly charged species in the mass 182 to 187 range that are the isotopes of tungsten and rhenium, originating from vaporization of the filament. The group near mass 61 may be triply charged tungsten and rhenium. At this measured vaporization rate (concentration of 1×10^3 molecules/cm^3), the useful filament lifetime is estimated at 10 yr. The remaining peaks are again thought to be artifact hydrocarbons.

Figure 17-4 is a reduced spectrum derived from raw data by subtracting from each peak amplitude the counts in the adjacent valleys due to background noise and scattered ions. Small-angle scattering of ions from neutrals in the mass spectrometer is a strong function of pressure but does occur to some

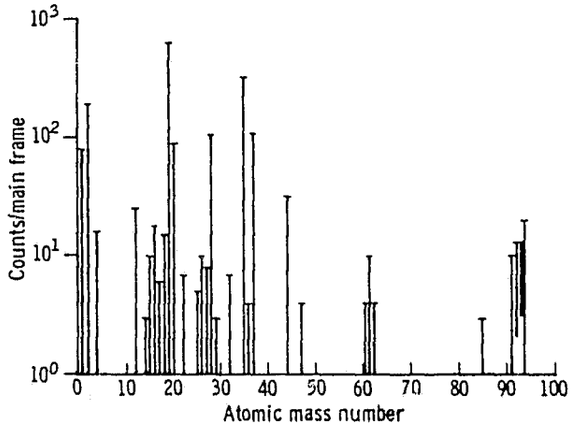

FIGURE 17-4.–Reduced spectrum taken 100 hr before sunrise of the third lunar night after deployment (16:30:00 G.m.t., Mar. 5, 1973). The solar zenith angle is 140°. Corrections have been applied for background counting rates.

extent in daytime data where the peak amplitudes are very large, that is, more than 1×10^5 counts/main frame in some cases. However, the corrections from scattering are typically less than 5 percent and frequently less than 1 percent. The accuracy of peak amplitudes at this stage of data analysis is estimated to be ±30 percent with some of the very small peaks having an uncertainty of a factor of 2. Most of the error comes from using the quick-look-type charts as the data source. The data are shown as counts/main frame as a function of atomic mass number. Differences between the mid- and high-mass overlapping ranges are removed by averaging. Counting rates (sec^{-1}) can be obtained by multiplying each peak amplitude by 1.65. The example given in figure 17-4 is data from the third lunar night, a few calendar days later than the spectrum of figure 17-3. At this time, the ion source temperature had been reduced from its normal operating level of 270 K to near 200 K by turning the ion source off for approximately 30 min before the measurement.

The minimum nighttime total gas concentration observed to date is 4.6×10^5 molecules/cm^3, of which nearly 20 percent is hydrogen and 25 percent is mass 19, both of which are believed to be artifact. In addition, neon and helium, both believed to be native, exist at the 15-percent level. The total gas concentration at noon of the second lunation is 4×10^8 molecules/cm^3, of which 25 percent is hydrogen and 7 percent is mass 36 (HCl), with the remaining peaks all lower in abundance. Water vapor is 5 percent of the total. All the large peaks are believed to be dominated by outgassing of the instrument, the LM, the landing site, and so forth, in the heat of the day.

Diurnal variation of helium-4 (^{4}He) is shown in figure 17-5, starting with first activation of the instrument on December 27 at a solar zenith angle of −155°. Time progresses to the right through the lunar night and into the day. The first lunation continues to sunset (−90°). The complete second lunation is also shown ending at sunset (Feb. 22, 1973). The dashed curve indicates regions where the instrument was not operating. No significance is attached to the lack of tracking of the two curves because the differences are within the errors associated with reading quick-look data. Helium concentration, plotted along the ordinate, is shown to vary from approximately 2×10^3 molecules/cm^3 at lunar noon to 4×10^4 molecules/cm^3 near midnight. Because of

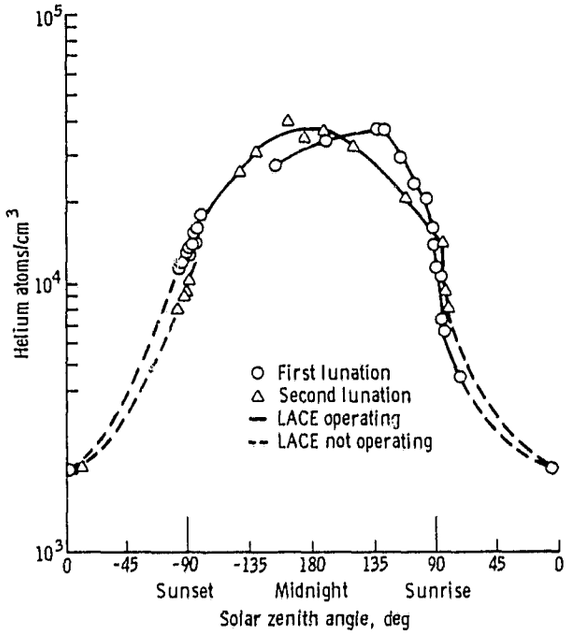

FIGURE 17-5.–Diurnal variation of ^{4}He. Concentration is plotted as a function of solar zenith angle with nighttime in the center of the figure. The distribution is typical for a noncondensable gas.

the very low level of the daytime helium (only three data counts after a correction for residual helium within the instrument is made based on preflight measurements of the helium and hydrogen ratio of laboratory spectra), the night-to-day ratio of helium can only be roughly estimated to be in the range of 15 to 30. This distribution is generally what would be expected of a noncondensable gas; that is, one that does not freeze out at the lunar nighttime temperature of 85 to 90 K (ref. 17-5).

The present measurement agrees with the daytime helium concentration of 3×10^3 molecules/cm^3 predicted by Johnson et al. (ref. 17-2). Hodges et al. (ref. 17-8) have done a Monte Carlo calculation of the distribution of solar wind helium around the Moon and found an equatorial night-to-day concentration ratio of 24, which should be slightly greater than at the 20° latitude of the instrument location. This distribution leads to a theoretical nighttime concentration of 4.1×10^4 molecules/cm^3 and a daytime value of 1.7×10^3 molecules/cm^3 for the same solar wind flux used by Johnson et al. (ref. 17-2); that is, 1.3×10^7 molecules/cm^2/sec. These values are in good agreement with the measurements, considering

the large variability of the solar wind flux (ref. 17-10).

The helium nighttime maximum occurring significantly before dawn (the coldest surface temperature occurs just before dawn) indicates that, because of the large-scale size of the helium trajectory (115 km at night), significant helium is lost from predawn and postsunset to the day side, from which thermal escape is a rapid loss mechanism.

The ^{40}Ar diurnal distribution is shown in figure 17-6. The coordinates are similar to those of figure 17-5. The difference between the nighttime minimums of the three lunations is believed to be due to a continual decrease in outgassing of the instrument with time. A significant feature is the large predawn increase in concentration. The very low, late night concentration of less than 200 molecules/cm^3 (which must be considered to be an upper limit of ^{40}Ar because the peak amplitude is essentially zero) indicates that it is a condensable gas and freezes out as the surface temperature falls below its freezing point. As the dawn terminator approaches the site but before any local heating occurs, the ^{40}Ar peak increase is due to argon being released from the warming surface and traveling several scale heights into the night side before being adsorbed by the lunar surface. The only other peak that exhibits this marked behavior is mass 36, probably ^{36}Ar. When the terminator passes the site and rapid local heating occurs, outgassing of hydrocarbon peaks dominates the argon contribution to mass 40. The trough just after 90° may be due to local depletion of argon from the surface all along the terminator. The trough is visible because of the delay in local sunrise after terminator crossing due to topographical conditions. It may be expected that the argon concentration would decrease slowly during the day until the onset of the rapid decrease after sunset. This would reflect the typical behavior of a condensable gas. However, argon may not condense on the surface until late night when the temperature reaches its freezing point.

The mass 36 peak exhibits a predawn enhancement but of a magnitude less than 10 percent of that of the ^{40}Ar, further supporting the evidence that the major contribution to the mass 36 peak is HCl when the ion source temperature is at its normal nighttime equilibrium value of 270 K. An upper limit for ^{36}Ar at night is 200 molecules/cm^3. As a comparison, the diurnal concentration of CO_2 (44 amu), which is a condensable gas at the night lunar surface temperature, is also given in figure 17-6. This peak shows no predawn enhancement but does show a very sharp increase at local sunrise and a similarly sharp decrease at sunset. Because the instrument is located in the Taurus-Littrow valley, local sunrise occurs nearly 8 hr after terminator crossing of the site longitude; local sunset occurs approximately 6 hr early. The lag in the CO_2 decrease beyond sunset very likely results from a thermal lag in the instrument and from other equipment degassing at the site.

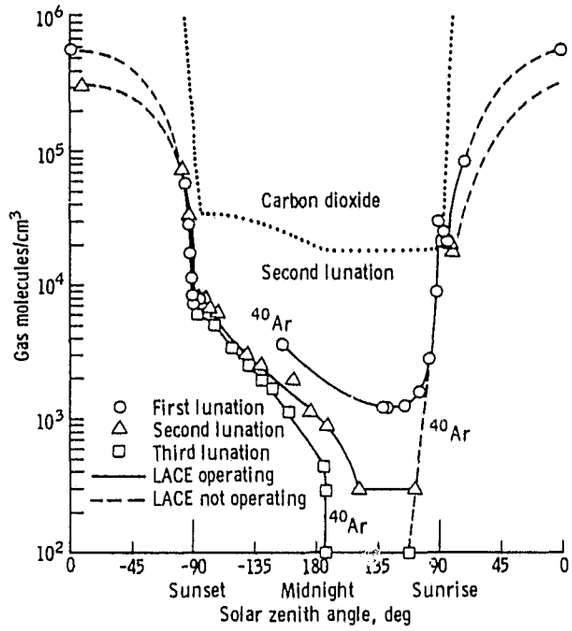

FIGURE 17-6.–Diurnal variation of ^{40}Ar. Coordinates are similar to those of figure 17-5. Predawn enhancement suggests boiloff of condensed gas from the warm approaching terminator region. Daytime increases are due to outgassing of hydrocarbon gases from the instrument, the LM, and the landing site. Carbon dioxide is shown as an example of a gas not showing predawn enhancement.

The concentrations of two other gases, nitrogen and CO at mass 28 and oxygen (at mass 32), are plotted in figure 17-7. Again, the coordinates are similar to those of the two previous figures. The behavior closely tracks that of CO_2, with no predawn enhancement. Oxygen would be expected to freeze out at night more readily than argon because its freezing point is several degrees higher than that of argon, and the ion source temperature reduction tests indeed showed a zero amplitude peak for mass 32. The conclusion is that essentially all the oxygen is

artifact, and an upper limit on the lunar oxygen is in the low 10^2 molecules/cm^3 range.

Conversely, mass 28, whether it is nitrogen or CO (no distinction is made at this time), would not condense at night temperatures and should have its maximum concentration at night. However, it is believed that the concentration of 3×10^4 molecules/cm^3 is still at least partially artifact because of the large decrease (a factor of 4) from the first lunation to the second. This appears to be merely an outgassing rate decrease. Perhaps several lunations hence, the value may stabilize and mass 28 will become a candidate for a native gas.

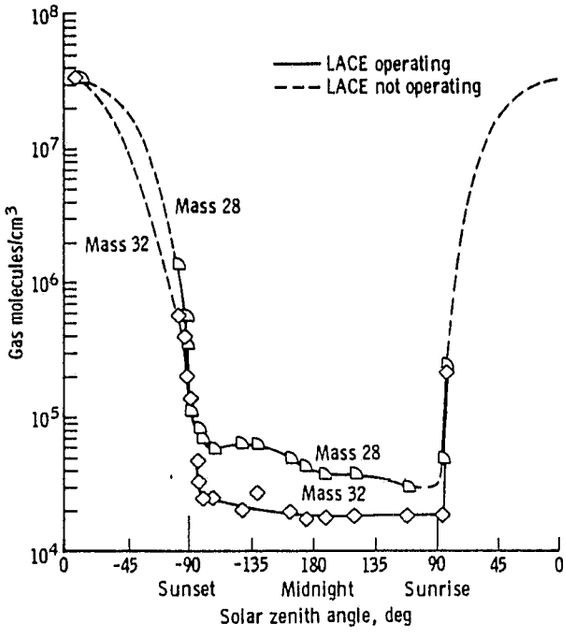

FIGURE 17-7.–Mass 28 (nitrogen and carbon monoxide) and mass 32 (oxygen) concentrations as a function of solar zenith angle during the second lunation.

CONCLUSIONS

From the data obtained during the first three lunations after deployment of the LACE instrument, three gases–helium, neon, and argon–have been identified as being native to the lunar atmosphere. A summary of the measured concentrations of these gases compared with several predictions is presented in table 17-I. The helium concentrations and the diurnal ratio are in excellent agreement with predictions based on the solar wind as a source, indicating that the basic tenets of the theory of a noncondensable gas are correct. However, the neon measured concentration is a factor of 20 below predictions, indicating possibly some adsorption or retention on the night side of the Moon. If true, this phenomenon is unexpected because of the very low freezing temperature (27 K) of neon. The Apollo 16 lunar orbital mass spectrometer experiment (ref. 17-11) did detect neon on the night side near the sunset terminator at a concentration approximately 1×10^5 molecules/cm^3. This is approximately a factor of less

TABLE 17-I.–*Concentrations of Gases Determined from Current Lunar Mass Spectrometer Data, Cold Cathode Gage Data, and Predictions*

Gas	*Mass spectrometer data, molecules/cm^3*		*Cold cathode gage data, molecules/cm^3*		*Predicted data, molecules/cm^3*	
	Day	*Night*	*Day*	*Night*	*Day*	*Night*
Hydrogen (H_2)	1×10^8	1×10^5			[a]3.6×10^3	[a]2.3×10^4
Helium	2×10^3	4×10^4			[b]3×10^3 [a]1.7×10^3	[a]4.1×10^4
Neon		[c]7×10^4			[b]5×10^4	[b]1.3×10^6
^{36}Ar		[c]2×10^3			[b]3×10^2	[b]8×10^3
^{40}Ar		[c]2×10^3				
[d]Total	4×10^8	4.6×10^5	1×10^7	2×10^5		

[a]Predicted by R. R. Hodges, Jr., in unpublished data.
[b]Reference 17-2.
[c]Upper limit; argon freezes out at night.
[d]Total gas concentrations from mass spectrometer during second lunar day and third lunar night after deployment; from cold cathode gage after 10 lunations.

than 2 higher than the present value and is within the experimental errors of the measurements. This discrepancy between theory and measurement for neon is a serious problem and is one of the major tasks to be considered in the future.

Argon appears to be adsorbed on the late night (coldest) part of the lunar surface as none of its isotopes are detected at this time. A significant predawn enhancement of ^{40}Ar indicates a release of the gas from the warm approaching terminator region. The ^{36}Ar and ^{38}Ar are masked by HCl peaks at this time. Future presunrise tests with a cooled ion source should reveal the actual amounts of ^{36}Ar and ^{38}Ar. Clearly, argon does not behave as a noncondensable gas and, therefore, cannot be compared to predictions. Furthermore, ^{40}Ar probably results mainly from potassium-40 decay and subsequent "weathering" of lunar surface materials, so its presence is evidence of a truly native lunar gas.

The remaining peaks of the spectra are all considered to be dominated by artifact gases at this time. The total nighttime gas density of 4.6×10^5 molecules/cm^3 is a factor of 2 higher than the measured values from the Apollo 14 and 15 cold cathode gage experiments. This is not surprising (notwithstanding errors in calibration of both instruments) because the mass spectrometer ion source is warmer than the cold discharge source of the gage and therefore would have a higher outgassing rate. However, the residual being measured by both instruments is clearly not entirely neon but a multitude of gases, including helium.

As the instrument, the LM, and the landing site continue to be cleansed in the high daytime temperatures, the passage of several more lunations should produce much cleaner spectra and yield more definitive data on concentrations of true lunar gases or, at a minimum, reduce the upper limits now determined.

ACKNOWLEDGMENTS

The authors wish to express their appreciation to the many people at the University of Texas at Dallas and at the Bendix Aerospace Corporation who contributed to the success of this experiment. Major contributions to the design, fabrication, and testing of the mass spectrometer were made by many of the personnel at the University of Texas at Dallas.

REFERENCES

17-1. Johnson, F. S.: Lunar Atmosphere. Rev. Geophys. Space Phys., vol. 9, no. 3, Aug. 1971, pp. 813-823.

17-2. Johnson, Francis S.; Carroll, James J.; and Evans, Dallas E.: Lunar Atmosphere Measurements. Proceedings of the Third Lunar Science Conference, vol. 3, MIT Press (Cambridge, Mass.), 1972, pp. 2231-2242.

17-3. Hoffman, J. H.; Hodges, R. R., Jr.; and Evans, D. E.: Lunar Orbital Mass Spectrometer Experiment. Proceedings of the Third Lunar Science Conference, vol. 3, MIT Press (Cambridge, Mass.), 1972, pp. 2205-2216.

17-4. Siscoe, G. L.; and Mukherjee, N. R.: Upper Limits on the Lunar Atmosphere Determined From Solar Wind Measurements. J. Geophys. Res., vol. 77, no. 31, Nov. 1, 1972, pp. 6042-6051.

17-5. Hodges, R. R., Jr.; and Johnson, F. S.: Lateral Transport in Planetary Exospheres. J. Geophys. Res., vol. 73, no. 23, Dec. 1, 1968, pp. 7307-7317.

17-6. Hoffman, J. H.; Hodges, R. R.; and Evans, D. E.: Lunar Orbital Mass Spectrometer Experiment. Sec. 19 of Apollo 15 Preliminary Science Report. NASA SP-289, 1972.

17-7. Von Ardenne, Manfred: Tabellen der Elektronenphysik Ionenphysik und Ubermikroskopie. Vol. 1, Deutscher Verlag der Wissenschaften (Berlin), 1956, p. 488.

17-8. Hodges, R. R., Jr.; Hoffman, J. H.; Johnson, F. S.; and Evans, D. E.: Composition and Dynamics of Lunar Atmosphere. Lunar Science IV (Abs. of papers presented at the Fourth Lunar Science Conference (Houston, Tex.), Mar. 5-8, 1973), pp. 374-375.

17-9. Geiss, J.; Buehler, F.; Cerutti, H.; Eberhardt, P.; and Filleux, Ch.: Solar Wind Composition Experiment. Sec. 14 of Apollo 16 Preliminary Science Report. NASA SP-315, 1972.

17-10. Hundhausen, A. J.; Bame, S. J.; Asbridge, J. R.; and Sydoriak, S. J.: Solar Wind Proton Properties: Vela 3 Observations from July 1965 to June 1967. J. Geophys. Res., vol. 75, no. 25, Sept. 1, 1970, pp. 4643-4657.

17-11. Hodges, R. R.; Hoffman, J. H.; and Evans, D. E.: Lunar Orbital Mass Spectrometer Experiment. Sec. 21 of Apollo 16 Preliminary Science Report. NASA SP-315, 1972.

Absolute Calibration of Apollo Lunar Orbital Mass Spectrometer

P. R. Yeager and A. Smith

NASA Langley Research Center, Hampton, Virginia 23365

J. J. Jackson and J. H. Hoffman

University of Texas, Dallas, Texas
(Received 2 June 1972; in final form 9 November 1972)

Recent experiments were conducted in Langley Research Center's molecular beam system to perform an absolute calibration of the lunar orbital mass spectrometer which was flown on the Apollo 15 and 16 missions. Tests were performed with several models of the instrument using two test gases, argon and neon, in the 10^{-13}–10^{-9} Torr range. Sensitivity to argon at spacecraft orbital velocity was 2.8×10^{-4} A/Torr enabling partial pressures in the 10^{-14} Torr range to be measured at the spacecraft altitude. Neon sensitivity was nearly a factor of 5 less. The response of the instrument to off-axis beams shows a cosine-to-cosine^2 dependence. Test data support the feasibility of using the lunar orbital mass spectrometer as a tool to gather information about the lunar atmosphere.

Introduction

The scientific objectives of the mass spectrometer experiment, carried on the flights of Apollo 15 and 16, are to obtain data on the composition and distribution of the lunar ambient atmosphere, and to detect transient changes in its composition. Data from the experiment will permit study of the lunar atmosphere sources, sinks, and transport mechanisms. Detection of changes in the composition will permit study of gases venting from the lunar surface or originating from man-made sources.

Mechanisms of release of gases from the surface, for example, solar wind bombardment or volcanism, perhaps can be affirmed by knowing what the effluent gases are. Likewise, data on released gases may afford some knowledge of the chemical processes underlying the lunar surface.

The experiment will provide a means for determining the natural distributions of gases in the lunar atmosphere. This information is essential if the sources, sinks, and transport of these gases are to be understood. Since the lunar atmosphere is a classical example of an exosphere, its global structure can be used to test theories on exospheric transport which is an important process in the terrestrial atmosphere.

Because of the importance of the measurements to be made and the need for high accuracy, it becomes necessary to perform absolute calibrations to determine sensitivity factors and operating characteristics of the mass spectrometers to be used in making the lunar measurements. To insure the highest possible accuracy, laboratory calibrations were performed on four models of the lunar orbital mass spectrometer (Qualification model, Flight 1, Flight 2, and Flight 3 models) in the Langley Research Center's Molecular Beam System (MBS)[1] using two test gases, argon and neon, for which sensitivity factors were established.

The mass spectrometer electronic and analyzer package was mounted in the guard vacuum (10^{-9}–10^{-8} Torr range) of the MBS with the ion source inlet, a plenum, in line with the beam axis, separated from the guard vacuum by a Teflon seal. Provisions were incorporated to vary the mass spectrometer inlet plenum with respect to the molecular beam axis, representing spacecraft pitch and yaw motions, to determine the angular response of the instrument for off-axis molecular beams.

The MBS used for this experiment incorporates a combined technique of pressure attenuation, molecular beaming, and cryopumping to produce accurately known pressures in the 10^{-13}–10^{-9} Torr range. Test data results generally agree with theory for both axial and off-axis molecular beams and demonstrate that the test chamber will adequately support calibrations of mass spectrometers for ground and flight experiments.

Description of Test Apparatus

Molecular Beam System

A molecular beam has been described as a stream of molecules effusing from a small aperture source into an evacuated chamber, where its direction is defined by collimating apertures. The molecular beam system[1] used for this experiment is shown schematically in Fig. 1 and pictorially in Fig. 2. A high-pressure gas source (number 2, Fig. 1), measured by a rotating piston gage, is required to maintain inlet pressures from 0.1–10^4 Torr, at a constant known temperature between 295 and 301 K. This known pressure is reduced from four to seven orders of magnitude through a selected porous plug, in the manner of Owens,[2] into a molecular furnace (number 4, Fig. 1). From there the gas effuses through a well-defined aperture in the furnace with a cosine distribution. All but the core of this effused gas is stripped off by liquid-helium-cooled aperture surfaces, the remaining core of gas (number 9, Fig. 1) forming the molecular beam. The beam passes through a liquid-helium-temper-

 Copyright © 1973 by the American Vacuum Society

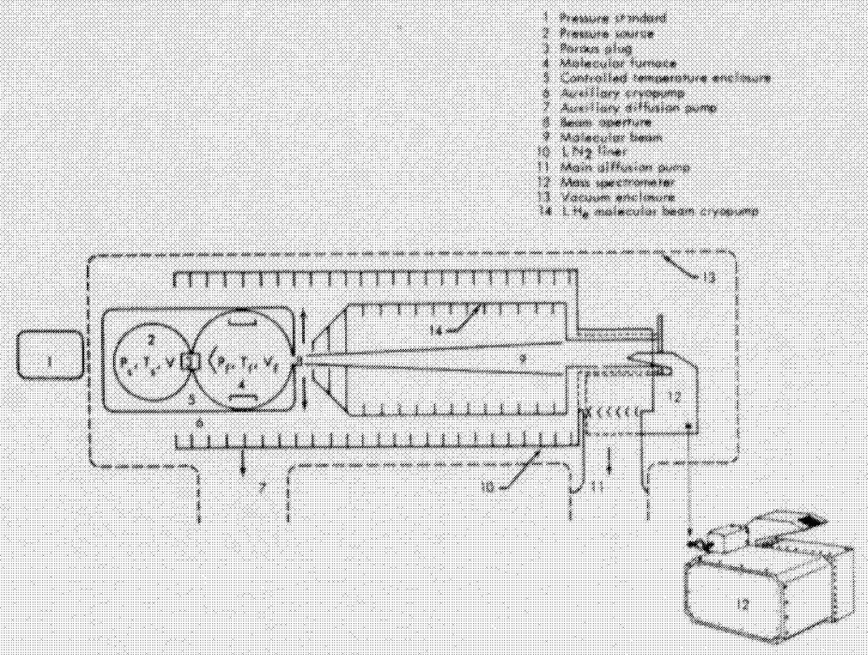

FIGURE 1. Molecular beam apparatus. Schematic drawing showing the interior of the system and position of the mass spectrometer.

ature inner tube to the mass spectrometer inlet plenum. The porous plug used in this application was a silicate glass plug, the conductance (C_p) of which was experimentally determined (*in situ*) for all test gases. For a known volume of gas attached to the porous plug in a steady-state flow condition, molecular conservation requires that

$$P(t) = P_0 e^{-C_p t/V}.$$

When the initial source pressure P_0, the pressure $P(t)$, volume V, and time t are known, the conductance can be determined from experimental data over a given pressure range. Figure 3 shows porous plug calibration data over several time differentials for argon and neon. Table I shows the values of conductance obtained and a maximum uncertainty in the porous plug conductance measurements. This uncertainty was obtained by choosing the difference between a maximum and minimum conductance value for the six readings and dividing by the mean value ($\bar{C}_p$). This procedure was used to reflect the largest magnitude of uncertainty. For these data, a mean value of conductance at 298 K was found to be 1.18×10^{-6} liters/sec for argon and 1.64×10^{-6} liters/sec for neon. Since the molecular beam flux is a

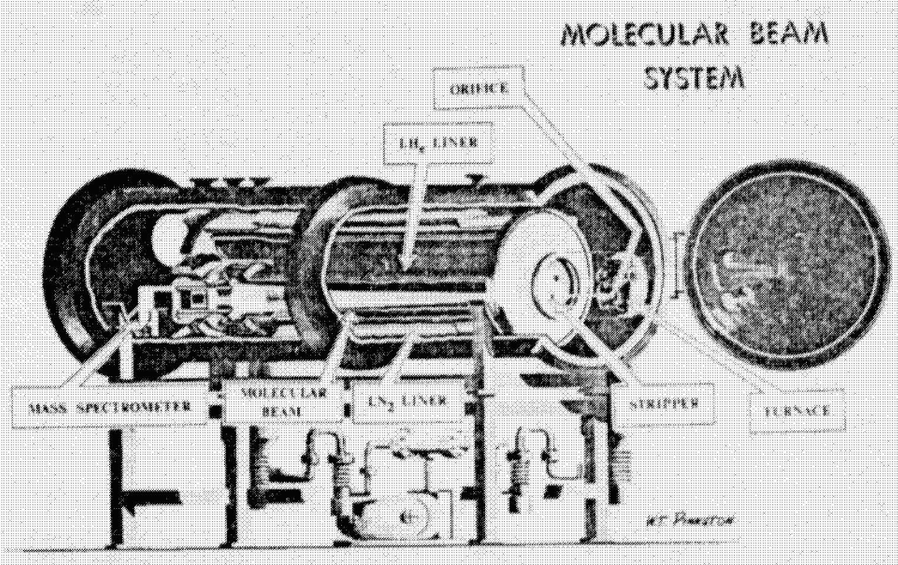

FIGURE 2. Molecular beam system. Pictorial view of the system showing a cross-sectional sketch of its interior, liquid nitrogen liner, and liquid helium liner.

TABLE I. Porous plug conductance data.

Gas	Calibrated porous plug conductance (C_p) for six readings ($\times 10^{-6}$ liters/sec)						Mean value of conductance $\bar{C}_p = [\frac{1}{6}\sum_{i=1}^{6}(C_p)_i]$	Uncertainty in porous plug conductance measurements $= \pm\frac{(C_p)_{max}-(C_p)_{min}}{\bar{C}_p}$
Argon	1.18	1.13	1.16	1.20	1.23	1.18	1.18×10^{-6} liters/sec	±4.2%
Neon	1.60	1.62	1.63	1.65	1.63	1.64	1.64×10^{-6} liters/sec	±3.1%

function of the furnace temperature, accurate monitoring of this temperature is essential. The furnace and gas source temperatures were maintained essentially at a constant value with variations of less than 0.2 K. Therefore, errors in the temperature measurement were considered negligible. Gas molecules, upon entering the molecular furnace, equilibrate to the wall temperature since the pressure is sufficiently low for molecular flow conditions to exist. The molecular beam effusing from the furnace aperture, at the furnace temperature, can be shown[1] to have a flux density of

$$\Gamma_b = \frac{1}{2}\left(\frac{r_a}{l}\right)^2 \frac{C_p}{C_a}\left(\frac{2}{\pi m k T_f}\right)^{\frac{1}{2}} P_s \frac{\text{molecules}}{\text{cm}^2\cdot\text{sec}},$$

where C_a = conductance of furnace aperture, 3.4 liters/sec for argon and 4.8 liters/sec for neon at 298 K; C_p = Conductance of porous plug, 1.18×10^{-6} liters/sec for argon and 1.64×10^{-6} liters/sec for neon at 298 K; k = Boltzmann's constant; l = Distance from beam aperture to plenum inlet, 207 cm; m = mass per molecule (grams/molecule); P_s = source pressure (dynes/cm²); r_a = furnace aperture radius, 0.33 cm; T_f = furnace temperature, 298 K; and Γ_b represents the number of molecules per second impinging on each square centimeter of the inlet (plenum) opening. Table II gives the comparison of source pressure, beam flux, and beam pressure.

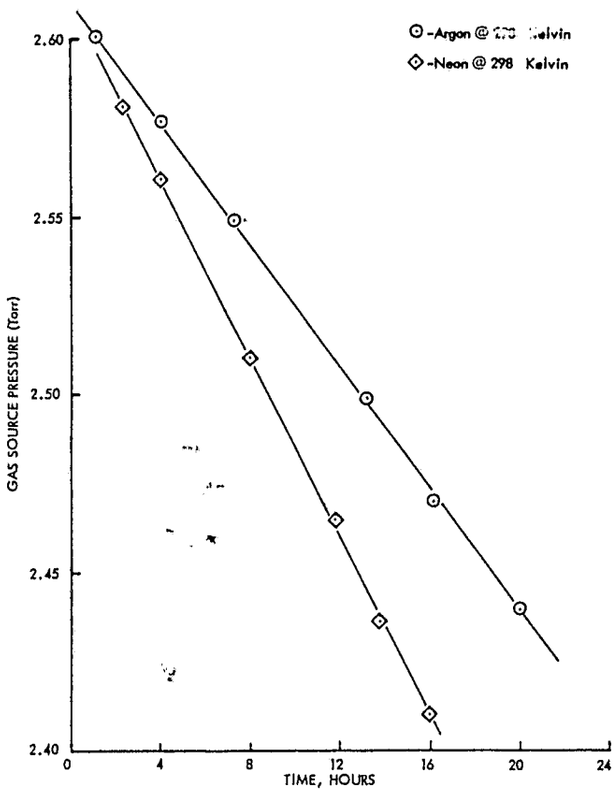

FIGURE 3. Porous plug calibration. Data on porous plug given as source pressure vs time to determine the plug conductance.

The mass spectrometer is shown mounted in the MBS pictorially in Fig. 4, where the electronic package is in the guard vacuum of the system and the inlet plenum axis is aligned with the beam axis. An externally controlled mechanical linkage was used to set the beam–plenum axis angle (equivalent to the spacecraft yaw axis) from 0° to 40° with reference to a horizontal axis perpendicular to the beam axis. Pitch angles of −5°, 0°, and +5° with reference to a vertical axis perpendicular to the beam axis were set manually with the system open. Separate measurements were made using combinations of the three pitch angles and various yaw angles up to 40°. The mass spectrometer inlet was completely enclosed by a liquid-helium-temperature copper tube, an extension of the beam collimating tube, such that backscattering of molecules into the inlet was essentially eliminated. Thermocouples were attached to the mass spectrometer inlet to monitor its temperature. Provision was also made to vary the temperature of the mass spectrometer source inlet using an externally controlled heating element.

Mass Spectrometer

The lunar orbital mass spectrometer is a magnetic deflection type mounted on a 7.3-m boom extending

TABLE II. Relationship of source pressure to beam flux and pressure.

Source pressure (psi)	Flux (mol/cm² sec)	Beam pressure[a] (P_b) (Torr)
Argon		
0.1	1.45×10^{9}	9.6×10^{-12}
0.3	4.25×10^{9}	2.9×10^{-12}
1.0	1.45×10^{10}	9.6×10^{-12}
3.0	4.25×10^{10}	2.9×10^{-11}
10.0	1.45×10^{11}	9.6×10^{-11}
30.0	4.35×10^{11}	2.9×10^{-10}
50.0	7.25×10^{11}	4.8×10^{-10}
Neon		
0.1	2.05×10^{9}	9.6×10^{-12}
0.3	6.15×10^{9}	2.9×10^{-12}
1.0	2.05×10^{10}	9.6×10^{-12}
3.0	6.15×10^{10}	2.9×10^{-11}
10.0	2.05×10^{11}	9.6×10^{-11}
20.0	4.10×10^{11}	1.9×10^{-10}

(Data for gases at 298 K)

[a] $P_b = \frac{2}{3\pi}\left(\frac{r_a}{l}\right)^2 \frac{C_p}{C_a} P_s$.

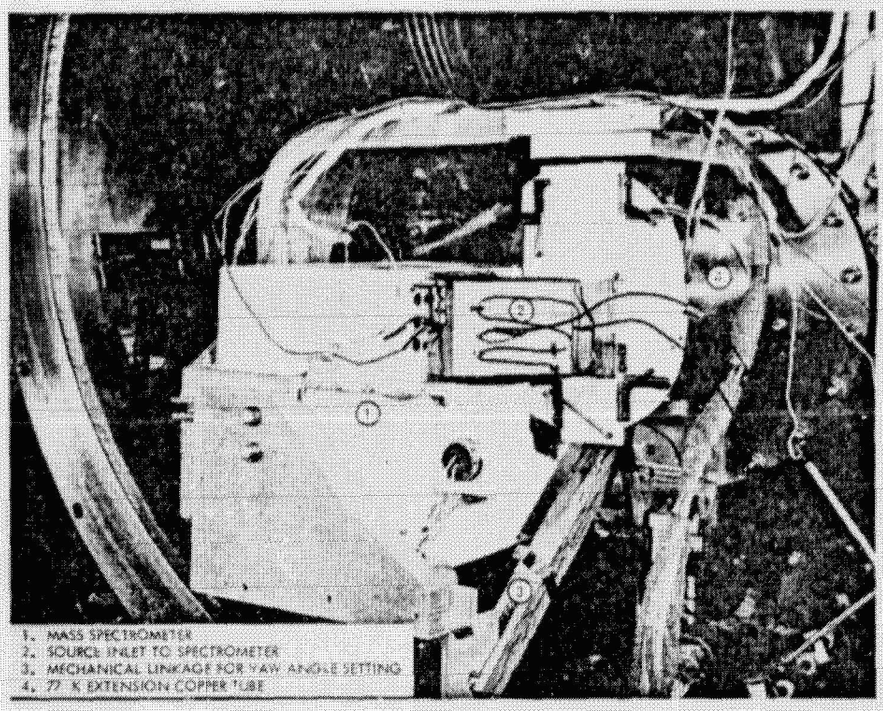

FIGURE 4. Mounting of mass spectrometer in molecular beam system. Pictorial view of mass spectrometer and electronic package as positioned during the test. Note also the source inlet to spectrometer, mechanical linkage for yaw angle setting, and 77 K extension copper tube.

from the Scientific Instrument Module in Bay 1 of the Apollo 15 and 16 service modules.[3] Dimensions of the instrument are approximately $0.30\times0.32\times0.23$ m, and the weight is 11 Kg. The operational configuration of the mass spectrometer is shown in Fig. 5.

The instrument analyzes the gases it collects by determining the concentration of each species of molecule with mass number between 12 and 66 atomic mass units (amu). Its gas inlet plenum mounted on the outboard side away from the spacecraft is oriented in the $-X$ direction of the Command and Service Module (CSM) to minimize collection of contaminant gases vented from the CSM. When the spacecraft is oriented to orbit the moon with the $-X$ axis forward (flying backward), the native gases of the lunar atmosphere are scooped into the plenum. To determine the background contamination from the CSM or other sources, the $+X$ spacecraft axis is pointed forward, preventing native gases from entering the plenum.

Molecules entering the plenum are ionized by electron bombardment in the ion source, accelerated by an electric field, and collimated into a beam that passes into a magnetic field wherein the ions follow trajectories that are a function of the ion momentum. Two special trajectories, shown in Fig. 6, lead to two collector slits where the ions are detected simultaneously in two mass ranges (12–28 and 28–66 amu).

Standard ion counting techniques determine the quantity of each ion species detected. Data are stored in two 21-bit accumulators, the outputs of which are compressed pseudologarithmically into two 10-bit data words (maintaining 7-bit accuracy) which convey the information to earth on the down-link telemetry channel. Voltage scan is employed using a stepping high-voltage power supply. Dwell time on each voltage step is 1/10 sec, thus requiring 59 sec to scan the entire spectrum. Background counting rate determination and internal calibration of the data system require 3 sec between sweeps. The minimum number of steps per mass number below mass 54 is 12; and, the mass resolution is such that at mass 39 amu there is less than 0.3% contribution from the mass 40 (argon) peak.

Tests and Results

In order to calibrate both mass ranges of the mass spectrometer, neon for the low-mass channel and argon for the high-mass range, were selected as the test gases. Using these gases, partial pressures ranging from 10^{-13}–10^{-9} Torr were obtained in the molecular beam facility.

The test sequence was basically as follows: The mass spectrometer inlet plenum was initially set at $-5°$ pitch and 0° yaw. The chamber was evacuated and the test

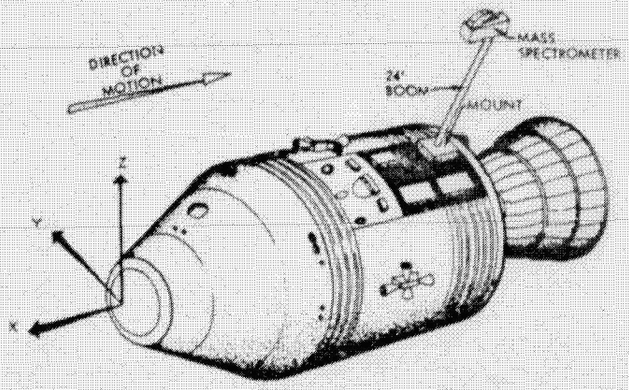

FIGURE 5. Mass spectrometer operational configuration. The mass spectrometer inlet plenum shown as positioned during space flight. The inlet plenum faces away from the spacecraft and is oriented in the $-X$ direction of the Command and Service Module.

REPRODUCIBILITY OF THE

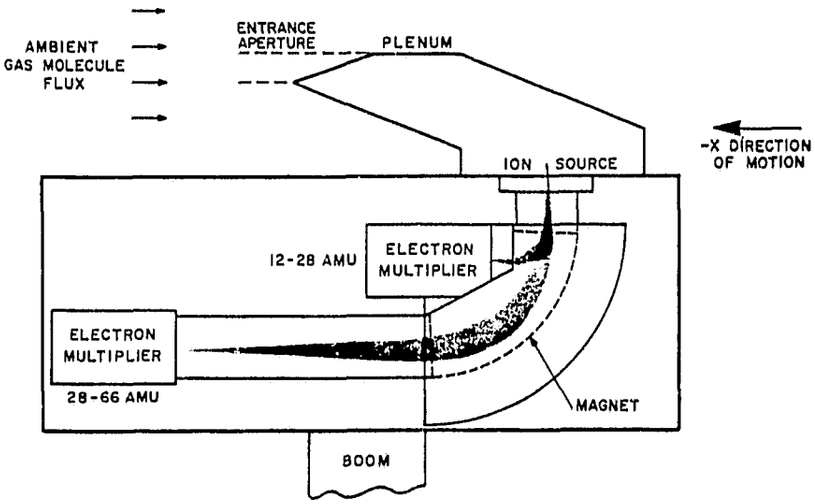

FIGURE 6. Analyzer trajectories. Ions emerge from the source and enter a uniform magnetic field, produced by a permanent magnet. Two special trajectories of 4.158- and 6.350-cm radii determine the location of collection slits for the low-mass and high-mass ion detectors.

chamber wall filled with liquid helium. This reduced the background pressure in the test chamber to the low 10^{-14}-Torr region as indicated on a Redhead gage (these gage readings are only an indicator that the chamber is pumping properly and are not used in the molecular beam flux calculations). Background readings were taken on the mass spectrometer. Then the beam source pressure was set at 1.0 psi argon and a minimum of three scans of the argon spectrum was taken on the mass spectrometer. Table II gives the relationship between source pressure and beam flux. After the first set of readings, the source pressure was reduced to zero in order to again make background readings. Source pressures of 3.0, 10.0, 30.0, and 50.0 psi were then set and mass spectrometer scans taken for each reading. Between each pressure point, the source was evacuated to obtain background readings. The data were recorded as ion counts for each peak in the spectrum less the background counts for that peak. The above procedure was repeated for yaw settings of 10°, 20°, 30°, and 40°. After completion of the argon tests, the complete procedure was repeated using neon as the test gas. Source pressure for neon was limited to 30.0 psi due to the fairly rapid background pressure buildup by the neon at higher pressures.

The above tests were repeated for pitch angles of 0° and +5°. Other data were taken for various inlet plenum temperatures between 238 and 300 K, and certain pressure sweeps were repeated using each of the two filaments in the mass spectrometer ion source.

From the above tests, it was possible to make a rather complete evaluation of the performance of the mass spectrometer. The data were analyzed to give comparison of filament performance, establish linearity of the instrument, assess output as a function of pitch and yaw angles, verify the effects of inlet (plenum) temperature variations, and determine the sensitivity of the instruments for the two test gases.

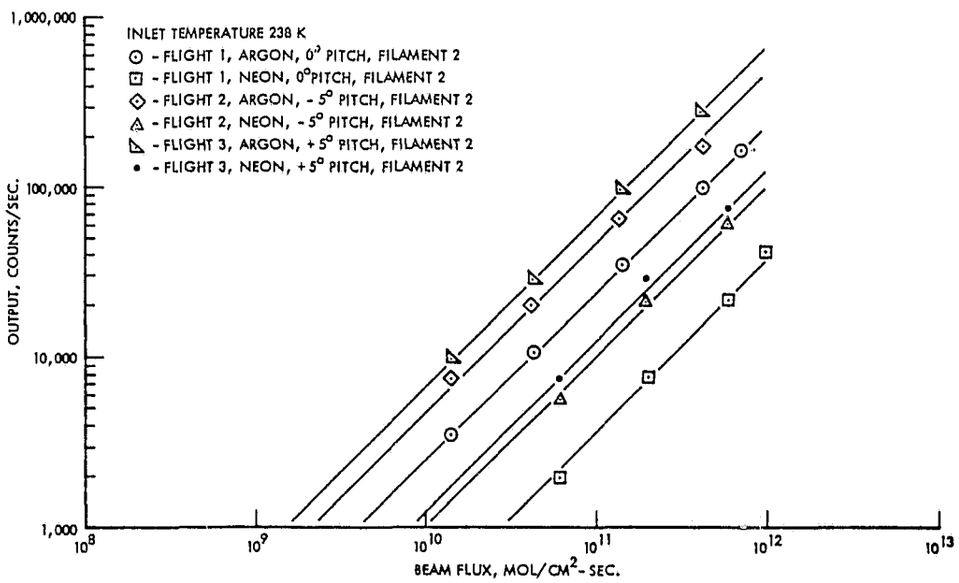

FIGURE 7. Variation of output for neon and argon for three flight instruments.

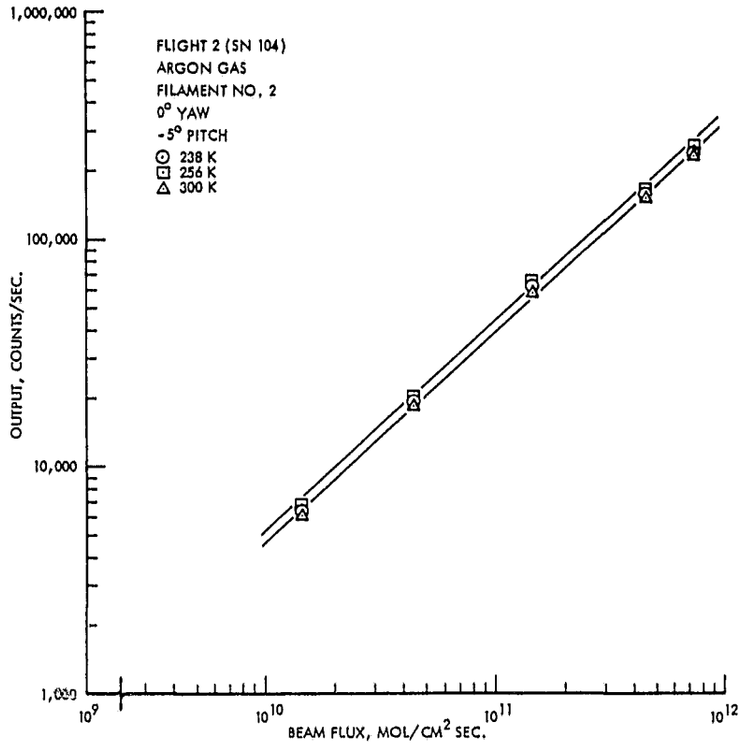

FIGURE 8. Variation in output with inlet (plenum) temperature over the range 238–300 K.

Figure 7 shows the output, in counts/second, of Flights 1, 2, and 3 instruments vs beam flux for both argon and neon. The data show the instrument to be linear over the range tested, with any deviation from linearity well within the beam accuracy (6%). The linearity test was extended to several decades using minor isotopes of the test gases. The data are presented in terms of beam flux rather than pressure since the speed ratio of the incoming gas between the calibration beam and actual flight differs by about a factor of 5. The actual equilibrium pressure in the inlet must be calculated for each gas molecule speed (gas temperature or ram velocity in flight). The technique for calculating the equilibrium pressure in an enclosure exposed to a gas beam is given in Ref. 1. Employing this technique, it was found that the sensitivity limit of the instrument to lunar orbital velocity gases was $\sim 10^{-14}$ Torr.

The relative sensitivity of the two filaments on

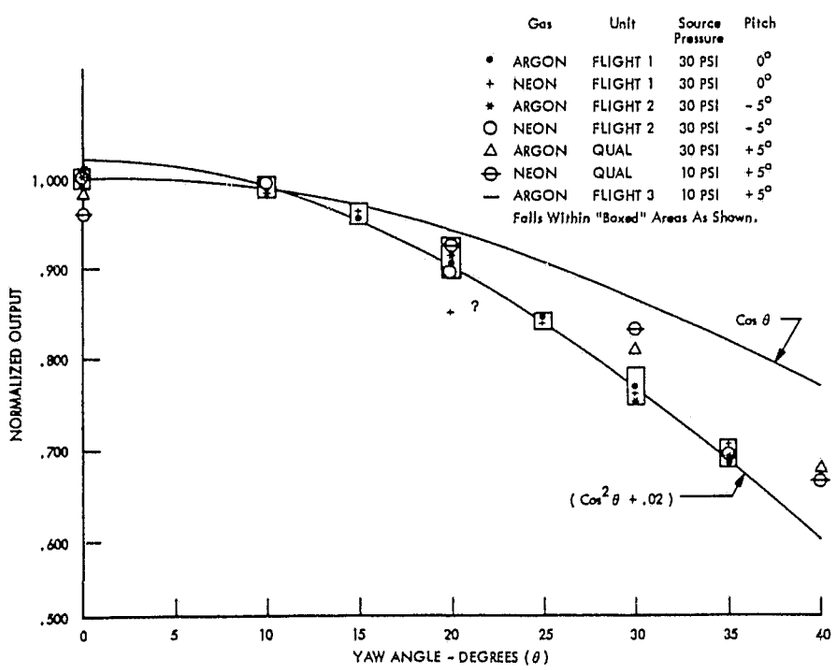

FIGURE 9. "Best fit" of data to $\cos\theta/\cos^2\theta$. Data were obtained to show the variations in output for the flight units with change in yaw angle. Up to 20°, the output portrays a cosine function; between 20° and 40° it is closer to a cosine² function.

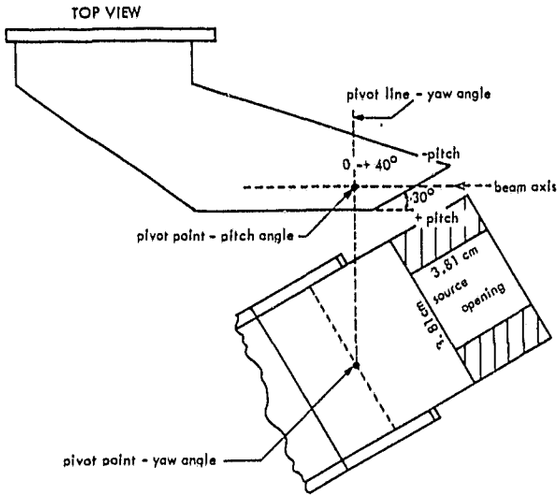

FIGURE 10. Inlet configuration. Cross-sectional view of the inlet opening. The opening is not perpendicular to the direction of the beam, but is at a 60° angle as it is in flight, and becomes more nearly so at negative pitch angles.

Flight 1 and Flight 2 instruments is of the order of 15% for argon. There is more variation in sensitivity between instruments than there is between filaments in a given instrument.

Figure 8 gives the variation in output for inlet (plenum) temperature variation from 238 to 300 K as measured by the Flight 2 instrument. The variations lie within the relative error bars of the measurements (5%) and are certainly much less than the square root of temperature ratio (12%). This probably results from actual variation of ion source temperature being less than the temperature sensors on the source housing indicated.

Figure 9 shows the variations in output for the flight units with change in yaw angle. Up to about 20° the output falls off according to the cosine law, as would be expected. However, between 20° and 40° the decrease is closer to a cosine^2 function. This seems to be due to incoming molecules not reaching equilibrium with the walls before they are measured or escape from the plenum. Up to 20° yaw, the input beam hits the rear wall of the plenum only. Beyond 20°, the beam begins to strike the side wall from which gas molecules may more readily escape without being measured. Pitch angle tests showed higher ion currents at negative than at positive angles. This is probably due to the shape of the inlet and the resulting in and out gas fluxes. As can be seen in Fig. 10, the inlet opening is not perpendicular to the direction of the beam but is at a 60° angle, as it is in flight (the plane through this opening is set to exclude the spacecraft from the mass spectrometer field of view), but the opening becomes more nearly perpendicular to beam direction at negative pitch angles. This results in the effective beam opening being smaller than the actual physical size for an incoming beam, but remains the geometrical opening for the out-going flux. The measured pitch angle response follows a cosine law.

Conclusion

The calibration of the lunar orbital mass spectrometer to known fluxes of gas molecules, performed in the Molecular Beam System at Langley Research Center, showed the instrument capable of measuring gases of partial pressures down to 10^{-14} Torr at spacecraft velocity with a linear response over several orders of magnitude. The corresponding sensitivity was 2.8×10^{-4} A/Torr. The argon to neon ratio of a factor of 5 is in good agreement with the ionization cross sections for the electron energy used (70 eV). The plenum temperature studies show relative insensitivity to temperature with a constant input flux, possibly indicating that the ion source temperature variation was less than the temperature sensors on its housing reported. Response to off-axis beams shows a cosine law dependence for small angles (up to 20°) and a cosine^2 dependence beyond that. During flight, the instrument was mounted on a long boom which is susceptible to thermal twisting. Photographs of the instrument at full boom extension showed that the boom's yaw and pitch behavior (twisting and bending) followed very closely that predicted by models of the boom showing that calibrations in pitch and yaw were required. Twist is in the yaw direction and was nearly 40°. Pitch is equivalent to boom bending and was less than 3°.

The Flight 2 instrument was flown on Apollo 15, 26 July–7 August 1971.[4] Flight 1 instrument was flown on Apollo 16, 16–28 April 1972. Preliminary data reduction showed large numbers of peaks in the mass spectra of relatively large amplitude in lunar orbit with a considerable reduction (factors of 5–10) in amplitude of all peaks during transearth coast. The gas molecules seen in lunar orbit do not appear to have a significant velocity with respect to the spacecraft since the densities observed are not a function of the angle of attack of the mass spectrometer plenum, indicating they are probably of spacecraft origin or are coorbiting with the spacecraft.

[1]A. Smith, TN D-5308, July 1969, NASA.
[2]C. L. Owens, J. Vac. Sci. Technol. 2, 104 (1965).
[3]J. H. Hoffman, Int. J. Mass Spectrom. Ion Phys. 8, 403 (1972).
[4]J. H. Hoffman, R. R. Hodges, Jr., and D. E. Evans, "Lunar Orbital Mass Spectrometer Experiment," Geochimica et Cosmochimica Acta (to be published).

COMPOSITION AND PHYSICS OF THE LUNAR ATMOSPHERE

J. H. Hoffman, R. R. Hodges, Jr., F. S. Johnson
The University of Texas at Dallas, Dallas, Texas

D. E. Evans
NASA/Johnson Space Center, Houston, Texas

Presented at

Sixteenth Plenary Meeting

COMMITTEE ON SPACE RESEARCH

(COSPAR)

Konstanz, F.R.G.

May 31, 1973

UTD No. SP-73-012 COSPAR No. i.16

Abstract

The existence in the lunar atmosphere of helium, neon, argon and possibly molecular hydrogen has been confirmed by the Apollo 17 mass spectrometer. The observed helium concentrations and distribution agree closely with model predictions for a non-condensable gas based on a solar wind source, thermal escape and a Monte Carlo random walk calculated longitudinal distribution. Heavier gases are lost by photoionization and subsequent sweeping away by the solar wind electric field. The observed nighttime neon concentration of 8×10^4 molecules cm^{-3} is consistent with expected amounts. Argon, however, is adsorbed on the lunar surface late at night when the surface temperature is lowest. It shows the expected pre-dawn enhancement exhibited by condensable gases released into the atmosphere at the sunrise terminator. Hydrogen appears to exist in the molecular rather than atomic state. Its observed concentration is less than a factor of 3 higher than that predicted by a model similar to that used for helium. The total nighttime concentration of known species (H_2 He, Ne, Ar) in the lunar atmosphere is 2×10^5 molecules cm^{-3}.

INTRODUCTION

The moon does indeed have an atmosphere, but it is so tenuous that it acts as a collisionless gas, the molecules traveling in ballistic trajectories between encounters with the surface of the moon. Trajectory heights and horizontal travel are determined by the surface temperature and molecular mass.

The major source of known gases in the lunar atmosphere is the solar wind [1]. Its ions impinge directly on the lunar surface and become imbedded in the surface materials, but once the surface is saturated with a given constituent of the solar wind, that constituent must be released from the surface at the same average rate as it is accrued. When released, the neutralized molecules form an atmosphere. Those molecules released with sufficiently high velocity will escape from the moon. This is the dominant loss process for hydrogen and helium. Heavier gases, for which thermal escape is slow, are distributed around the moon by diffusion, their local concentration being a function of temperature, ($T^{-5/2}$) [2], unless they condense or are adsorbed on the cold nightside. A noncondensable gas will then have a night-to-day concentration ratio of about 30. For a condensable gas, a rapid release occurs at the sunrise terminator forming a locally enhanced concentration. Gases from this region can travel eastward throughout the dayside region or westward into the nightside several scale heights before being readsorbed on the surface, thus giving rise to a pre-dawn enhancement.

The light gases do not follow the $T^{-5/2}$ concentration law, but their distribution about the moon can be handled by a Monte Carlo calculation. Assuming a symmetric daytime temperature distribution about the subsolar point and a gradually decreasing night temperature to 90K at the sunrise terminator, the diurnal ratio for helium and hydrogen has been shown to be 24 and 6.5 respectively [3] with the maximum for both occurring at night.

Heavy gas molecules, not lost by thermal escape, are photoionized and accelerated by the solar wind electric field [4]. As their speeds increase, the ions begin to react to the solar wind magnetic field, eventually traveling in cycloidal paths. Since the radius of gyration is large compared to the moon, about half the ions escape from the moon and half impinge on the surface to be re-released into the atmosphere as neutral gas molecules.

Using these concepts and measured solar wind fluxes, expected gas concentrations have been derived for both the subsolar and antisolar points. These are summarized in Table 1.

Apollo 17 carried a miniature mass spectrometer to the Taurus Littrow site to identify the gas species in the lunar atmosphere and determine their concentrations. Because of the very tenuous nature of the lunar atmosphere, the instrument was designed [5] with an extremely high sensitivity, of the order of 100 molecules cm^{-3} for most gases, such as nitrogen and argon. It features an electron bombardment ion source, simultaneous scanning of three mass ranges (1 to 4, 12 to 48, and 27 to 110 amu), ion counting techniques, and a unique floating point data compression scheme which maintains 7-bit (1%) accuracy throughout a 21-bit (2×10^6) range of data counts. Calibration was done using a molecular beam system at NASA Langley Research Center [6].

Initial operation of the instrument occurred on December 27, 1972. Data reported herein have been taken during the first five lunations since deployment.

RESULTS

Quick-look strip chart type records have been used for data reduction to date. An example of such a record is given in reference [5]. The accuracy of data from this type of record (not the final data form) is considered to be ±30% with the smaller amplitude peaks having a factor of 2 uncertainty.

Because of the very high sensitivity of the instrument, daytime spectra are characterized by large amplitude peaks at nearly every mass number. These gases result from outgassing of the instrument, lunar module and landing site, and, except for helium, are all considered artifact at this time.

Nighttime spectra are generally quite clear of contaminant peaks but exhibit dominant peaks at 19, 35 and 37 amu. These are believed to be from fluorine and chlorine which are probably artifacts, but their origins are unknown. Hydrogenated halogen peaks occurring at masses 20, 36 and 38, are probably formed in the ion source by a reaction with hydrogen as their abundance is a strong function of ion source temperature.

In order to be assured that any given mass peak in the spectrum is not artifact (produced by outgassing of the ion source electrodes), a cool-down test of the ion source is performed periodically. Normal nighttime ion source temperature is 270K. Removing filament power for nearly an hour causes the ion source temperature to drop to approximately 195K. Subsequent turn-on of the filament produces a relatively clean spectrum for the first spectrum scan. That is, peaks due to outgassing have decreased markedly, some to zero amplitude, while those gases not originating in the ion source produce essentially unchanged peak amplitudes.

There exists positive identification of at least three gases native to the lunar atmosphere, helium, neon and argon. In addition, recent ion source cool-down tests show hydrogen to exist in the molecular form at a concentration of 6.5×10^4 molecules cm^{-3}. While this may still be only an upper limit on lunar molecular hydrogen, since the mass 2 peak was dominated by hydrogen outgassing from the ion source early in the operation of the instrument, recent measurements have shown a stable peak amplitude which is only slightly depressed during the cool down tests, suggesting that the ambient level is being sampled. The existence of hydrogen in molecular form is consistent with the result from the Far UV spectrometer experiment flown on Apollo 17, which set a daytime upper limit for atomic hydrogen of 10 atoms cm^{-3} [7]. These results also showed a daytime upper limit for H_2 to be less than the instrument detection limit of 6×10^3 molecules cm^{-3}. This value combined with the Monte Carlo model diurnal ratio of 6.5 [3] gives an inferred nighttime upper limit of 4×10^4 cm^{-3}, which is close to the presently measured value. Using a solar wind flux of 3×10^8 molecules cm^{-2} sec^{-1} Hodges [3] obtained a daytime concentration of 3.6×10^3 and nighttime value of 2.3×10^4, a factor of nearly 3 lower than the observed value.

Earlier predictions of the hydrogen concentration in the lunar atmosphere [1] assumed no recombination at the surface and thus an atmosphere of H. The existence of H_2 has not been predicted.

The mass 1 peak is dominated by dissociatively ionized (in the instrument ion source) hydrogenated molecules and no measurement of its ambient lunar concentration can be expected from the instrument.

Figure 1 shows the helium concentration plotted as a function of solar zenith angle during the first five lunations after deployment of the instrument. The abscissa scale begins at the subsolar point and progresses through the lunation. Sunset, midnight and sunrise are identified. The scatter of the nighttime data is indicative of the variations that have been measured [8] in the solar wind flux of helium. Residence time is of the order of 7.6×10^4 sec [3] indicating a response time to fluctuations in the solar wind of a few tens of hours. The frequencies of the observed variations are consistent with this time scale.

The solid curve on Figure 1 is the helium distribution at 18° latitude from an updated Monte Carlo calculation based on a solar wind flux of 1.3×10^7 He ions cm^{-2} sec^{-1} observed by Geiss et al [9]. The agreement with the data is seen to be excellent. Maximum calculated diurnal ratio is 24; the measured value is approximately 20. The asymmetry about the antisolar point results from the temperature decrease throughout the night and the rotation of the moon.

During ion source cool-down tests occurring in the fourth and fifth lunar nights, the level of the artifact peak (HF) at mass 20 has been reduced sufficiently to give valid neon measurements. The average ^{20}Ne concentration is 8×10^4 cm^{-3}, which agrees favorably with the atmospheric model value of 1.2×10^5 cm^{-3} [10]. The observed isotopic ratio, $^{20}Ne/^{22}Ne$, is 14.2, close to the ratio of 13.7 from the solar wind composition experiment [9].

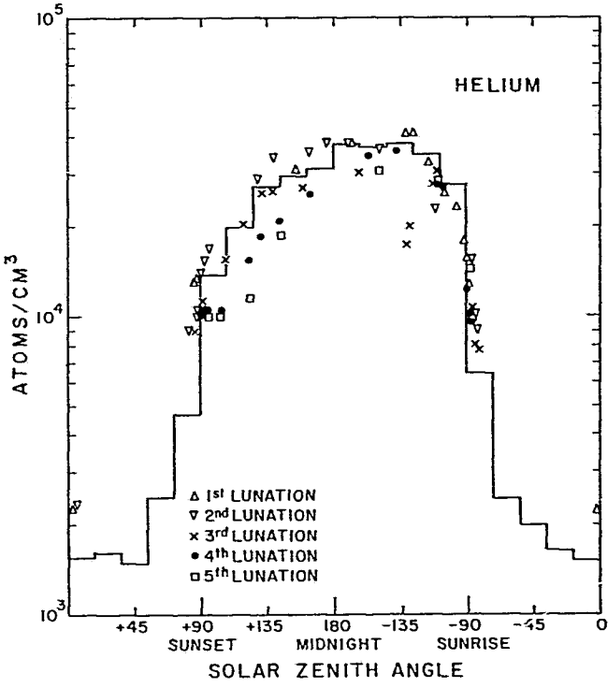

Figure 1. Diurnal variation of ^4He concentration as a function of solar zenith angle starting at subsolar point. Data points are from the first five lunations. Solid curve is theoretical distribution based on a Monte Carlo calculation.

The diurnal distribution of ^{40}Ar during the third, fourth and fifth lunar nights is shown in Figure 2. Coordinates are similar to those of Figure 1. Daytime data are masked by hydrocarbon peaks from outgassing of the instrument and site. By the time the sunset terminator (solar zenith angle of 90°) has crossed the landing site meridian (six hours after the sun has dipped below the mountains to the west), the site has cooled sufficiently that contaminent peaks no longer interfere with the ^{40}Ar measurement. The ^{40}Ar concentration at sunset is about 8 x 10^3 cm^{-3}. This steadily decreases through the night as the surface cools reaching a value of 10^2 cm^{-3} (the instrument detection limit) at -145° solar zenith angle. It appears that the argon is adsorbed on the cold nighttime surface. At about 20° before sunrise, the ^{40}Ar concentration begins to increase reaching a value of 3.5 x 10^4 at the terminator crossing of the site, a factor of nearly 5 larger than at sunset. Sunrise at the site is delayed 8 hours from the time the sun is at a zenith angle of 90° by shadowing from the mountains to the east, precluding significant local heating before this time. This behavior of argon matches closely that of a condensable gas as described above. The concentration of an artifact gas, CO_2, which does not exhibit a pre-dawn enhancement, is shown for comparison. After sunrise, rapid heating occurs and hydrocarbon peaks again dominate the spectrum.

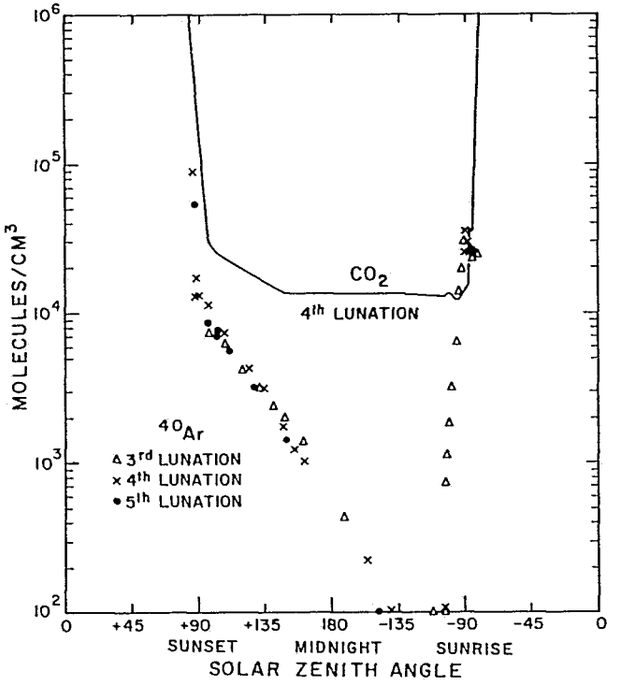

Figure 2. ^{40}Ar and CO_2 diurnal variation. Coordinates similar to Figure 1.

A more detailed picture of the pre-dawn and sunrise conditions is given in Figure 3. Gas concentrations are plotted as a function of solar zenith angle from -110° to -80°. After terminator crossing there appears to be a slight decrease in ^{40}Ar concentration as though the local source were being somewhat depleted of argon as would be expected after the terminator had passed.

Mass 36 also exhibits a pre-dawn enhancement, about 10% of that of ^{40}Ar. Because of the presence of HCl, only the enhanced portion of the peak is believed to be ^{36}Ar, yielding a concentration of 3 x 10^3 cm^{-3} at the terminator. The ^{36}Ar source is the solar wind, whereas ^{40}Ar is believed to come from degassing of the regolith. From the near equality of the ^{36}Ar and excess ^{40}Ar trapped in the soil [11], the atmospheric ratio would be expected to be closer to unity. Perhaps the soil is not saturated with ^{36}Ar and hence most of the impinging solar wind flux of ^{36}Ar is permanently trapped.

Other gases shown in Figure 3 (masses 28 and 44) do not appear to exhibit a pre-dawn enhancement. Mass 28, if it is N_2, would probably not be adsorbed at the night lunar temperature and would therefore not show a pre-dawn enhancement. If it is CO, it would likely be adsorbed and would be expected to follow the argon pattern. Native CO_2 (mass 44) would also be expected to show a pre-dawn enhancement. The negative result places an upper limit on both native CO and CO_2 at the sunrise terminator of 3 x 10^3 cm^{-3}. Mass 32, O_2, also exhibits no pre-dawn enhancement, and several ion source cool down tests have shown a zero amplitude peak for O_2. An upper limit is in the low 10^2 cm^{-3} range.

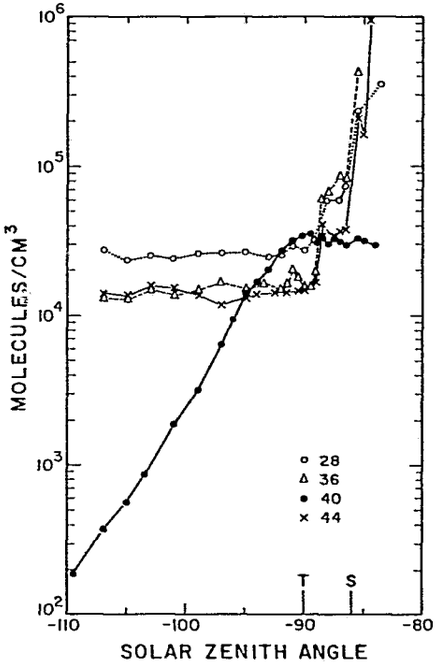

Figure 3. Concentrations of masses 28, 36, 40, and 44 as a function of solar zenith angle from -110° to -80°. "T" is time of terminator crossing landing site longitude. "S" is sunrise at landing site and the time of onset of local heating.

The total gas concentration measured near the antisolar point on the fourth lunation is 2 x 10^5 molecules cm^{-3} without the mass 19, 35 and 37 peaks included. All other peaks in the spectrum are of significantly lower amplitude. This value is the same as that obtained by the Cold Cathode Gauge Experiment on Apollos 14 and 15 [1]. However, addition of the 19, 35 and 37 peaks (F and Cl) doubles the nighttime gas concentration. It is unclear whether these gases were present at the Apollo 14 and 15 site and were being measured as part of the nighttime gas concentration by the cold cathode gauges. Daytime comparisons are not meaningful at this time due to the high outgassing rate still prevailing at the Apollo 17 site. CCGE daytime readings were not made until the ninth lunation.

CONCLUSION

The existence of three gases in the lunar atmosphere is confirmed by the Apollo 17 mass spectrometer. Helium and neon follow the expected behavior of non-condensable gases, and have concentrations close to those predicted by lunar atmospheric models considering the solar wind as their source. Argon behaves on the nightside as a condensable gas exhibiting a pre-dawn enhancement, with the $^{40}Ar/^{36}Ar$ ratio approximately 10. In addition, nighttime molecular hydrogen measurements are within a factor of 3 of a Monte Carlo model prediction, and close to an upper limit inferred from application of the model's night-to-day ratio to the Far UV spectrometer experiment's daytime value. The existence of hydrogen in the molecular form has not been predicted.

The sum of all the known gases in the nighttime lunar atmosphere (H_2 He, Ne, Ar) equals that measured by the cold cathode gauges at the Apollo 14 and 15 sites: 2 x 10^5 molecules cm^{-3}. Table 1 lists a summary of these gas concentrations. All other peaks in the spectrum are considered artifact at this time. As the degassing of the site continues, other gas species may eventually be identified as native lunar gases.

ACKNOWLEDGMENTS

This work was supported by NASA Contract NAS9-12074 and by Bendix Aerospace Subcontract SC-830 of NASA Contract NAS9-5829. Special thanks are due the crew of Apollo 17 who so successfully deployed the instrument on the moon.

Table 1. Summary of Gases in the Lunar Atmosphere

Gas	Observation Molecules cm^{-3}		Model[a] Molecules cm^{-3}	
	Day	Night	Day	Night
H_2	–	6.5 x 10^4	3.6 x 10^3	2.3 x 10^4
^4He	2 x 10^3	4 x 10^4	1.7 x 10^3	4.1 x 10^4
^{20}Ne	–	8 x 10^4	4.7 x 10^3	1.2 x 10^5
^{36}Ar	–	3 x 10^3 b	–	–
^{40}Ar	–	3.5 x 10^4 b	–	–
	–	8 x 10^3 c	–	–
O_2	–	<2 x 10^2	–	–
CO_2	–	<3 x 10^3	–	–
CO	–	<3 x 10^3	–	–

Total (Nightime):
Mass Spectrometer 2 x 10^5
CCGE 2 x 10^5

a. Ref [3], [10].

b. Sunset terminator.

c. Sunrise terminator.

References

[1] F. S. Johnson, J. M. Carroll and D. E. Evans, Proc. Third Lunar Sci. Conf., Geochim. et Cosmochim. Acta, Suppl. 3, 3, 2231 (1972).

[2] R. R. Hodges and F. S. Johnson, J. Geophys. Res. 73, 7307 (1968).

[3] R. R. Hodges, Jr., Submitted to J. Geophys. Res.

[4] R. H. Manka and F. C. Michel, Proc. Second Lunar Sci. Conf., Geochim. et Cosmochim. Acta, Suppl. 2, 2, 1717 (1971).

[5] J. H. Hoffman, R. R. Hodges, Jr., F. S. Johnson and D. E. Evans, Apollo 17 Prelim. Sci. Report, NASA Report, in press.

[6] J. H. Hoffman, R. R. Hodges, Jr., F. S. Johnson and D. E. Evans, Apollo 15 Prelim. Sci. Report, NASA Report SP-289 (1972).

[7] W. G. Fastie, Private Communication.

[8] A. J. Hundhausen, S. J. Bame, J. R. Asbridge and S. J. Sydoriak, J. Geophys. Res., 75, 4643 (1970).

[9] J. Geiss, F. Beuther, H. Cerutti, P. Eberhardt and C. Filleux, Apollo 16 Prelim. Sci. Report, NASA Report SP-315 (1972).

[10] R. R. Hodges, Jr., J. H. Hoffman, F. S. Johnson and D. E. Evans, Proc. Fourth Lunar Sci. Conf., Geochim. et Cosmochim. Acta, Suppl. 4, in press.

[11] A. Yaniv and D. Heymann, Proc. Third Lunar Sci. Conf., Geochim. et Cosmochim. Acta, Suppl. 3, 2, 1967 (1972).

GEOCHIMICA ET COSMOCHIMICA ACTA
Journal of The Geochemical Society and The Meteoritical Society
SUPPLEMENT 4

PROCEEDINGS
OF THE
FOURTH LUNAR SCIENCE CONFERENCE
Houston, Texas, March 5-8, 1973

Sponsored by
The NASA Johnson Space Center
and
The Lunar Science Institute

PERGAMON PRESS

Printed in the U.S.A.

Proceedings of the Fourth Lunar Science Conference
(Supplement 4, *Geochimica et Cosmochimica Acta*)
Vol. 3, pp. 2855–2864

Composition and dynamics of lunar atmosphere

R. R. HODGES, JR., J. H. HOFFMAN, and F. S. JOHNSON

The University of Texas at Dallas
Dallas, Texas

D. E. EVANS

Johnson Space Center
Houston, Texas

Abstract—The model of lunar atmosphere is updated to take into account new information on the dynamics and amounts of H_2, ^4He, ^{20}Ne, ^{36}Ar, and ^{40}Ar. Helium and neon appear to be in close balance with the solar wind, although ^{36}Ar is depleted in the atmosphere, suggesting that surface materials are not saturated with argon. Atmospheric carbon compounds, which should result from the solar wind influx of carbon, remain undetected, as do nitrogen compounds. However, evidence of a volcanic gas release is presented, which suggests the transient presence of these elements.

INTRODUCTION

THE LUNAR atmosphere is so tenuous that it is a collisionless gas, except for molecular encounters with the surface of the moon. In the absence of particle interactions, hydrodynamic processes do not exist. However, the statistical distribution of molecular trajectories over the moon causes pseudo-collective phenomena, similar to tides, waves and winds, to exist.

In the preliminary analysis of data from the Apollo 17 lunar surface mass spectrometer a diurnal tidal oscillation of helium is clearly present (Hoffman *et al.*, 1973). The nighttime concentration of He is about 20 times that in the daytime, in close agreement with the theoretical model of Hodges (1973).

Helium is unique in lunar mass spectrometric data because there is no contaminant source of a substance with mass of 4 amu. Inasmuch as degassing of remnant spaceflight hardware produces artifacts at virtually all other mass numbers in the daytime, recognition of a native species requires correlation of some part of its diurnal variation with a theoretical model. For example, Hodges and Johnson (1968) pointed out that a gas which condenses on the cold surface of the dark side of the moon will form a pocket of gas over the sunrise terminator due to release of adsorbed gases from the rapidly warming surface. This phenomenon includes a presunrise increase in concentration due to particles which travel westward into the nighttime hemisphere from their point of release near the sunrise terminator. In the Apollo 17 mass spectrometer data it is evident that both ^{36}Ar and ^{40}Ar have precisely this presunrise behavior, but the post sunrise data at masses 36 and 40 amu are complicated by the release of contaminants from the spaceflight hardware at the ALSEP site.

In addition to these diurnal effects, it is important to understand the characteristics of volcanic events, and particularly the differences of such events from artifact gas releases.

This paper presents a review of the present state of knowledge of the dynamics of the lunar atmosphere from both theoretical and experimental viewpoints. It includes data on both diurnal variation and transient volcanic events, which are used to update the model of the composition of the lunar atmosphere.

SOURCES OF LUNAR ATMOSPHERE

The solar wind is probably the dominant source of lunar atmosphere. Solar wind ions impact the moon with energies the order of 1 keV per amu, which is sufficient to imbed the ions in surface materials. Present abundances of most trapped solar wind gases in returned soil samples are lower than would be expected if a significant fraction of the impinging solar wind were currently being trapped. Thus it is likely that the soil is saturated with trapped gases and that a detailed balance of the solar wind influx and the release of previously trapped gases exists.

An important verification of this hypothesis is the close balance of the solar wind flux and the lunar atmospheric content of helium (Hodges, 1973). A counter example is the surprisingly small amount of atomic hydrogen detected by the Apollo 17 orbital ultraviolet spectrometer (Fastie *et al.*, 1973), which may be explained by postulating that most of the hydrogen released from the soil is molecular (H_2). The solar wind balanced H_2 model of Hodges (1973) is compatible with the lowest upper bound on H_2 that could be inferred from the data reported by Fastie *et al.* (1973). Contaminant H and H_2 in available mass spectrometric data precludes elucidation of this problem, except to set a nighttime upper bound on H_2 at $6.5 \times 10^4\ cm^{-3}$ (Hoffman *et al.*, 1973).

The amounts of nitrogen, carbon, oxygen, neon, and argon in the solar wind are significant, and the soil is apparently saturated with these elements. Mass spectrometric data suggest that neither N nor C exists in atomic form in the lunar atmosphere. Presumedly molecular nitrogen could be formed, but the preponderance of protons in the impinging solar wind would more likely lead to formation of NH_3. A similar process should lead to production of CH_4. Neither ammonia nor methane, which freeze at 196°K and 91°K respectively, appears in the nighttime lunar atmosphere. Their daytime levels are obscured by contaminants, which should eventually dissipate from the Apollo 17 lunar surface mass spectrometer data. The large amounts of oxygen in the soil may lead to formation of CO and possibly NO, although the reactions to produce these gases would probably be reversible. Oxygen ions of the solar wind must react rapidly with the soil, precluding oxygen in the atmosphere. Neon and argon have been detected on the moon (Hodges *et al.*, 1972b, and Hoffman *et al.*, 1973).

It is clear from the lack of a dense atmosphere that the rate of volcanic degassing of the moon is somewhat less than on earth. Hodges *et al.* (1972a) have found an upper bound on lunar venting to be $1.5 \times 10^{-16}\ g\ cm^{-2}\ sec^{-1}$, which is several orders of magnitude less than would occur if the release rate were the same per

unit mass as for earth (cf. Johnson *et al.*, 1972). Despite this low average level of volcanic activity, rather convincing evidence of currently active, sporadic volcanism in certain regions of the moon is found in the alpha particle data reported by Gorenstein *et al.* (1973). The time scale of this activity is the order of 21 years, the lifetime of the ^{210}Pb in the decay of ^{222}Rn. It is possible that these events occur so infrequently as to have no more than a transient effect on the lunar atmosphere.

The radioactive decay of uranium and thorium in the moon produces alpha particles, and hence helium, at several times the rate of solar wind influx of helium. However the bulk of these atoms must be permanently trapped within the moon. A test of this hypothesis will be obtained with the Apollo 17 lunar surface mass spectrometer when the moon passes through the high latitude part of the geomagnetic tail, during which time the solar wind source of helium will be eliminated. If the atmospheric helium dissipates at the expected rate (about 1 day^{-1}), the solar wind source will be confirmed. Otherwise a lunar source must be considered.

Decay of ^{40}K in surface materials is probably the main source of ^{40}Ar in the lunar atmosphere. Subsequent photoionization and acceleration of the resulting ions by solar wind fields causes some of the ^{40}Ar to be retrapped in the soil along with solar wind ^{36}Ar, so that the isotopic composition of impacted argon in the soil may be indicative of the amount of ^{40}Ar in the atmosphere (Manka and Michel, 1971).

Identification of Noncondensable Gases

On the dark side of the moon, where the temperature falls below 100°K, most gases are adsorbed. Analogy with a laboratory cold trap suggests that hydrogen, helium, nitrogen, and neon would not condense at night. Of these only helium is easily identifiable, because of the absence of 4 amu contaminants in mass spectra from the moon. However, neon has also been detected as the excess of the 20 amu measurement when contaminants have been accounted for (Hodges *et al.*, 1972b, and Hoffman *et al.*, 1973).

Figure 1 shows the presently available data on the concentration of ^{20}Ne at the lunar surface, along with a fitted theoretical distribution ($n \propto T^{-5/2}$, as derived by Hodges and Johnson, 1968), plotted as functions of longitude measured from the subsolar meridian. Circles are from the Apollo 16 orbital mass spectrometer, and squares are preliminary data from the Apollo 17 ALSEP mass spectrometer. Water ($H_2{}^{18}O$) was a large contaminant in the orbital neon data, and the circles represent all of the data where the water contribution was low enough that it could be subtracted with reasonable accuracy. Even so, the lower bound of the statistical uncertainty of each data point includes zero. These data are generally about a factor of 4 lower than the preliminary value of neon concentration given by Hodges *et al.* (1972b), the difference being due to improved laboratory data on the cracking pattern of water in the mass spectrometer ion source. The paucity of data from the Apollo 17 lunar surface instrument reflects the difficulty in

REPRODUCIBILITY OF THE
ORIGINAL PAGE IS POOR

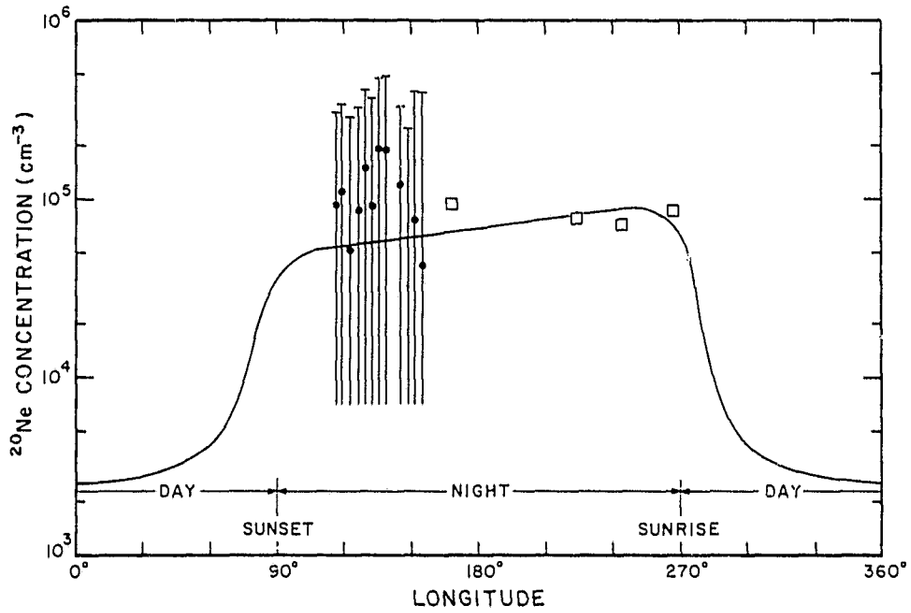

Fig. 1. A hypothetical equatorial distribution of ^{20}Ne at the lunar surface, predicted by the $T^{-5/2}$ law, is shown by the solid curve. Data from the Apollo 16 orbital mass spectrometer are represented by circles, while those from the Apollo 17 lunar surface mass spectrometer are represented by squares.

obtaining a neon measurement. This is accomplished by a complicated command sequence which lowers the ion source temperature sufficiently to condense the contaminant at 20 amu, which is HF (Hoffman *et al.*, 1973).

There is an order of magnitude discrepancy between the predicted neon concentration of Johnson *et al.* (1972); i.e., about 1.3×10^6 cm^{-3} at night, and the data given in Fig. 1, necessitating a reexamination of the theory. Subsequent discussion shows that a surprising increase in the calculated rate of loss of neon from the moon arises when the $T^{-5/2}$ concentration distribution is substituted for the previously used stepped model.

The amount of neon in the lunar atmosphere must be in equilibrium with the solar wind influx, i.e.,

$$\pi R^2 \Phi_{sw} = \frac{N_s}{2\tau_i} \tag{1}$$

where R is the lunar radius, Φ_{sw} is the solar wind flux of neon, N_s is the total number of atoms in sunlight, and τ_i is the photoionization lifetime. The factor 2 in the denominator gives an approximate accounting for the fraction of photoions which impact the moon and subsequently return to the atmosphere (Johnson, 1971).

Approximating the vertical distribution of neon as barometric and the surface

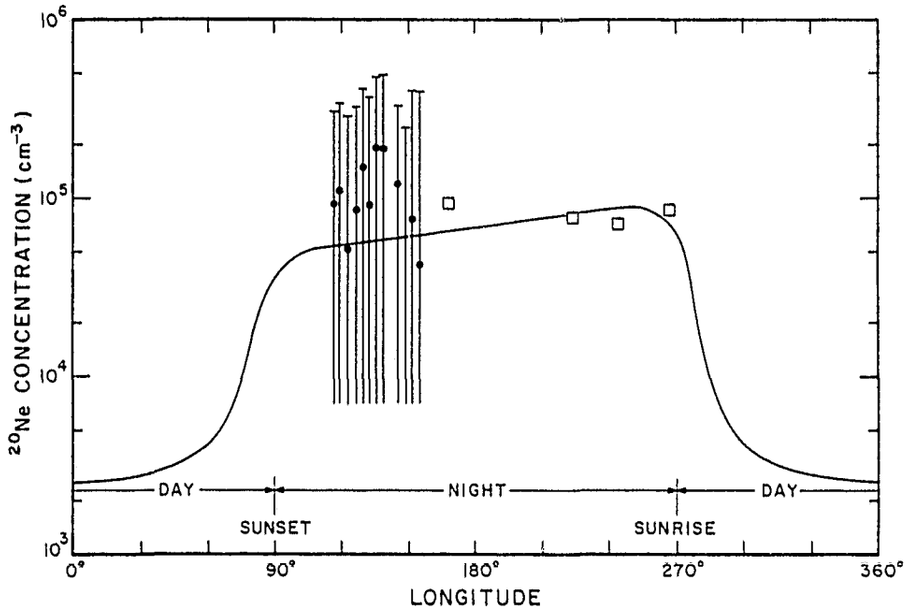

Fig. 1. A hypothetical equatorial distribution of ^{20}Ne at the lunar surface, predicted by the $T^{-5/2}$ law, is shown by the solid curve. Data from the Apollo 16 orbital mass spectrometer are represented by circles, while those from the Apollo 17 lunar surface mass spectrometer are represented by squares.

obtaining a neon measurement. This is accomplished by a complicated command sequence which lowers the ion source temperature sufficiently to condense the contaminant at 20 amu, which is HF (Hoffman *et al.*, 1973).

There is an order of magnitude discrepancy between the predicted neon concentration of Johnson *et al.* (1972); i.e., about $1.3\times10^6\,\mathrm{cm}^{-3}$ at night, and the data given in Fig. 1, necessitating a reexamination of the theory. Subsequent discussion shows that a surprising increase in the calculated rate of loss of neon from the moon arises when the $T^{-5/2}$ concentration distribution is substituted for the previously used stepped model.

The amount of neon in the lunar atmosphere must be in equilibrium with the solar wind influx, i.e.,

$$\pi R^2\Phi_{sw}=\frac{N_s}{2\tau_l} \tag{1}$$

where R is the lunar radius, Φ_{sw} is the solar wind flux of neon, N_s is the total number of atoms in sunlight, and τ_l is the photoionization lifetime. The factor 2 in the denominator gives an approximate accounting for the fraction of photoions which impact the moon and subsequently return to the atmosphere (Johnson, 1971).

Approximating the vertical distribution of neon as barometric and the surface

temperature distribution as symmetrical about the moon–sun axis, N_s is given by

$$N_s = 2\pi R^2 \int_0^{\pi/2} d\psi\, nH \sin\psi + 2\pi \int_{-\infty}^{0} dz \int_R^0 d\rho\rho\, ne^{(\sqrt{z^2+\rho^2})/h} \tag{2}$$

where n is concentration at the surface, H is scale height, ψ is the lunarcentric angle from the subsolar point, while z and ρ are lunarcentric cylindrical coordinates, with z measured toward the sun. The first integral represents the number of atoms in the daytime hemisphere while the second gives those over the night side at altitudes great enough to be in sunlight. Temperature is approximated by radiative equilibrium in daytime ($\propto \cos^{1/4}\psi$) and constant at night. Letting $n \propto T^{-5/2}$, integration of expression 2 results in

$$N_s = 2\pi R^2 n_N H_N \left\{ \frac{8}{5}\left(\frac{T_N}{T_D}\right)^{3/2}\left[1 - \frac{3}{8}\left(\frac{T_N}{T_D}\right)^{5/2}\right] + e^{R/H_N} K_2\left(\frac{R}{H_N}\right)\right\} \tag{3}$$

where the subscript N denotes nighttime value, T_D is the daytime maximum temperature, and K_2 is the modified Bessel function of the second kind and of order 2. The first of the bracketed terms is due to the daytime integral; and for a day to night temperature ratio of 4 its value is 0.20. The last term represents the nighttime integral; and is 0.21 for $T_N = 95°K$.

The abundance of ^{20}Ne in the solar wind is about 1/570 that of ^{4}He according to Geiss *et al.* (1972), while the amount of ^{4}He is 0.045 that of hydrogen (Johnson *et al.*, 1972). Assuming an average proton flux of 3×10^8 cm^{-2}sec^{-1}, the solar wind flux of ^{20}Ne should be 2.4×10^4 cm^{-2} sec^{-1}. Using this flux, a photoionization lifetime of 10^7 sec, and the evaluation of expression 3 above in Equation 1, gives 2.3×10^5 cm^{-3} for the nighttime ^{20}Ne concentration. This is about $\frac{1}{3}$ the amount predicted by Johnson *et al.* (1972), with most of the difference being due to the previous neglect of photoionization near the terminators.

Manka (1972) has suggested that the photoionization lifetime of neon should be 6×10^6 sec, which would further reduce the theoretical nighttime concentration to 1.4×10^5 cm^{-3}. A slight further reduction in the theoretical value can be made on the basis that the moon spends only about 25 of each 29 days in the solar wind (with the other 4 days in the geomagnetic tail), reducing the influx of neon in that proportion, and hence reducing the predicted nighttime concentration of neon to 2.0×10^5 cm^{-3} or 1.2×10^5 cm^{-3}, depending on which photoionization lifetime is used. Table 1 gives the present theoretical estimates and experimental values on the noncondensable gases on the moon. Theoretical values for neon reflect the uncertainty regarding the photoionization lifetime. Atomic hydrogen, nitrogen and noncondensable compounds containing nitrogen and carbon are omitted because they are not present in significant quantities in the nighttime atmosphere.

Condensable Gases

In available mass spectroscopic data the only obvious condensable gases of the lunar atmosphere are ^{40}Ar and ^{36}Ar, while the presence of ^{222}Rn has been identified in alpha particle data (Gorenstein *et al.*, 1973). Other species, such as ^{38}Ar, NH_3, or

REPRODUCIBILITY OF THE ORIGINAL PAGE IS POOR

Table 1. Noncondensable gases of the lunar atmosphere.

	H_2		^4He		^{20}Ne
Solar wind flux ($cm^{-2}sec^{-1}$)	3×10^8 (protons)		1.3×10^7		2.4×10^4
Residence time (sec)	6.5×10^3	(a)	7.9×10^4	(a)	$1\text{-}3\times10^7$
Surface concentration (cm^{-3})					
Subsolar theory	2.0×10^3	(a)	1.6×10^3	(a)	$4\text{-}7\times10^3$
Subsolar experiment			2×10^3	(b)	
Antisolar theory	1.2×10^4	(a)	3.8×10^4	(a)	$1\text{-}2\times10^5$
Antisolar experiment	$<6.5\times10^4$	(b)	4×10^4	(b)	$\sim10^5$

(a) Hodges (1973)
(b) Hoffman *et al.* (1973)

CH_4, may also exist, but their abundances are not sufficient to overcome the artifact background in the mass spectrum.

Identifiable features of the diurnal variations of a native condensable gas include concentration minima near both the subsolar and antisolar regions, with the former being due to transport effects and the latter due to adsorption on the cold nighttime surface of the moon. Since artifacts dominate the daytime data, only the nighttime behavior has been detected.

To elucidate the nature of a condensable gas it is helpful to use the diffusion approximation of exospheric transport (Hodges, 1972)

$$\Phi_s = \frac{\alpha}{1-\alpha}\frac{n\langle v\rangle}{4} + \Omega\frac{\partial}{\partial\phi}nH - \nabla_h^2 n\langle v\rangle H^2 \tag{4}$$

where Φ_s is the upward flux near sunrise due to release of adsorbed gas, α is the fraction of the downcoming flux adsorbed by the surface, $\langle v\rangle$ is mean particle speed, Ω is the rate of angular rotation of the moon, ϕ is longitude measured from the subsolar meridian, and ∇_h^2 is the horizontal part of the Laplacian operator in a sun-referenced coordinate system. In the daytime hemisphere α is zero; while at night it must be small as compared to unity for the differential equation to be valid.

To simplify solution of equation 4 it is helpful to restrict the problem to the equator, where meridional flow of the atmosphere must vanish, and then to approximate the flow as though the lunar surface were cylindrical. In addition the release of adsorbed gas is assumed to take place very near the sunrise terminator, so that Φ_s can be approximated as a line source. Then equation 4 becomes 1-dimensional, and its solution can be found easily by integration.

Figure 2 shows a theoretical distribution of ^{40}Ar at the equator, where the longitudinal dependence of the surface adsorption fraction, α, has been chosen to insure that the solution matches the indicated experimental data points from the Apollo 17 lunar surface mass spectrometer. Just prior to sunrise the appropriate value of α is 0.054 while that immediately following sunset is 7×10^{-4}. The difference in these values of α is explainable as an indication of the temperature depen-

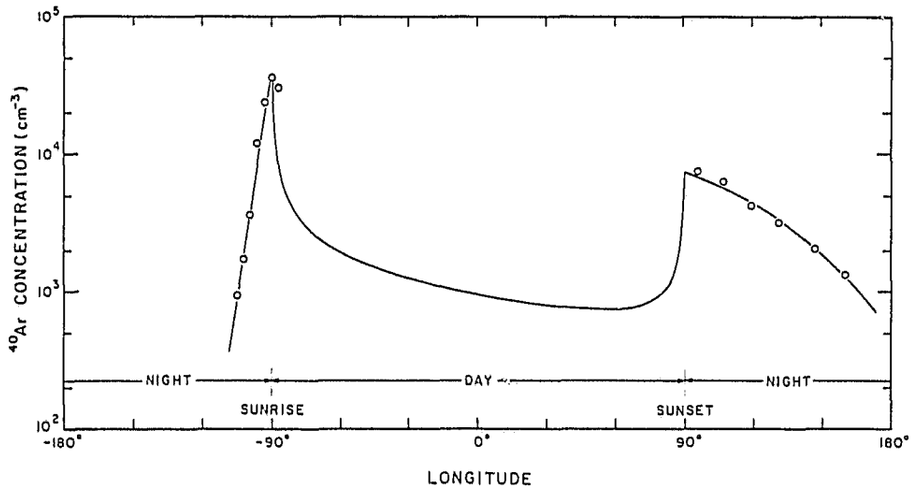

Fig. 2. Equatorial distribution of ^{40}Ar computed from Equation 4, with surface adsorption fraction chosen to fit the Apollo 17 mass spectrometer data.

dence of the adsorption mechanism, wherein adsorption becomes increasingly more likely as the temperature approaches the freezing temperature of argon (~84°K).

A similar diurnal variation of ^{36}Ar has been detected, but at a much lower level. In addition, a persistent nighttime contaminant at mass 36 amu precludes accurate determination of the level. However, it is clear that the ratio of ^{36}Ar to ^{40}Ar in the lunar atmosphere is the order of 0.1. This result is perhaps surprising in view of the near equality of ^{36}Ar and excess ^{40}Ar trapped in the soil (cf. Yaniv and Heymann, 1972). It suggests that the soil is not saturated with ^{36}Ar, and hence that most of the impinging solar wind flux of ^{36}Ar is permanently trapped. The amount of ^{20}Ne in returned samples exceeds that of ^{36}Ar by a factor greater than 2 (cf. Eberhardt *et al.*, 1972, or Heymann *et al.*, 1972). Since solar wind argon impacts the moon with almost twice the energy of neon, and hence is implanted deeper, the saturation level of argon might be expected to exceed neon. Thus the hypothesis that the soil is saturated with neon but not with argon is plausible. Owing to the small influx of ^{36}Ar there is no conflict of saturation with the present amount in the soil and a shallow mixing depth (< 10 meters) of the regolith over geologic time.

An estimate of the release rate of ^{40}Ar into the atmosphere can be made by a crude adaptation of the equatorial variation in Fig. 2 to a global distribution, and subsequent determination of the amount of the gas in sunlight, as was done for neon earlier. Using a photoionization lifetime of 1.6×10^6 sec (Manka, 1972), the average flux of ^{40}Ar emanating from the lunar surface is about 2.6×10^3 cm^{-2} sec^{-1}.

EVIDENCE OF LUNAR VOLCANISM

In all of the data from the orbital mass spectrometers on Apollo 15 and Apollo 16, and preliminary data from the Apollo 17 lunar surface instrument, only one probable volcanic event has been discovered. Figure 3 shows measurements at masses 14, 28, and 32 amu from the Apollo 15 orbital mass spectrometer. The sudden excursions of these three masses occurred at 0822 hours GMT on August 6, 1971, as the spacecraft passed over 110.3°W, 4.1°S (i.e., northwest of Mare Orientale and in lunar night). No coincident change occurred at any other mass in the spectrum from 12 to 67 amu. Excursions with amplitudes similar to that at 32 amu would have been detected at all masses except 16, 17, 18, and 44 amu, which were dominated by large contaminant levels (Hodges *et al.*, 1972a). The absence of other substances in this event may be a temporal artifact, caused by a short

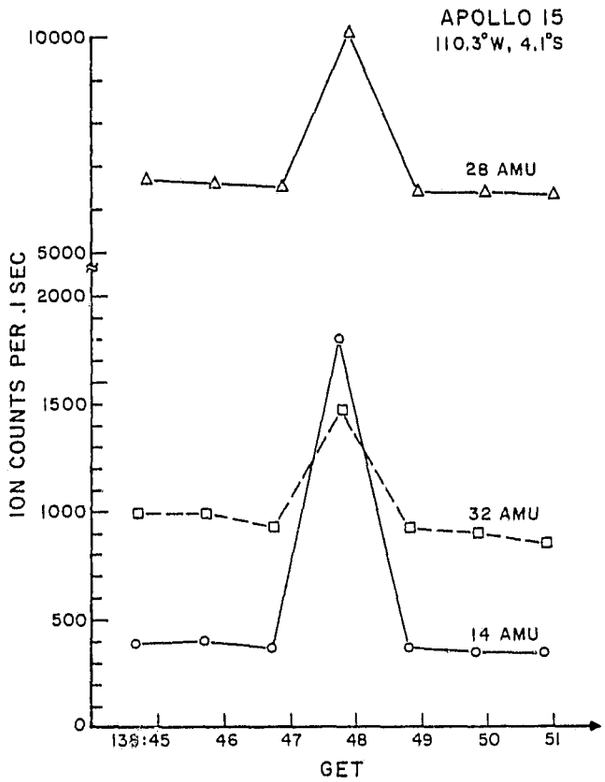

Fig. 3. Event of probable volcanic origin in data from the Apollo 15 orbital mass spectrometer. Ground elapsed time (GET) of 138:48 corresponds to 0822 hours GMT on August 6, 1971. Argon sensitivity corrected for orbital velocity ram effect was 2000 atoms/cc/count/sec, and the ion source used a 70 eV electron beam.

REPRODUCIBILITY OF THE ORIGINAL PAGE IS POOR

lived disturbance that did not span the entire duration of one sweep of the mass spectrum (62 sec).

It is practical to rule out some conjectured causes of this event. There is no evidence of recurrence of this pattern of gas release that would suggest a spacecraft origin. The lone crew member was asleep when the event occurred, and all monitors of spacecraft operation were nominal. A similar type of perturbation of only 14 and 28 amu shown in Fig. 4 was produced by the release of a large quantity of N_2 from the panoramic camera whenever its control was switched (by the crewman) to "operate." The panoramic camera produced no effect at 32 amu, while the ratio of 28 amu to 14 amu was typical of the cracking pattern of N_2, and different from that of the supposed volcanic event of Fig. 3. Thus accidental release of N_2 from the camera is not a plausible explanation of the event.

While the above comparison seems to indicate that the volcanic gas at 28 amu was not entirely N_2, the absence of a large effect at 12 amu seems to rule out the dominance of CO as well. A mixture of N, N_2, and a small amount of CO would be

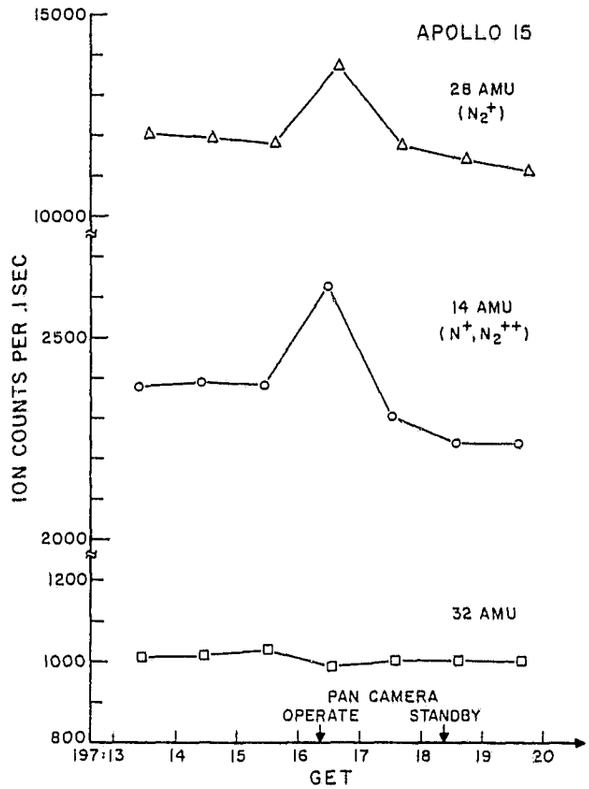

Fig. 4. Typical panoramic camera event due to sudden release of N_2.

plausible, however. Mass 32 amu could have been O_2, or possibly SO_2 if the duration of the event were short enough to have dissipated by the time the instrument measured 64 amu (about 20 sec after the 32 amu measurement).

In a word, the event shown in Fig. 3 asks more questions than it answers. The origin of its component gases is difficult to explain in terms of volcanism. Certainly N and O_2 are unlikely constituents. On the positive side, the rate of gas release necessary to have produced this event can be extrapolated from the work of Hodges *et al.* (1972a) to be the order of 1 kg/sec, or about 20 kg total, which is small in volcanic terms, albeit a significant contribution to the lunar atmosphere.

Acknowledgments—It is a pleasure to acknowledge the efforts of C. M. Peters and H. D. Hammack in the processing of mass spectrometric data. This research was sponsored by NASA under Contracts NAS9-10410 and NAS9-12074.

REFERENCES

Eberhardt P., Geiss J., Graf H., Grögler N., Mendia M. D., Mörgeli M., Schwaller H., Stettler A., Krähenbühl U., and von Gunten H. R. (1972) Trapped solar wind noble gases in Apollo 12 lunar fines 12001 and Apollo 11 breccia 10046. *Proc. Third Lunar Sci. Conf., Geochim. Cosmochim. Acta*, Suppl. 3, Vol. 2, pp. 1821–1856. MIT Press.

Fastie W. G., Feldman P. D., Henry R. C., Moos V. W., Barth C. A., Lillie C., Thomas G. E., and Donahue T. M. (1973) The Apollo 17 orbital ultraviolet spectrometer experiment (abstract). In *Lunar Science—IV*, p. 233. The Lunar Science Institute, Houston.

Geiss J., Buehler F., Cerutti H., Eberhardt P., and Filleux Ch. (1972) Solar wind composition experiment. *Apollo 16 Preliminary Science Report*, NASA SP-315, pp. 141–149.

Gorenstein P., Golub L., and Bjorkholm P. (1973) Spatial nonhomogeneity and temporal variability in the emanation of radon from the lunar surface: Interpretation (abstract). In *Lunar Science—IV*, p. 307–308. The Lunar Science Institute, Houston.

Heymann D., Yaniv A., and Lakatos S. (1972) Inert gases from Apollo 12, 14, and 15 fines. *Proc. Third Lunar Sci. Conf., Geochim. Cosmochim. Acta*, Suppl. 3, Vol. 2, pp. 1857–1863. MIT Press.

Hodges R. R. Jr. (1972) Applicability of a diffusion model to lateral transport in the terrestrial and lunar exospheres. *Planet. Space Sci.* **20**, 103–115.

Hodges R. R. Jr. (1973) Helium and hydrogen in the lunar atmosphere (submitted to *J. Geophys. Res.*).

Hodges R. R. Jr. and Johnson F. S. (1968) Lateral transport in planetary exospheres. *J. Geophys. Res.* **73**, 7307–7317.

Hodges R. R. Jr., Hoffman J. H., Yeh T. T. J., and Chang G. K. (1972a) Orbital search for lunar volcanism. *J. Geophys. Res.* **77**, 4079–4085.

Hodges R. R. Jr., Hoffman J. H., and Evans D. E. (1972b) Lunar orbital mass spectrometer experiment. *Apollo 16 Preliminary Science Report*, NASA SP-315, pp. 211–216.

Hoffman J. H., Hodges R. R. Jr., and Evans D. E. (1973) Lunar atmospheric composition results from Apollo 17 *Proc. Fourth Lunar Sci. Conf., Geochim. Cosmochim. Acta.* In press.

Johnson F. S. (1971) Lunar atmosphere. *Rev. Geophys. Space Phys.* **9**, 813–823.

Johnson F. S., Carroll J. M., and Evans D. E. (1972) Lunar atmospheric measurements. *Proc. Third Lunar Sci. Conf., Geochim. Cosmochim. Acta*, Suppl. 3, Vol. 3, pp. 2231–2242. MIT Press.

Manka R. H. (1972) Lunar atmosphere and ionosphere. Ph.D. Thesis, Rice University, 1972.

Manka R. H. and Michel F. C. (1972) Lunar atmosphere as a source of lunar surface elements. *Proc. Second Lunar Sci. Conf., Geochim. Cosmochim. Acta*, Suppl. 2, Vol. 2, pp. 1717–1728. MIT Press.

Yaniv A. and Heymann D. (1972) Atmospheric Ar^{40} in lunar fines. *Proc. Third Lunar Sci. Conf., Geochim. Cosmochim. Acta*, Suppl. 3, Vol. 2, pp. 1967–1980. MIT Press.

Helium and Hydrogen in the Lunar Atmosphere

R. R. HODGES, JR.

The University of Texas at Dallas, Dallas, Texas 75230

Solar wind ions impinge on the surface of the moon, become neutralized, and are subsequently released to become part of the neutral lunar atmosphere. Of the gas species supplied by the solar wind, only helium and hydrogen are light enough to be lost from the moon by Jeans' thermal escape mechanism. To study the behavior of helium and hydrogen, a Monte Carlo technique has been used, in which random ballistic trajectories of individual molecules are traced over a spherical moon. In the computation, a particle is 'created' on the sunlit surface, and the locations of its subsequent encounters with the surface are recorded until it escapes. Global distributions of helium and hydrogen concentrations have been computed, based on the hypothesis that the release of neutral gases from the lunar surface is confined to daytime and correlated with the solar wind influx. The resulting helium model is in good agreement with the measurements from the Apollo 17 lunar surface mass spectrometer. In view of the absence of atomic hydrogen in the lunar atmosphere and the need for a loss mechanism for the solar wind influx of protons, a molecular hydrogen atmosphere model is proposed in which predicted amounts of H_2 are below presently established upper bounds.

The atmosphere of the moon is sufficiently tenuous to be entirely an exosphere. Except for localized effects of orographic features, the lunar surface serves as a nearly classical exobase for noncondensable gases such as hydrogen, helium, and perhaps some heavier gases such as neon and nitrogen, which are unlikely to be adsorbed on the cold nighttime surface (~90°K). *Hodges and Johnson* [1968] and *Hodges* [1972] have derived the theory of exospheric transport for the heavier gases, which are expected to be distributed at the lunar surface approximately as the $-5/2$ power of temperature. Sources of these gases and their probable abundances have been discussed by *Bernstein et al.* [1963], *Hinton and Taeusch* [1964], *Johnson* [1971], *Siscoe and Mukherjee* [1972], and *Johnson et al.* [1972].

One of the significant features of the preliminary data from the Apollo 17 lunar surface mass spectrometer is the presence of a small amount of native helium [*Hoffman et al.*, 1973*a*, *b*]. Other species in the spectrum, including H and H_2, behave characteristically as the contaminants noted by *Johnson et al.* [1972] in the Apollo 14 and 15 cold cathode gage data, i.e., by increasing in amount as temperature increases and decreasing as temperature decreases. Helium does the opposite, as should be expected of a native noncondensable gas [cf. *Hodges and Johnson*, 1968].

Existing theory of exospheric transport does not provide a detailed description of the diurnal oscillation of light lunar gases, mainly because of difficulties inherent in accounting for the large diurnal temperature excursions of the surface of the moon (~80°–390°K). A Monte Carlo technique has been developed to model the behavior of the lunar atmosphere. Subsequent discussion will show results of its application to hydrogen and helium.

ASSUMPTIONS AND APPROXIMATIONS

The scale of size of typical trajectories of gas particles in the lunar atmosphere is the scale height (which is about 115 km for He at night and 4 times that in daytime). It greatly exceeds the vertical scales of orographic features. Hence it is reasonable to approximate the exobase of the moon as a smooth surface of constant gravitational potential. Owing to the slow rotation of the moon, a spherical surface is an adequate approximation.

A more crucial assumption involves the nature of encounters of gas molecules with the lunar surface. Even during nighttime at high latitudes, where the temperature probably falls below 80°K, it is not likely that hydrogen or

Copyright © 1973 by the American Geophysical Union.

helium should be adsorbed by the surface, and hence adsorption is neglected in the following theory. If this is an erroneous assumption, it will cause the nighttime concentration to be overestimated. It is assumed that molecules, after colliding with the surface, immediately reenter the lunar atmosphere with Maxwellian velocity distribution and complete accomodation with the surface temperature. Since the surface material is mainly a fine-grain soil, the probability of localized multiple collisions is high, and hence accomodation is likely.

A major source of lunar hydrogen and helium is thought to be solar wind ions, which impinge on the daytime surface, become neutralized, and then enter the atmosphere [cf. *Hinton and Taeusch,* 1964; *Hodges and Johnson,* 1968; *Johnson,* 1971]. It is assumed that the solar wind is unperturbed as it impinges on the dayside of the moon, so that the influx of hydrogen or helium is proportional to the cosine of the lunar-centric angle from the subsolar point to the point of interest. In lieu of a better approximation, the source strength of these elements in neutral gases emitted from the surface is assumed to be in local balance with the influx. Near zero phase the moon is in the tail of the magnetosphere of the earth, and the source becomes the magnetospheric plasma; this complication is not treated in this paper.

Loss of hydrogen and helium from the moon is mainly due to thermal escape. Residence times for H, H_2, and He given by the present theory are roughly 10^3, 6×10^3, and 8×10^4 sec, respectively. Escape due to photoionization has a time constant of the order of a month and thus may be neglected. Collisional ionization and charge exchange with solar wind and magnetospheric protons are also considered to be negligible.

Two temperature models have been used in the calculations. These models are empirical approximations of temperature distributions calculated by M. G. Langseth and S. J. Keihm (private communication, 1973). The first model (Figure 1) is based on a deduced thermal property profile for the Apollo 15 site and is thought to be appropriate for mare regions of the moon. The second model has nighttime temperatures 10°K higher than those shown in Figure 1 and the same daytime temperatures except very near the terminator. This warmer model is based on thermal property data from the Apollo 17 site. In subsequent use, these models are referred to as being cold and warm, respectively. Owing to the fact that the only atmospheric mass spectrometer on the moon is that at the Apollo 17 site, the warm model is probably best suited for comparison of theory and experiment.

Computationally, the daytime temperature is presumed to be in radiative equilibrium with solar radiation except near the terminator. A subsolar point temperature of 384° has been used. On the nighttime side the temperature is found via interpolation of temperatures at specified points on meridians spaced 12° apart.

THEORETICAL MODEL

The usual approach to the theoretical study of exospheric lateral flow is to express the problem as the Fredholm equation

$$\Phi(\theta, \phi) = (\tfrac{1}{4}n\langle v\rangle)_{\theta,\phi} - \iint d\phi'\, d\theta' \sin\theta' n(\theta', \phi') K(\theta, \phi \mid \theta', \phi') \quad (1)$$

where Φ is the net vertical flux at the surface (i.e., the source strength), whereas the terms on the right-hand side are upgoing and downcoming flux, respectively. Concentration is denoted by n, and $\langle v\rangle$ is the mean particle speed. The kernel K is the response of the downcoming flux at (θ, ϕ) to a unit amplitude point source at (θ', ϕ'), where θ and ϕ are colatitude and longitude, respectively.

For lunar hydrogen and helium the boundary condition of this relation is that Φ equal the local escape flux plus the lateral flux needed to transport each particle from its point of origin (as a neutralized solar wind ion) to its last encounter with the lunar surface prior to escape. The high probability of thermal escape of these gases and the relatively long time of ballistic flight (>500 sec according to *Hodges* [1972]) tend to make the lateral flux an important part of Φ and hence to make direct solution of (1) quite difficult.

An alternative to the direct solution of (1) is to use a Monte Carlo model, in which the paths of a succession of individual particles are traced from creation to escape. This use amounts to considering the total content of the lunar

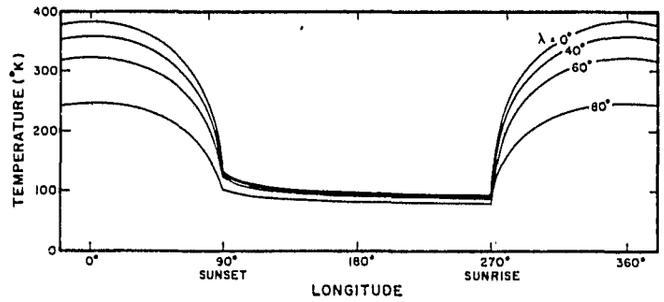

Fig. 1. Cold nighttime model of lunar surface temperature. Longitude is measured from the subsolar meridian, and λ denotes latitude. The warm model has a 10°K increase in temperature at night.

atmosphere to be one molecule. It is valid because there is no opportunity for particle collisions to be significant in the tenuous gas on the moon. The downcoming part of the vertical flux is proportional to the number of surface encounters of the particle in a unit area of the surface, and the concentration is proportional to that flux divided by $\langle v \rangle$. Absolute concentration is also proportional to the strength of the source of gas.

Figure 2 shows angular relationships used to describe the points of origin (subscript o) and impact (subscript i) of a particle trajectory. The horizontal extent of the trajectory is specified by δ, χ is the zenith angle of the initial velocity $\mathbf{v}$ of the particle, and ψ is the azimuth of the lateral projection of $\mathbf{v}$.

The process for solution of the problem is illustrated schematically in Figure 3. It begins with selection of a starting point on the daytime surface. The solar angle of this point of origin is denoted τ_o and is chosen from a random distribution of deviates of the function $\cos \tau$, which represents the distribution of the flux of solar wind ions on the lunar surface. In practice, this function is generated by

$$\tau_o = \cos^{-1}\left[\frac{1}{2}\left(1 - \frac{n}{N}\right)^{1/2} + \frac{1}{2}\left(1 - \frac{n-1}{N}\right)^{1/2}\right] \qquad (2)$$

where n is a uniform, integer deviate in the range 1–N. The azimuth μ_o is chosen at random in the range 0–2π. A coordinate transformation is then used to determine θ_o and ϕ_o.

A set of three Gaussian deviates is generated to determine the velocity from a Maxwellian distribution. The Gaussian deviates, denoted X_i, are found by using the relation given by *Zelen and Severo* [1965],

$$X_i = (-2 \ln p_i)^{1/2} \cos 2\pi q_i \qquad (3)$$

where p_i and q_i are uniform deviates between 0 and 1. The variance of each X_i is 1, and hence the identification can be made that

$$X_i = (m/kT_o)^{1/2}(v_i - \delta_{i1}\omega R_M \sin \theta_o) \qquad (4)$$

where m is particle mass, v_i is the ith component of the velocity vector $\mathbf{v}$, k is Boltzmann's constant, T_o is the temperature at the point of origin (θ_o, ϕ_o), δ_{i1} is the Kronecker delta function, ω is the synodic rate of angular rotation of the moon, and R_M is the lunar radius. The three X_i are combined to give particle speed and the angles of departure of the orbit, χ and ψ, which are defined in Figure 2.

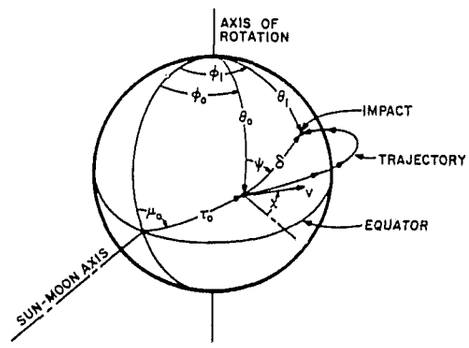

Fig. 2. Definitions of angles that specify points of origin and impact and the direction of departure of a particle from the surface of the moon.

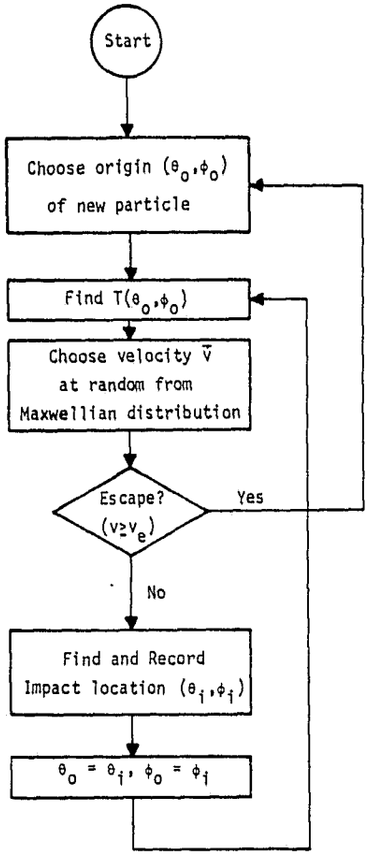

Fig. 3. Schematic diagram of the process used to trace numerically the flights and surface impacts of molecules in the lunar atmosphere.

A test is then made to determine if v is greater than the lunar surface escape velocity v_e. If so, the escape event is recorded, and a new particle is created. In effect, this preserves a detailed balance of the content of the single-particle atmosphere.

If the particle does not escape, the angular distance to its point of impact, δ, is found from elementary orbital mechanics via the relation

$$\cos \delta = 1 - \frac{8(v/v_e)^4 \sin^2 \chi \cos^2 \chi}{1 - 4(v/v_e)^2[1 - (v/v_e)^2] \sin^2 \chi} \quad (5)$$

This angle and the previously determined azimuth ψ are used to find the coordinates of impact:

$$\theta_i = \cos^{-1} \{\cos \theta_o \cos \delta + \sin \theta_o \sin \delta \cos \psi\} \quad (6)$$

$$\phi_i = \phi_o + \sin^{-1} \{\sin \delta \sin \psi / \sin \theta_i\} \quad (7)$$

The impact at θ_i, ϕ_i is then recorded by adding 1 to an accumulator corresponding to the appropriate zone of the lunar surface. Figure 4 shows how 75 accumulation zones are distributed over one hemisphere. Latitude and longitude intervals are chosen so that all zones have identical areas. Owing to the equatorial symmetry inherent in the formulation of the problem, an impact in the lower hemisphere is recorded at the conjugate point in the upper hemisphere.

Because of the assumption of no surface adsorption and that of thermal accommodation upon impact, a particle that strikes the surface is immediately identified as entering the lunar atmosphere at the point of impact. Thus θ_o and ϕ_o are replaced by the impact coordinates θ_i and ϕ_i, respectively, and the process of determining its next destination is begun.

The accuracy of the calculating technique can be assessed by examination of its solution to a simple problem: an isothermal nonrotating moon with uniformly distributed gas source. Obviously, this should lead to a uniform atmospheric distribution. In addition, the fraction of trajectories that are hyperbolic and lead to escape should be equal to the fraction of par-

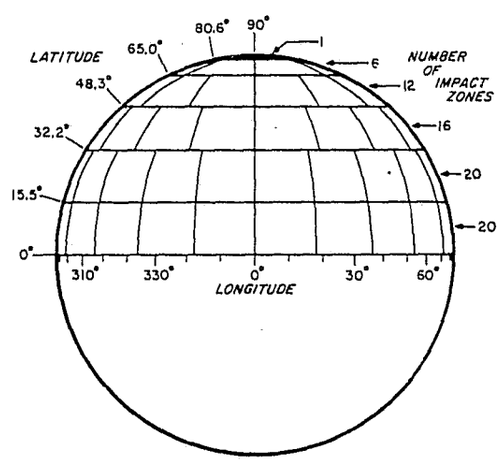

Fig. 4. Impact accumulation zone boundaries on the sunlit side of the moon. There are 75 equal area zones arranged in circumferential bands so as to cover the entire upper hemisphere.

ticles of a Maxwellian distribution with velocities greater than v_e. Integration of the Maxwellian distribution gives this fraction to be

$$\eta = \operatorname{erfc} E^{1/2} + 2(E/\pi)^{1/2}e^{-E} \qquad (8)$$

where

$$E = mv_e^2/2kT \qquad (9)$$

Table 1 summarizes data acquired from four such tests for values of T/m ranging from 25 to 200. Each test represents 10^6 trajectories. Escape results agree quite well with (8), confirming the random selection of Gaussian deviates. The variance of the number of impacts per accumulation zone decreases with increasing T/m, i.e., with increasing average trajectory length, which is about 2 scale heights [*Hodges*, 1972]. As a percentage of impacts, the variance increases slightly at the highest value of T/m, where escape has diminished the number of impacts considerably. It appears that 10^3 impacts per accumulation zone is adequate to insure good accuracy of calculations at $T/m = 100$ or 200, which correspond roughly to daytime He or H_2, respectively. At colder temperatures more impacts are necessary to achieve similar accuracy. Subsequent calculations represent 10^3 trajectories each, which is sufficient to provide of the order of 10^5 impacts per accumulation zone at night and more than 10^3 in daytime, assuring accuracies superior to the foregoing test results.

INTERPRETATION OF IMPACT DATA

The most-used phenomenological parameter of the lunar atmosphere, the gas concentration, defies rigorous determination. A measuring device detects a component of a flux; e.g., the Apollo 17 mass spectrometer responds to the downcoming part of the vertical flux, Φ_{down}. Since the downcoming part of the velocity distribution represents diverse conditions at surrounding points on the surface of the moon, it is non-Maxwellian. However, the only reasonable way to relate the measurement and concentration is via the Maxwellian relation

$$\Phi_{down} = n\langle v\rangle/4 \qquad (10)$$

In effect, (10) defines n in terms of the Maxwellian upward flux if newly produced particles are ignored.

Impact data from the Monte Carlo calculation represent a relative distribution of Φ_{down}. Conversion of these data to relative concentration can be done by dividing the impact counts by the square root of temperature. To make the results absolute, it is necessary to scale the relative concentration distribution so as to balance the rates of production and escape.

It is assumed that the source of new molecules is locally proportional to solar wind flux. Thus continuity at the surface is represented by

$$\Phi_{up} = \Phi_{down} + \Phi_{sw} \cos \tau \, u(\cos \tau) \qquad (11)$$

where Φ_{sw} is the solar wind flux of the ion species in question, τ is local solar zenith angle (cf. Figure 2), and u is the unit step function. The local rate of escape, which is part of the upward flux, is given by Jeans' formula

$$\Phi_{esc} = \Phi_{up}(1 + E)e^{-E} \qquad (12)$$

TABLE 1. Isothermal Test Results

	T/m = 25 or Nighttime He	T/m = 50 or Nighttime H_2	T/m = 100 or Daytime He Nighttime H	T/m = 200 or Daytime H_2
Scale height, km	128	256	511	1022
Escape trajectories				
Computation	0	334	7942	33,293
$\eta \times 10^5$ (equation 8)	0.5	350	7849	33,382
Impact accumulations				
Average $\langle D\rangle$	1,333.3	1328.9	1227.4	889.4
Variance σ	100.5	54.5	36.4	33.0
$\sigma/\langle D\rangle$	0.075	0.041	0.029	0.037

In this table, the value for the temperature T is given in degrees Kelvin, and the mass m is given in atomic mass units.

Integration of Φ_{esc} over the entire planet gives the total rate of escape, which must equal the total solar wind influx $\pi R_M^2 \Phi_{sw}$. By equating global escape and inflow rates and performing some algebraic manipulation involving use of (10) and (11), the absolute concentration is found to be

$$n = \frac{4D\Phi_{sw}}{\langle v \rangle} \cdot \left[\frac{1 - (1/\pi) \int d\Omega \cos\tau \, u(\cos\tau)(1+E)e^{-E}}{(1/\pi) \int d\Omega \, D(1+E)e^{-E}} \right] \tag{13}$$

where D is the relative distribution of Φ_{down}. Impact data are used for D in subsequent calculations.

The average residence time of atmospheric molecules is the ratio of total atmospheric content to the solar wind influx. Using the barometric law to approximate the vertical distribution leads to

$$\tau \cong (1/\pi\Phi_{sw}) \int d\Omega n H \tag{14}$$

where H is the scale height. This approximation is probably better for helium than hydrogen because of the large scale height of hydrogen.

HELIUM

Preliminary data from the Apollo 17 lunar surface mass spectrometer show helium to be an atmospheric constituent. Its nighttime concentration has a maximum of about 4×10^4 cm^{-3}, whereas the small amount of available daytime data suggests a night to day ratio of at least 20 [*Hoffman et al.*, 1973*a*, *b*]. *Johnson et al.* [1972] have made a rough estimate that the daytime helium concentration should be about 3×10^3 if it is in balance with the solar wind influx of He^+ ions. The large measured night to day ratio is in qualitative agreement with the theory of *Hodges and Johnson* [1968].

Johnson et al. [1972] have reviewed the solar wind data on helium and concluded that the average solar wind flux of He^+ is about 0.045 that of protons, or about 1.3×10^7 cm^{-2} sec^{-1}. This value is adopted here, but the results, which assume a balance of solar wind influx and thermal escape, may be scaled linearly to accommodate any other assumed influx rate.

Figure 5 shows computed longitudinal distributions of helium concentration at latitudes corresponding to area centers of the circumferential sets of impact accumulation zones. Solid lines are for the cold nighttime temperature model, and dashed lines represent the warm model. The amount of helium on the dayside is about the same for either model, reflecting the fact that both production and escape are confined to the daytime hemisphere. At night the helium concentration for the cold model is about 20% greater than that for the warmer case, even though the temperature difference is only 10°K. This finding is in agreement with the $T^{-5/2}$ law of exospheric equilibrium [*Hodges and Johnson*, 1968]. The asymmetry of the distributions about the antisolar direction (180° longitude) is due to decreasing temperature through the night, and the bias of the distribution toward sunrise is again in agreement with the

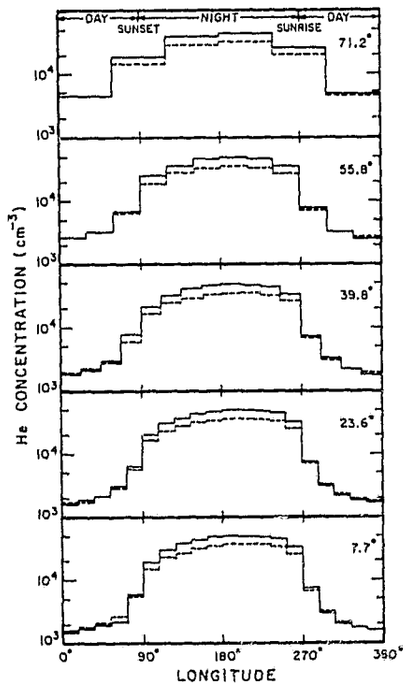

Fig. 5. Calculated longitudinal distributions of helium at latitudes corresponding to the circumferential bands of impact accumulation zones. Dashed lines represent warm temperature model results, and solid lines cold model results.

$T^{-5/2}$ law. Rotation of the moon also causes an eastward shift of the distribution, but not as great a shift as that due to temperature effects.

The ratio of nighttime maximum to daytime minimum near the equator is 32 for the cold nighttime temperature model and 24 for the warm model. Analogous night to day ratios from the 23.6° latitude data, which correspond approximately to the Apollo 17 mass spectrometer location (20°N), are 30 and 21, respectively. Because the warm nighttime temperature model is based on thermal property measurements at the Apollo 17 site, it is probably best to compare the mass spectrometer results with the warm temperature model atmosphere calculations. Figure 6 shows a composite of theoretical and experimental results, the latter having been presented by *Hoffman et al.* [1973*b*]. The daytime concentration is so low ($\sim 2 \times 10^3$ cm^{-3}) that the statistical uncertainty of the data is great enough to encompass the theoretical result. Owing to the fact that the daytime concentration is related to the source strength and is relatively insensitive to temperature model, it is unlikely that the actual midday concentration could greatly exceed the theoretical value of 1.6×10^3 cm^{-3}. What is important is the close agreement of the nighttime results, which supports the hypothesis that the source distribution of helium is closely related to the solar wind influx.

HYDROGEN

Prior to Apollo 17 it was generally thought that the proton flux of the solar wind ($\sim 3 \times 10^8$ cm^{-2} sec^{-1}) would produce an atomic hydrogen component in the lunar atmosphere. However, the orbital UV spectrometer on Apollo 17 detected no hydrogen [*Fastie et al.*, 1973]. The experiment does permit the setting of upper bounds on daytime concentrations of hydrogen, which are reported by W. G. Fastie (private communication, 1973) to be less than 10 cm^{-3} for H and 6×10^3 cm^{-3} for H_2.

Monte Carlo calculation of an atomic hydrogen lunar atmosphere resulted in a daytime concentration minimum of about 600 atoms cm^{-3} and a nighttime level of roughly 2×10^3 cm^{-3}. The great discrepancy between theory and experiment suggests that the impinging solar wind protons form molecular compounds on the lunar surface, which enter the atmosphere and subsequently escape. A nonthermal loss mechanism for hydrogen may also exist, but its nature must be such that it does not influence the loss of helium, which appears to be explainable by thermal escape alone.

Owing to the dominance of protons in the

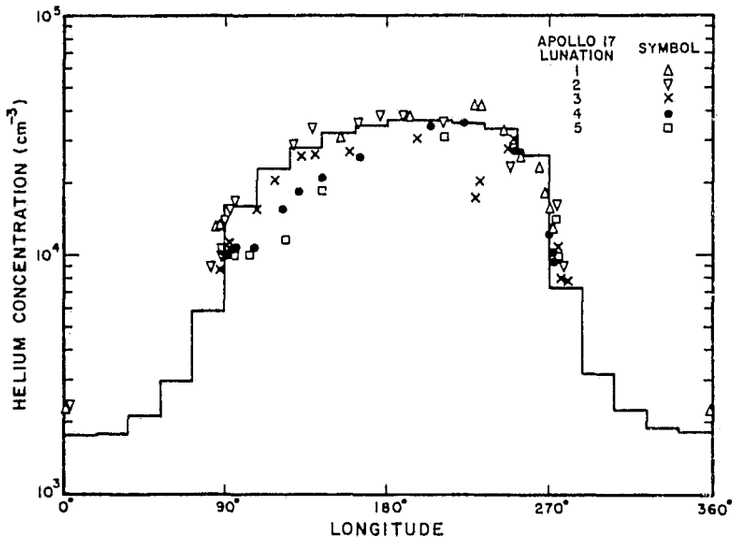

Fig. 6. Helium data from the Apollo 17 lunar surface mass spectrometer at 20°N [*Hoffman et al.*, 1973*b*] superimposed on the warm temperature model calculation for 23.6° latitude.

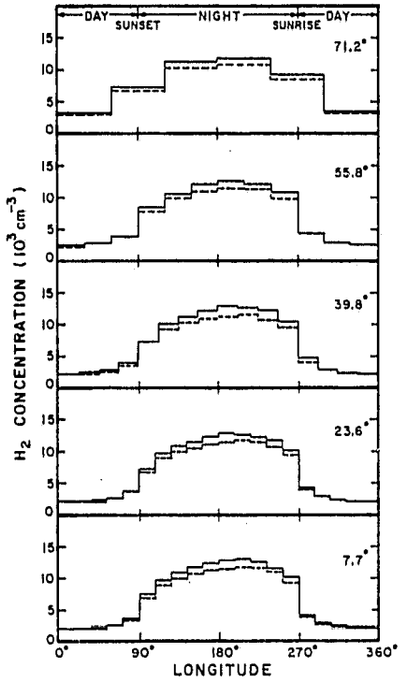

Fig. 7. Calculated longitudinal distribution of H_2 at latitudes corresponding to the circumferential bands of impact accumulation zones. Dashed lines represent warm temperature model results, and solid lines cold model results.

solar wind, the most likely hydrogen compound to be formed on the lunar surface is H_2. Figure 7 shows calculated longitudinal profiles of the H_2 concentration that account for all of the proton influx. The daytime concentration of about 2×10^3 cm^{-3} is less than the bound set by the Apollo 17 UV spectrometer data, and the nighttime maximum of about 1.3×10^4 cm^{-3} is less than the upper bound of 6.5×10^4 cm^{-3} from Apollo 17 mass spectrometer data reported by *Hoffman et al.* [1973*b*].

DISCUSSION

A summary of lunar atmosphere parameters resulting from the Monte Carlo calculations is presented in Table 2. Substantially greater nighttime reservoirs of both hydrogen and helium are predicted for the cold temperature model than for the warm model, reflecting a decrease in mobility with decreasing temperature. The tendency of particles to stay longer on the night side for the cold model is also shown in the longer residence times for the cold model.

Because the warm temperature model probably represents the region of the moon near the Apollo 17 site, it is tempting to draw conclusions based on the close fit of Apollo 17 mass spectrometer measurements of helium to the warm model distribution shown in Figure 6. The near agreement suggests that the source of helium is in balance with the solar wind influx and hence that nonthermal escape of part of the solar wind helium influx is negligible. If this interpretation is valid, then it constrains the possibilities for nonthermal escape of hydrogen and other solar wind related gases (e.g., neon, argon, nitrogen, and carbon compounds).

An alternative to the confining of the assumed source of helium to the sunlit part of the moon is to propose that some of the implanted helium is released at night. A test calculation was made of the distribution of helium that would result from a source that was independent of longi-

TABLE 2*a*. Summary of Hydrogen and Helium Distributions for Cold and Warm Models

	H_2		He	
	Cold Model	Warm Model	Cold Model	Warm Model
Residence time, sec	6.6×10^3	6.5×10^3	9.3×10^4	7.9×10^4
Concentration, cm^{-3}				
$\lambda = 7.7°$				
Day minimum	2.1×10^3	2.0×10^3	1.6×10^3	1.6×10^3
Night maximum	1.3×10^4	1.2×10^4	5.1×10^4	3.8×10^4
$\lambda = 23.6°$				
Day minimum	2.2×10^3	2.1×10^3	1.7×10^3	1.7×10^3
Night maximum	1.3×10^4	1.2×10^4	5.1×10^4	3.7×10^4

The solar wind flux of protons is 3×10^8 cm^{-2} sec^{-1}, and the solar wind He flux is 1.3×10^7 cm^{-2} sec^{-1}.

TABLE 2b. Summary of Hydrogen and Helium Distributions from Experimental Data

	H_2	He
Experimental data		
Day minimum	$<6 \times 10^3$ (UV)	$\sim 2 \times 10^3$ (MS)
Night maximum	$<6.5 \times 10^4$ (MS)	$\sim 4 \times 10^4$ (MS)

The UV denotes Apollo 17 orbital UV spectrometer (W. G. Fastie, private communication, 1973), and the MS denotes Apollo 17 mass spectrometer (20°N) [*Hoffman et al.*, 1973*b*].

tude. The result was about a factor of 2 increase in the reservoir of helium on the nightside obviously due to the creation of half of the new particles in nighttime, where lateral mobility is low and escape is unlikely. Any other source model that relies on release of a substantial amount of helium from the night surface would produce a similar increase in the night to day helium ratio, which is contradictory to the Apollo 17 mass spectrometer data.

Other plausible models of the neutral helium source include daytime release correlated with surface temperature or with the solar radiation flux. Then release could be characterized by a surface residence time. If this time were sufficiently long, production of neutral helium should proceed normally while the solar wind is interrupted as the moon passes through the geomagnetic tail. In this case the ion influx must be modified by the fraction of time that the moon actually spends in the solar wind, i.e., by about 25/29. The contribution of magnetotail plasma may also be important. These effects could change the absolute concentrations presented in this paper but would not alter the relative global distributions significantly.

Balance of atmospheric helium with the solar wind influx is not a strict necessity in view of the production of alpha particles throughout the moon by radioactive decay of uranium and thorium. However, this source of atmosphere has been neglected because the total amount of helium produced since formation of the moon can only exceed present uranium and thorium levels by about an order of magnitude and thus cannot approach a degree of saturation that would cause diffusion of newly formed helium atoms out of rocks.

The primary source of atmospheric hydrogen must also be the solar wind. If hydrogen escapes thermally from the moon, it must do so as H_2. Heavier hydrogen compounds, such as CH_4 or NH_3, probably escape, owing to photoionization and subsequent interaction with solar wind fields. However, the available amounts of C and N can only accommodate a small fraction of the proton influx. Nonthermal escape of hydrogen may be a possible alternative, but the mechanism must be peculiar to hydrogen and ineffective for helium as well as neon and ^{36}Ar, which also appear to be in near balance with the solar wind [*Hodges et al.*, 1973]. Thus atmospheric H_2 seems to be necessary to balance the loss of hydrogen with the influx of protons.

Acknowledgments. It is a pleasure to acknowledge the assistance of H. D. Hammack, in programing the numerical computations.

This research was supported by NASA contract NAS9-12074.

* * *

The Editor thanks P. M. Banks and R. H. Manka for their assistance in evaluating this paper.

REFERENCES

Bernstein, W., R. W. Fredricks, J. L. Vogl, and W. A. Fowler, The lunar atmosphere and the solar wind, *Icarus, 2,* 233, 1963.

Fastie, W. G., P. D. Feldman, R. C. Henry, V. W. Moos, C. A. Barth, C. Lillie, G. E. Thomas, and T. M. Donahue, The Apollo 17 orbital ultraviolet spectrometer experiment, in *Lunar Science IV,* edited by J. W. Chamberlain and C. Watkins, p. 233, Lunar Science Institute, Houston, Tex., 1973.

Hinton, F. L., and D. R. Taeusch, Variation of the lunar atmosphere with the strength of the solar wind, *J. Geophys. Res., 69,* 1341, 1964.

Hodges, R. R., Applicability of a diffusion model to lateral transport in the terrestrial and lunar exospheres, *Planet. Space Sci., 20,* 103, 1972.

Hodges, R. R., and F. S. Johnson, Lateral transport in planetary exosphere, *J. Geophys. Res., 73,* 7307, 1968.

Hodges, R. R., J. H. Hoffman, F. S. Johnson, and D. E. Evans, Composition and dynamics of lunar atmosphere, *Geochim. Cosmochim. Acta,* in press, 1973.

Hoffman, J. H., R. R. Hodges, and D. E. Evans, Lunar atmospheric composition results from Apollo 17, *Geochim. Cosmochim. Acta*, in press, 1973*a*.

Hoffman, J. H., R. R. Hodges, F. S. Johnson, and D. E. Evans, Composition and physics of the lunar atmosphere, paper presented at 16th Plenary Meeting, Cospar, Konstanz, West Germany, 1973*b*.

Johnson, F. S., Lunar atmosphere, *Rev. Geophys. Space Phys.*, *9*, 813, 1971.

Johnson, F. S., J. M. Carroll, and D. E. Evans, Lunar atmosphere measurements, *Geochim. Cosmochim. Acta*, *3*, suppl. 3, 2231, 1972.

Siscoe, G. L., and N. R. Mukherjee, Upper limits on the lunar atmosphere determined from solar wind measurements, *J. Geophys. Res.*, *77*, 6042, 1972.

Zelen, M., and N. C. Severo, Probability functions, in *Handbook of Mathematical Functions*, edited by M. Abramowitz and I. A. Stegun, Dover, New York, 1965.

(Received March 19, 1973;
accepted September 5, 1973.)

ICARUS 21, 415–426 (1974)

The Lunar Atmosphere

R. R. HODGES, Jr., J. H. HOFFMAN, AND
FRANCIS S. JOHNSON

The University of Texas at Dallas, Dallas, Texas 75230

Received October 24, 1973; revised December, 11 1973

In contrast to earth, the atmosphere of the moon is exceedingly tenuous and appears to consist mainly of noble gases. The solar wind impinges on the lunar surface, supplying detectable amounts of helium, neon and ^{36}Ar. Influxes of solar wind protons and carbon and nitrogen ions are significant, but atmospheric gases containing these elements have not been positively identified. Radiogenic ^{40}Ar and ^{222}Rn produced within the moon have been detected. The present rate of effusion of argon from the moon accounts for about 0.4% of the total production of ^{40}Ar due to decay of ^{40}K if the average abundance of potassium in the moon is 1000 ppm. Lack of weathering processes in the regolith suggests that most of the atmospheric ^{40}Ar originates deep in the lunar interior, perhaps in a partially molten core. If so, other gases may be vented along with the argon.

The atmosphere of the moon is so tenuous that it can be regarded as a collisionless exosphere in which atoms and molecules are gravitationally bound in ballistic trajectories between encounters with the lunar surface. Despite the small amount of gas, the vestige of atmosphere is an important indicator of lunar processes which produce atmospheric gases. Direct measurements of lunar gases by means of the Apollo cold cathode gage and mass spectrometer experiments, along with ancillary data from alpha particle and ultraviolet spectrometers and analyses of returned lunar samples, provide a basis for study of the relationship between the moon and its atmosphere.

Lack of a significant amount of lunar atmosphere can be attributed mainly to an efficient escape mechanism for particles that are too heavy to escape thermally. Neutral gas molecules or atoms are photoionized by solar radiation and then, in the absence of significant magnetization of the moon, the $\mathbf{v} \times \mathbf{B}$ field of the impinging solar wind accelerates the resultant ions. Roughly half of these ions impact the lunar surface, but the other half escape. The geomagnetic field inhibits this escape process over the earth, while induced ionospheric currents apparently cause a deflection of the solar wind around both Mars and Venus, thus causing ions produced below the deflection boundary to remain in the planetary atmosphere.

The present tenuous state of the lunar atmosphere is not inherent to the size, mass or orbit of the moon. Given a rate of volcanic release of gases in excess of the photoionization loss rate, a dense atmosphere would form. To understand this possibility, it is useful to consider the physics of a hypothetical dense atmosphere on the moon, of sufficient depth to form an ionosphere that is not in contact with the lunar surface. Gases which cannot escape thermally (i.e., gases other than hydrogen and helium) would presumably make up the bulk of this atmosphere. The photoescape rate would be limited to photoions formed above the level where ionospheric currents produce an ionosphere–solar wind boundary. This escape rate is also a lower bound on the rate of degassing of the moon needed to form a dense atmosphere, since surface chemical processes could also act as a sink. The relationship of the surface loss processes to the excess gas release rate

Copyright © 1974 by Academic Press, Inc.
All rights of reproduction in any form reserved.
Printed in Great Britain

would determine the surface concentration and hence the height of the region where the solar wind deflection occurs.

An approximation to the maximum rate of loss of lunar atmosphere is found by integration of the rate of photoionization over the sunlit side of the moon. The resulting mass outflow of a specific gas is $2\pi R^2 nm\, H/\tau$ where R is the radius of the ionosphere–solar wind boundary, n is concentration at that level, m is molecular mass, H is daytime scale height, and τ is photoionization time. Since the product mH is independent of molecular mass, the total loss rate is also given by the above expression if n is total neutral concentration and τ is an average photoionization time. Assuming that the solar wind is deflected near the base of the exosphere of the hypothetical atmosphere in question, the concentration n should be about $10^8\,\mathrm{cm}^{-3}$. Making the further assumptions of an average exobase temperature of 1000°K and a photoionization time of 10^7 sec, the net mass loss rate would be 1.7×10^3 g/sec, or a global average loss rate per unit area of roughly $4 \times 10^{-15}\,\mathrm{g\,cm^{-2}\,sec^{-1}}$. For purposes of comparison, the volcanic release rate, if at the same rate per unit planetary mass as for the earth, would be about $3 \times 10^{-12}\,\mathrm{g\,cm^{-2}\,sec^{-1}}$ of H_2O and $5 \times 10^{-13}\,\mathrm{g\,cm^{-2}\,sec^{-1}}$ of CO_2 (Johnson, 1969; 1971). Thus the absence of a lunar atmosphere is evidence that volcanic activity on the moon is at least several orders of magnitude less intense per unit mass than on earth.

The above argument does not rule out presently active lunar volcanism, but it does set a limit on the degassing rate over geologic time scales. However, based on Apollo 14 and 15 cold cathode gage data (Johnson *et al.*, 1972) a present upper bound of about $10^{-16}\,\mathrm{g\,cm^{-2}\,sec^{-1}}$ has been established by Hodges *et al.* (1972a). Since the cold cathode gage data obtained during lunar daytime may be mainly due to artifact gases released from remnant spaceflight hardware, it is entirely possible that this upper bound greatly over-estimates the actual degassing rate of the moon. Subsequent discussion of spectrometric data will show that some gases are presently evolving from the moon, and hence that a lower bound can be placed on the release rate.

In addition to the release of lunar gases, the impinging solar wind is an important and predictable source of atmosphere. Solar wind ions impact the moon with energies the order of 1 keV per amu and become imbedded in surface rocks. The soil is probably saturated with most solar wind gases, and a balance of ion inflow and neutral effusion from the lunar surface probably exists. This hypothesis is verified by the close balance between the solar wind influx and the lunar atmospheric content of helium, ^{20}Ne, and ^{36}Ar which will be discussed later.

Owing to the small amount of ambient gas on the moon, species identification is greatly complicated by contaminants of spacecraft origin. A distinguishing feature of a native gas is the diurnal tidal oscillation of its concentration, a collective effect that reflects statistics of encounters of particles with the moon but not with each other.

Atmospheric atoms and molecules travel in ballistic trajectories between encounters with the lunar surface. Neglecting adsorption or chemical reaction at the surface, global transport of gases is similar to a two-dimensional random walk process, the mean step size being approximately equal to two scale heights, and therefore proportional to temperature. Fig. 1 shows a portion of the path of a hypothetical atom

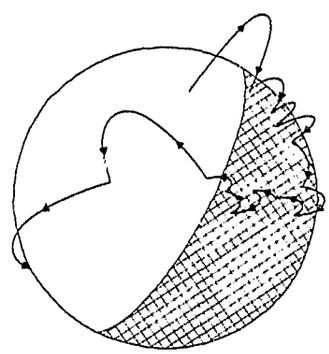

FIG. 1. Path of a hypothetical atom of the lunar atmosphere.

REPRODUCIBILITY OF THE ORIGINAL PAGE IS POOR

on the moon. Trajectories are generally longer over the warm sunlit side, resulting in the tendency for migration of particles to the colder nighttime side to be greater than that from night to day. Equilibrium of lateral transport requires that the distribution of a gas vary in concentration roughly as the $-5/2$ power of temperature (Hodges and Johnson, 1968; see also recent extensions of the theory by Hodges, 1972 and 1973a). Since the day-to-night temperature ratio is about 4 : 1, the expected nighttime gas concentration is approximately 32 times that in daytime.

Gases which are adsorbed on the nighttime side of the moon have both nighttime and daytime minima, the former being due to surface adsorption, and the latter, to the tendency of gases to avoid a temperature maximum. This leaves a meridional maximum at the terminator. Near sunrise, where the adsorbed gases are released as the surface warms, the maximum concentration is significantly greater than that at sunset.

Atmospheric Constituents

A summary of present knowledge of lunar atmospheric parameters is given in Table I. Theoretical values for hydrogen and helium are based on calculations by Hodges (1973b), which are in close agreement with independent calculations of Hartle and Thomas (1973). Daytime concentrations of hydrogen and helium may be expressed in two ways—in terms of downcoming bound particles which have completed at least one ballistic trajectory or as the total of bound and newly created upgoing molecules in initial trajectories. Hodges has related the bound particle definition of concentration to the downcoming molecular flux measured by the Apollo 17 lunar surface mass spectrometer, while Hartle and Thomas were concerned with the total concentration which is appropriate to analyses of optical data from the Apollo 17 orbital ultraviolet spectrometer. Owing to long residence

TABLE I

Summary of Lunar Atmosphere Parameters

	H	H_2	^4He	^{20}Ne	^{36}Ar	^{40}Ar
Solar wind influx (ions/sec)	2.8×10^{25}		1.3×10^{24}	2.2×10^{21}	8.0×10^{19}	—
Lunar venting (atoms/sec)	—	—	—	—	—	8.7×10^{20}
Photoionization time (sec)	10^7	10^7	10^7	6×10^6	1.6×10^6	1.6×10^6
Residence time (sec)[a]	1.2×10^3	7×10^3	8×10^4	4×10^7	10^7	10^7
Concentration (cm^{-3}):						
Theory day bound	6×10^2[c]	2×10^3	1.7×10^3			
Theory day total	2.7×10^3[c]	3.5×10^3	1.9×10^3	4×10^3	1.3×10^2	1.6×10^3
Theory night	1.6×10^3[c]	1.2×10^4	4×10^4	1.1×10^5	3×10^3[d]	4×10^4[d]
Experiment[b] day	$<10^1 cm^{-3}$	$<6 \times 10^3$	2×10^3	—	—	—
Experiment[b] night	—	$<3.5 \times 10^4$	4×10^4	10^5	3×10^3[d]	4×10^4[d]

[a] Hydrogen and helium escape thermally, while photoionization controls lifetimes of the other gases.

[b] Daytime upper bounds on H and H_2 are Apollo 17 orbital ultraviolet spectrometer results (Fastie *et al.*, 1973) while the remaining data are from Apollo mass spectrometer experiments.

[c] Amounts that would be present if released in atomic rather than molecular form.

[d] Sunrise terminator maxima are given for argon. Surface adsorption removes most of the nighttime argon.

times for neon and argon, differences between their respective bound and total concentrations are negligible.

Amounts of helium, ^{20}Ne and ^{36}Ar, which are known from Apollo 16 (Hodges *et al.*, 1973), and Apollo 17 mass spectrometer data (Hoffman *et al.*, 1973), are in balance with the solar wind influxes of these species. The lack of a large accumulation of hydrogen in the lunar soil suggests that the solar wind influx of protons is similarly converted to a neutral gas, presumably H_2, to equalize rates of accretion and escape. By analogy, it is reasonable to expect that the carbon and nitrogen influxes from the solar wind are also balanced by atmospheric escape, probably as methane and ammonia, respectively.

The presence of excess amounts of ^{40}Ar trapped in returned lunar samples has been recognized as evidence of ^{40}Ar as an atmospheric gas (Manka and Michel, 1971). More recently, ^{40}Ar has been identified in the lunar atmosphere by the Apollo 17 mass spectrometer (Hodges *et al.*, 1973; Hoffman *et al.*, 1973). Since the only known source of ^{40}Ar is radiogenic decay of ^{40}K within the moon, its presence in the atmosphere is evidence of a venting or degassing process which may involve other gases. The α-particle experiments on Apollo 15 and Apollo 16 have shown evidence of atmospheric ^{222}Rn and its long lived daughter ^{210}Po (Bjorkholm *et al.*, 1973; Gorenstein *et al.*, 1973). One interpretation of an imbalance of radon and polonium in the α-particle data is that sporadic venting of other gases may cause spatial and temporal fluctuations in the rate of effusion of radon. Whether venting rates of ^{40}Ar and ^{222}Rn are related is speculative at this time.

Subsequent sections on hydrogen, helium, neon and argon delineate the origins and geophysical implications of the data summarized in Table I. Additional discussion is presented on other candidate gases of the lunar atmosphere which have not been detected. Reasons to expect other gases include the large, mainly artifact, daytime gas levels detected by the Apollo 14 and Apollo 15 cold cathode gages and by the Apollo 17 mass spectrometer, which could hide some ambient, condensible constituents.

Hydrogen

Existence of atomic or molecular hydrogen in the lunar atmosphere seems necessary to balance the escape of hydrogen with the large solar wind influx of protons ($\sim 3 \times 10^8\,cm^{-2}\,sec^{-1}$) which impinges on the daytime side of the moon. Johnson *et al.* (1972), made a rough estimate that the surface concentration of H should be $5 \times 10^3\,cm^{-3}$ if hydrogen remained in atomic form. A more detailed calculation by Hodges (1973b) gave a nighttime maximum concentration of $1.6 \times 10^3\,cm^{-3}$ and a daytime minimum of $6 \times 10^2\,cm^{-3}$. An independent calculation by Hartle and Thomas (1973) is in close agreement if account is taken of the subtle difference in the definition of concentration adopted in the former study and that used by Hodges. However, the Apollo 17 orbital ultraviolet spectrometer showed that the daytime concentration of H is less than 10 atoms cm^{-3} (Fastie *et al.*, 1973), suggesting that the bulk of the solar wind hydrogen influx must reappear in molecular form.

Figure 2 shows the global distribution of bound H_2 from the Monte Carlo calculations of Hodges (1973b). The results are displayed as the average concentration in each of 75 equi-area zones covering one hemisphere of the moon. These zones are arranged in circumferential bands which are centered at the latitudes indicated on the graphs. The global temperature model used in these calculations was developed by M. G. Langseth and S. J. Keihm (private communication). Line widths in Fig. 2 give the range of concentrations resulting from a $\pm 5°K$ uncertainty in the nighttime temperature model. The amount of atmospheric H_2 was established by balancing the total rate of thermal escape of hydrogen with the rate of impact of solar wind protons on the moon. New molecules were assumed to evolve only from the daytime lunar surface, with the outflow rate of H_2 molecules equal to the local solar wind influx of proton pairs. In Fig. 2 the daytime minimum concentration

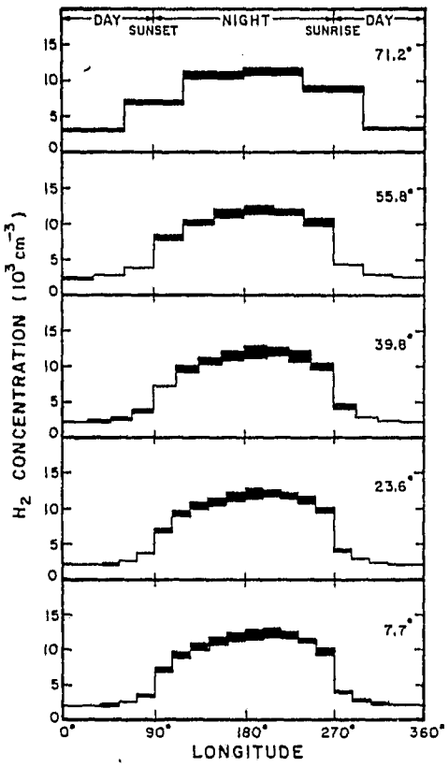

FIG. 2. Computed global distribution of H_2 on the moon (from Hodges, 1973b). Latitudes of the graphs correspond to geographic centers of data accumulation zones used in the calculation. The line widths show the range of values resulting from a $\pm 5°K$ uncertainty in the nighttime temperature model.

is about 2×10^3 cm^{-3}, while at night a level of 1.2×10^4 cm^{-3} is reached. These results in Fig. 2 agree fairly well with those of Hartle and Thomas (1973) if differences in definitions of concentration are taken into account. Near the subsolar point the solar wind contribution of new molecules amounts to an equivalent concentration of 1.5×10^3 cm^{-3}, making the theoretical total amount of H_2 somewhat less than the uv upper limit of 6×10^3 cm^{-3} established by Feldman and Fastie (1973). At night the lowest concentration of H_2 yet recorded by the Apollo 17 mass spectrometer is 3.5×10^4 cm^{-3}, or about three times the theoretical level. Temptation to accept this measurement as a true atmospheric level, rather than as an upper bound possibly influenced by contamination, must be tempered by the subsequent discussion of the distribution of lunar helium, which is quite accurately predicted by the theory.

If H_2 does exist on the moon, the average molecular residence time against thermal escape is only about 7×10^3 sec. This is short enough that the response of atmospheric H_2 to sudden changes in the solar wind should reveal the surface reaction time for formation and release of H_2. Hence, it is important that continued attempts be made to obtain realistic *in situ* measurements of molecular hydrogen.

HELIUM

The Apollo 17 mass spectrometer data clearly show helium to be an ambient lunar atmosphere gas (Hoffman *et al.*, 1973). Figure 3 shows preliminary mass spectrometer data superimposed on a theoretical graph of the diurnal variation of helium appropriate to the Apollo 17 landing site (from Hodges, 1973b). The small amount of daytime data is due to limited usage of the instrument during daytime, when artifact gas levels are quite high and extended operation could have resulted in irreversible contamination of the ion source electrodes. Owing to the low ambient level of He in daytime, it is probable that the daytime data points may include a significant artificial bias due to contamination. The important facet of Fig. 3 is the close agreement of experiment and theory over the night hemisphere, where the bulk of the gas is found. This is strong support for the hypothesis that the total solar wind influx of helium—assumed to be 0.045 times the proton flux in accordance with Johnson *et al.* (1972)—is balanced by thermal escape.

Figure 4 shows the theoretical global distribution of bound helium calculated by Hodges (1973b). Average residence time for this model is about one day. The pattern is almost an ideal example of exospheric equilibrium. The nighttime asymmetry about the antisolar meridian is

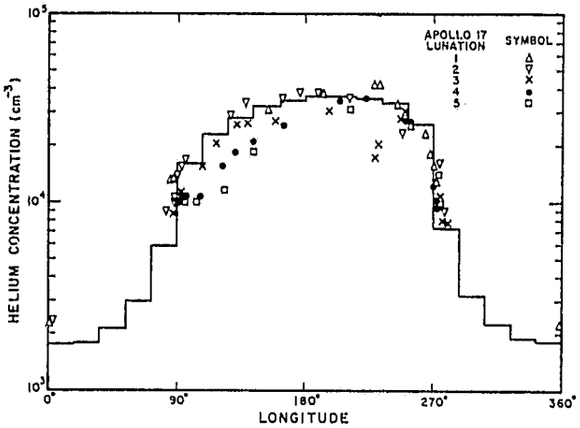

FIG. 3. Preliminary data from the Apollo 17 mass spectrometer superimposed on a calculated diurnal variation of helium (from Hodges, 1973b).

related to a continual decrease in surface temperature through the night.

NEON

Calculations by Hinton and Taeusch (1964), Johnson (1971), Johnson *et al.* (1972), and Hodges *et al.* (1973) have shown ^{20}Ne to be the most probable dominant gas of solar wind origin on the moon, although successive refinements of theory have resulted in a significant decrease in the expected amount. At present there is a fairly good agreement between theory and experimental results.

Figure 5 is a superposition of a theoretical global model distribution of ^{20}Ne and the existing experimental results. The paucity of data points reflects the difficulties that have plagued attempts to measure neon. Data shown on the 7.7° latitude graph are surface values extrapolated from the Apollo 16 orbital mass spectrometer measurements at latitudes between 7° and 10° (Hodges *et al.*, 1972b; 1973). These points are the only data in which the spectral peak at mass 20 amu was not overwhelmed by $H_2{}^{18}O$ arising from a spacecraft source of water. Scatter of the points is well within the large statistical uncertainties of the data that result from subtraction of about a 90% water contribution from the mass 20 amu measurements.

Available measurements from the Apollo

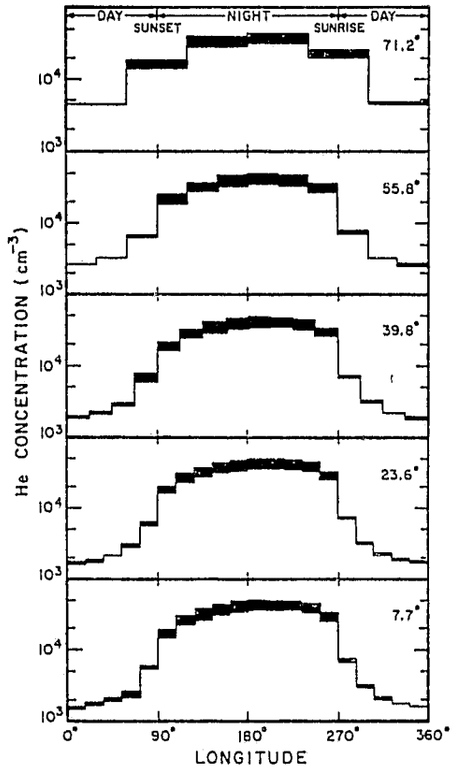

FIG. 4. Computed global distribution of helium on the moon (from Hodges, 1973b). Latitudes of the graphs correspond to geographic centers of data accumulation zones used in the calculation. The line widths show the range of values resulting from a ±5°K uncertainty in the nighttime temperature model.

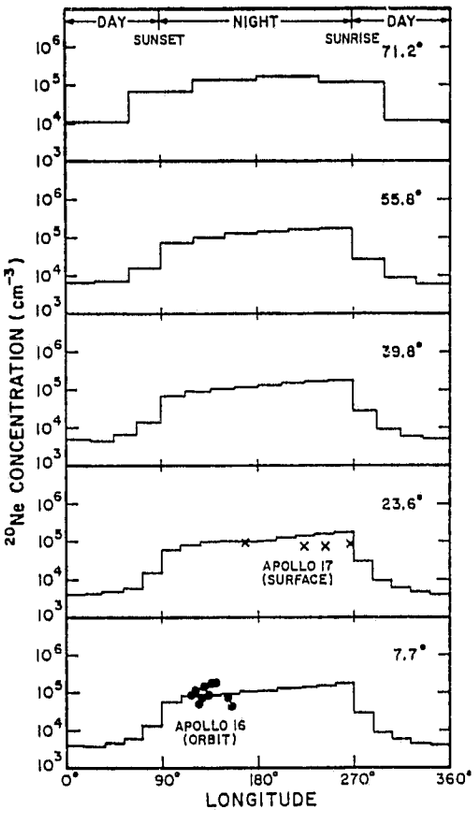

FIG. 5. Computed global distribution of ^{20}Ne on the moon based on a solar wind flux of $2.4 \times 10^4 \text{cm}^{-2}\text{sec}^{-1}$ and a photoionization lifetime of 6×10^6sec. Latitudes of the graphs correspond to geographic centers of data accumulation zones used in the calculation. Experimental results from the Apollo 16 orbital mass spectrometer and the Apollo 17 lunar surface mass spectrometer are superimposed on the calculated graphs at appropriate latitudes.

17 mass spectrometer at 20°N (Hoffman *et al.*, 1973) are shown on the computed graph for 23.6° latitude. Each point was obtained by a complex process in which the instrument was turned off and allowed to cool sufficiently to condense a significant mass 20 amu contaminant, ^{19}F, which is produced in the ion source, probably from decomposition of vestiges of contaminant halogen and hydrogen compounds ingrained in materials from which the source was constructed. These measurements also provide an isotopic abundance ratio of ^{20}Ne to ^{22}Ne of about 14, which is in reasonable agreement with the solar wind ratio of 13.7 measured by Geiss *et al.* (1972).

The theoretical model results from application of the Monte Carlo technique of Hodges (1973b). It employs the assumption of no surface adsorption and complete conversion of the solar wind influx of neon ions to neutral, atmospheric atoms. A solar wind flux of $2.4 \times 10^4 \text{cm}^{-2}\text{sec}^{-1}$ was adopted on the basis of the measurements by Geiss *et al.* (1972) which show the ratio of ^{4}He to ^{20}Ne in the solar wind to be about 570. This flux has been corrected for the fraction of time the moon spends in the geomagnetic tail, and hence not in the solar wind, about 4 days per lunation. It has also been assumed that the dominant loss mechanism for atmospheric neon is photoionization with a lifetime of 6×10^6 sec, as suggested by Manka (1972). These photoions are accelerated by the $\mathbf{v} \times \mathbf{B}$ field of the solar wind so that about half escape while the other half impact the moon and are subsequently recycled into the atmosphere.

Close agreement of theory and experiment suggests that the assumptions of the model are essentially correct. The failure of the Apollo 17 data to rise late in the night may be interpreted as an indication of a very slight amount of surface adsorption. Comparison with subsequent argon calculations indicates that the fraction of surface encounters which result in adsorption is probably the order of 10^{-4}.

ARGON

The dominant isotope of argon in the lunar atmosphere is ^{40}Ar, which is radiogenic and produced within the moon from ^{40}K. In addition, ^{36}Ar of solar wind origin is present at a level of about 10%. One of the interesting features of argon is that it is adsorbed by the lunar surface at night and released just after sunrise. Its residence time as an atmospheric atom includes long periods on the nighttime surface, and hence, technically not in the atmosphere.

Figure 6 gives a global atmospheric model for ^{40}Ar that was computed by use of a modification of the Monte Carlo

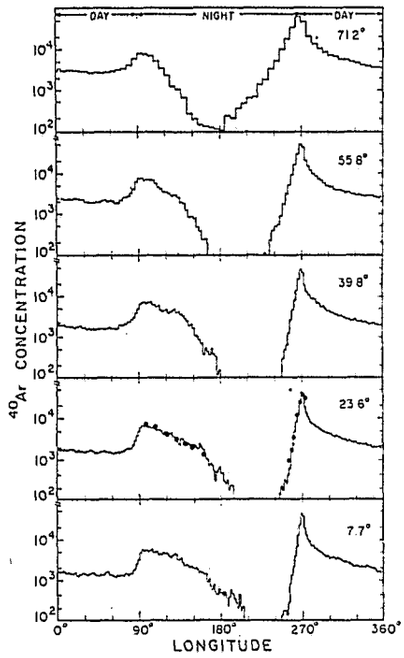

FIG. 6. Computed global distribution of ^{40}Ar on the moon. Latitudes of individual graphs correspond to geographic centers of data accumulation zones used in the calculation. Preliminary experimental results from the Apollo 17 mass spectrometer are superimposed on the graph for 23.6° latitude.

technique of Hodges (1973b) which included nighttime surface adsorption and sunrise release processes. This model is the culmination of a series of calculations in which the fit at 23.6° latitude with the Apollo 17 mass spectrometer data was optimized by successive iteration of the temperature dependence of adsorption probability. The resulting adsorption function is shown in Fig. 7 where the solid line represents the temperature range of the Apollo 17 data, and the dashed lines are extrapolations. Of course such syntheses do not give unique answers, and thus other adsorption functions may give equally good agreement with the experimental data. In an extreme case in which the cold temperature limit of the adsorption probability was increased from 0.05 (used above) to unity, the only significant change was a slight increase in the amount of gas in polar regions where the cold nighttime temperature insures adsorption.

Assuming a photoionization lifetime of 1.6×10^6 sec for argon (Manka, 1972) and the escape of half the photoions due to solar wind $v \times B$ acceleration, the global average rate of loss of argon from the atmospheric distribution shown in Fig. 6 is 2.3×10^3 atoms $cm^{-2}sec^{-1}$. If the average lunar abundance of potassium is about 1000 ppm,

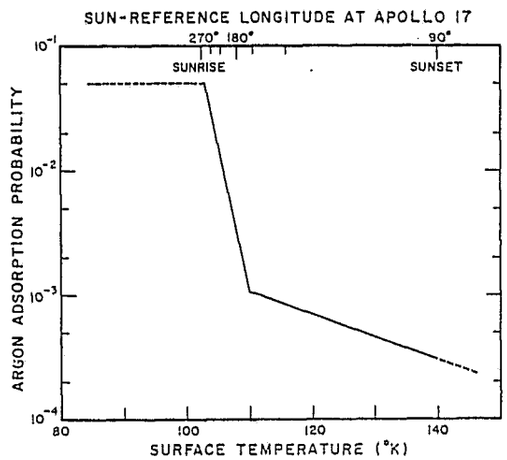

FIG. 7. Solid part of graph shows synthesized probability of adsorption of argon as a function of surface temperature and sun referenced longitude at the Apollo 17 site (lower and upper abscissas, respectively). Dashed lines are arbitrary extrapolations used for other nighttime temperatures.

the total rate of production of ^{40}Ar amounts to roughly 6×10^5 atoms $cm^{-2} sec^{-1}$ at the surface. Thus, the rate of loss of atmospheric ^{40}Ar from the moon corresponds to about 0.4% of the total production. Another way to view this rate of loss is that it corresponds to release of the entire argon production from the upper 3 km of the lunar soil.

The mechanism for conduction of such a large fraction of the ^{40}Ar production into the atmosphere from its point of origin within rocks is obscure. On earth, where potassium is probably concentrated mainly in the crust, the weathering of rocks has released the observed amount of atmospheric argon. Assuming the earth to be similar in composition to chondrites, Turekian (1964) has estimated that the present terrestrial atmospheric ^{40}Ar represents release of 10% of the total produced over geologic time. However, there is no evidence of ongoing weathering on the moon to a sufficient depth to account for the argon release there.

It is not reasonable to postulate an enhanced abundance of ^{40}K below the surface of the moon because of heat flow considerations. The energy generated by the assumed 1000 ppm amount would correspond to a heat outflow of about 10^{-6} watts cm^{-2} which is a substantial fraction of the measured heat flows—the order of 3×10^{-6} watts cm^{-2} according to Langseth *et al.* (1973).

As mentioned previously, the amount of ^{36}Ar on the moon is roughly 10% of the ^{40}Ar. The solar wind flux of ^{36}Ar ions is about $8 \times 10^2 cm^{-2} sec^{-1}$ (Johnson *et al.*, 1972). Since these ions impinge only on the side of the moon facing the sun, the average global influx is 1/4 the solar wind flux, or $2 \times 10^2 cm^{-2} sec^{-1}$, which is about 10% of the ^{40}Ar effusion rate calculated above. Thus, the sustenance of ^{36}Ar at about 10% of the amount of ^{40}Ar requires that the rate of supply of ^{36}Ar to the atmosphere be essentially in balance with the solar wind influx.

The average rate of embedding of ^{36}Ar in lunar surface materials is the sum of the averages of solar wind influx and half the photoionization rate, which amounts to twice the average solar wind influx, or about $4 \times 10^2 cm^{-2} sec^{-1}$. Embedding of photoionized atmospheric ^{40}Ar occurs at just half the average photoionization rate, which is also equal to the previously calculated escape rate of $2.3 \times 10^3 cm^{-2} sec^{-1}$. Balance of atmospheric supply and solar wind influx of ^{36}Ar implies saturation of the surface materials with argon, and the balance of effusion and embedding rates requires that the ratio of trapped ^{40}Ar to ^{36}Ar be the order of 6. This presents a slight dilemma since the ratio of trapped ^{40}Ar and ^{36}Ar varies from .5 to 2 in most returned lunar soil samples. However, gas release rates obtained during linear heating of soil samples typically show a fairly high ratio of ^{40}Ar to ^{36}Ar at low temperatures (Baur *et al.*, 1972; Frick *et al.*, 1973). This may be interpreted to imply a higher ratio of ^{40}Ar to ^{36}Ar near grain surfaces, where exchange of effusing neutral atoms and impacting ions is most likely to occur.

The isotope of argon at mass 38 amu is mainly of solar wind origin, and thus its abundance in the atmosphere should be in the same ratio to ^{36}Ar as the abundance ratio of these isotopes in lunar soil samples, which is generally the same as the terrestrial ratio, i.e., ^{38}Ar is about 20% as abundant as ^{36}Ar. In the Apollo 17 mass spectrometer data there are interferences at masses 36 and 38 amu due to an HCl contaminant, which apparently is produced in the same reaction that forms HF (discussed earlier in connection with neon). The argon diurnal effect is sufficiently above the contaminant background at 36 amu that the ^{36}Ar presence is obvious. However, a more detailed analysis of the data is needed to positively verify the existence of ^{38}Ar in the lunar atmosphere.

Other Solar Wind Gases

Solar abundances of O, C and N probably exceed that of Ne (Cameron, 1968), but atomic and molecular forms of these elements derived from the solar wind do not show evidence of a recognizable diurnal atmospheric oscillation in the Apollo 17 mass spectrometer data. The only reasonable interpretation of this fact is that

ambient levels are small compared to the artifact background.

Atomic oxygen ions of the solar wind probably react with lunar materials, as the moon is less than fully oxidized, even though oxygen is the major constituent of the moon. Thus the lack of evidence of O or O_2 in the atmosphere is understandable.

Atmospheric forms of C and N are more reasonably expected. By analogy with the previously discussed hypothesis of the formation of H_2, it is expected that CH_4 and NH_3 should also be formed and released to the atmosphere (Hodges *et al.*, 1973). The large amount of oxygen in the soil may lead to production of CO, CO_2 and NO, but these reactions may also be reversible. The alternative to atmospheric forms of C or N is that most of the solar wind influx of these elements is now being permanently implanted in the soil.

Other Gases of Lunar Origin

The only gases of lunar origin that have been positively identified, ^{40}Ar and ^{222}Rn, were anticipated on the basis of geophysical considerations. However, the rate of effusion of ^{40}Ar is significantly more than might be expected in view of the lack of evidence of a crustal excess of potassium or an efficient weathering mechanism. Since the outflow of ^{40}Ar may be accompanied by other gases, it is important to consider possible argon release mechanisms.

One possibility is that most of the atmospheric ^{40}Ar is produced deep in the lunar interior. Latham *et al.* (1973) have identified a highly attenuating zone for seismic shear waves beginning at a depth of 1000 km to 1100 km. If the attenuation is due to high temperatures and partial melting, then an outflow of argon from the core could result. This would undoubtedly result in trapping of the gas in some regions and in a global venting rate that depends on the distribution of deep fissures. Alternatively, radiogenic argon could have diffused into voids within the moon over a long period and some of these reservoirs could now be venting argon into the atmosphere. An attractive feature of either hypothesis is that it can explain, through seismic changes in venting rates, a great variability in the level of ^{40}Ar in the lunar atmosphere over geologic time. Yaniv and Heymann (1972) have proposed such variations to explain the dispersion of the ^{40}Ar to ^{36}Ar ratio in the lunar soil samples.

The regolith must be ruled out as an important source of atmospheric argon simply because of the magnitude of the loss rate, which corresponds to release of ^{40}Ar at its rate of production throughout the upper 3 km of soil. Impact gardening may release a small fraction of the trapped argon from the soil, but the depth of this effect cannot be great enough to make a substantial contribution. Diffusion of argon out of small grains to a great depth also seems an unlikely explanation because this mechanism would not have produced a varying supply of argon.

If argon is indeed vented from the lunar interior, then it may carry with it other common volcanic gases. By analogy with earth, water vapor would seem to be a candidate gas, although there is no evidence of atmospheric water in the Apollo 17 mass spectrometer data. The photodissociation time for H_2O is quite short, and its dissociation products are chemically active, so that the rate of effusion of water vapor from the moon may in fact be significant without being detectable.

A transient gas event was detected by the Apollo 15 orbital mass spectrometer (Hodges *et al.*, 1973) as the spacecraft passed northwest of Mare Orientale (110.3° W, 4.1°S) in lunar night. Briefly, this event consisted of a sudden burst of gases at masses 14, 28 and 32 amu. Similar excursions could have been detected at all other parts of the spectrum between 12 amu and 67 amu except at 16, 17, 18 and 44 amu, which unfortunately were dominated by contaminants. The absence of other mass numbers in this event may have been a temporal effect caused by a duration of the disturbance that was shorter than the time required to scan the mass spectrum (62 sec). The ratio of masses 14 and 18 amu was greater than the cracking pattern of

REPRODUCIBILITY OF THE ORIGINAL PAGE IS POOR

N_2, while the absence of mass 12 amu rules out a significant amount of CO or CO_2. A mixture of N, N_2 and a small amount of CO or CO_2 would fit the observed spectral distribution of mass peaks. The excursion at 32 amu could have been O_2, or more likely a fragment of SO_2 from a very short burst that lasted less than the 20 seconds needed to scan the spectrum from 32 amu to 64 amu. The total amount of gas needed to produce this event has been estimated to be about 20 kg. The volcanic origin of some of the gases that might have been involved in the above event, i.e. N, N_2 and O_2, were not generally anticipated. However, CO, CO_2, SO_2 and H_2O seem likely candidates, based on a terrestrial analogy.

Acknowledgments

The assistance of Mr. H. D. Hammack in programming of numerical computations is gratefully acknowledged. This research was supported by NASA under contracts NAS9-5964, NAS9-10410 and NAS9-12074.

References

Baur, H., Frick, U., Funk, H., Schultz, L., and Signer, P. (1972). Thermal Release of Helium, Neon, and Argon from Lunar Fines and Minerals. *Proc. Third Lunar Sci. Conf., Geochim Cosmochim Acta*, Suppl. 3, Vol. 2, 1947.

Bjorkholm, P., Golub, L., and Gorenstein, P. (1973). Detection of radon emanation from the lunar regolith during Apollo 15 and 16 (abstract), *In* "Lunar Science IV." (J. W. Chamberlain and Carolyn Watkins, eds.). Lunar Science Institute, Houston, Texas, 78.

Cameron, A. G. W. (1968). A new table of abundances of the elements in the solar system, *In* "Origin and Distribution of the Elements," (L. H. Ahrens, ed.). Pergamon, 124.

Fastie, W. G., Feldman, P. D., Henry, R. C., Moos, H. W., Barth, C. A. Thomas, G. E., and Donahue, T. M. (1973). A search for far ultraviolet emissions from the lunar atmosphere. *Science* **182**, 710.

Feldman, P. D., and Fastie, W. G. (1973). Fluorescence of molecular hydrogen excited by solar extreme ultraviolet radiation. Submitted to *Astrophys. J. Letters*.

Frick, U., Baur, H., Funk, H., Phinney, D., Schultz, L., and Signer, P. (1973). Diffusion of argon in lunar fines, or little orphan argon retrapped (abstract), *In* Lunar Science IV, (J. W. Chamberlain and Carolyn Watkins, eds.). Lunar Science Institute, Houston, Texas, 266.

Geiss, J., Buehler, F., Cerutti, H., Eberhardt, P., and Ch. Filleux (1972). Solar Wind Composition Experiment. Apollo 16 Preliminary Science Report, NASA SP-315, 14-1.

Gorenstein, P., Golub, L., and Bjorkholm, P. (1973). Spatial nonhomogeneity and temporal variability in the emanation of radon from the lunar surface: interpretation (abstract). *In* "Lunar Science IV," (J. W. Chamberlain and Carolyn Watkins, eds.). Lunar Science Institute, Houston, Texas, 307.

Hartle, R. E., and Thomas, G. E. (1973). Neutral and ion-exosphere models for lunar hydrogen and helium. Submitted to *J. Geophys. Res.*

Hinton, F. L., and Taeusch, D. R. (1964). Variation of the lunar atmosphere with the strength of the solar wind. *J. Geophys. Res.* **69**, 1341.

Hodges, R. R. (1972). Applicability of a diffusion model to lateral transport in the terrestrial and lunar exospheres. *Planet. Space Sci.* **20**, 103.

Hodges, R. R. (1973a). The differential equation of exospheric lateral transport and its application to terrestrial hydrogen. *J. Geophys. Res.* **78**, 7340.

Hodges, R. R. (1973b). Helium and hydrogen in the lunar atmosphere, *J. Geophys. Res.*, **78**, 8055.

Hodges, R. R., and Johnson, F. S. (1968). Lateral transport in planetary exospheres. *J. Geophys. Res.* **73**, 7307.

Hodges, R. R., Hoffman, J. H., Yeh, T. T. J. and Chang, G. K. (1972a). Orbital search for lunar volcanism. *J. Geophys. Res.* **77**, 4079.

Hodges, R. R., Hoffman, J. H., and Evans, D. E. (1972b). Lunar Orbital Mass Spectrometer Experiment. Apollo 16 Preliminary Science Report, NASA SP-315, 21-1.

Hodges, R. R., Hoffman, J. H., Johnson, F. S., and Evans, D. E. (1973) Composition and dynamics of lunar atmosphere. *Proc. Fourth Lunar Sci. Conf., Geochim Cosmochim Acta, Suppl. 4*, **3**, 2855.

Hoffman, J. H., Hodges, R. R., and Evans, D. E. (1973). Lunar atmospheric composition results from Apollo 17, *Proc. Fourth Lunar Sci. Conf., Geochim Cosmochim Acta., Suppl. 4*, **3**, 2865.

Johnson, F. S. (1969). Origin of planetary atmosphere. *Space Sci. Rev.*, **9**, 303

Johnson, F. S. (1971). Lunar atmosphere. *Rev. Geophys. Space Phys.*, **9**, 813.

Johnson, F. S., Carroll, J. M., and Evans,

D. E. (1972). Lunar atmospheric measurements. *Proc. Third Lunar Sci. Conf., Geochim Cosmochim Acta*, Suppl. 3, Vol. 3, 2231.

LANGSETH, M. G., CHUTE, J. L., AND KEIHM, S. (1973). Direct measurements of heat flow from the moon (abstract), *In* "Lunar Science IV," (J. W. Chamberlain and Carolyn Watkins, eds.). Lunar Science Institute, Houston, Texas, 455.

LATHAM, G., DORMAN, J., DUENNEBIER, F., EWING, M., LAMMLEIN, D., AND NAKAMURA, Y. (1973). Moonquakes, meteoroids, and the state of the lunar interior (abstract). *In* "Lunar Science IV," (J. W. Chamberlain and Carolyn Watkins, eds.) Lunar Science Institute, Houston, Texas, 457.

MANKA, R. H. (1972). Lunar Atmosphere and Ionosphere. Ph.D. Thesis, Rice University.

MANKA, R. H., AND MICHEL, F. C. (1971). Lunar atmosphere as a source of lunar surface elements. *Proc. Second Lunar Sci. Conf., Geochim Cosmochim Acta*, Suppl. 2, Vol. 2, 1717.

TUREKIAN, K. K. (1964). Degassing of argon and helium from the earth. *In* "The Origin and Evolution of Atmospheres and Oceans," (P. J. Brancazio and A. G. W. Cameron, eds.). John Wiley, N. Y., 74.

YANIV, A., AND HEYMANN, D. (1972). Atmospheric Ar^{40} in lunar fines. *Proc. Third Lunar Sci. Conf., Geochim. Cosmochim Acta*, Suppl. 3, Vol. 2, 1967.

Proceedings of the Fifth Lunar Conference
(Supplement 5, Geochimica et Cosmochimica Acta)
Vol. 3 pp. 2955–2961 (1974)
Printed in the United States of America

Episodic release of ^{40}Ar from the interior of the moon

R. R. HODGES, JR. and J. H. HOFFMAN
The University of Texas at Dallas, Richardson, Texas 75080

Abstract—Measurements of lunar atmosphere made by the mass spectrometer at the Apollo 17 landing site during the first 9 lunations of 1973 show an apparently cyclical variation of radiogenic ^{40}Ar, with maximum to minimum abundance ratio of about 2. There seems to be a 6–7 month periodicity in the oscillation, but the limited data base makes a fixed oscillatory pattern uncertain. The significance of the variation of atmospheric argon lies in the implication that its source is episodic in nature, ranging in strength from about 1% of the total rate of production of ^{40}Ar in the moon to near zero. This requires a presently active mechanism for transient venting of gas from deep within the moon.

INTRODUCTION

THE ATMOSPHERE of the moon is a good indicator of both the effusion of gases from the interior of the planet and of the interaction of the moon with its radiation and particle environment in the solar wind and in the geomagnetic tail. Owing to the short lifetime of atmospheric gases (a few months at most), their abundances give information regarding presently active lunar processes. This contrasts sharply with the returned sample analyses, which tend to give integrated information on time scales in excess of 10^6 years.

The major native constituent of the lunar atmosphere is probably radiogenic ^{40}Ar, which is produced as a result of the decay of ^{40}K within the moon. Argon supplied by the solar wind should probably have an excess of ^{36}Ar, whereas the atmospheric abundance ratio of ^{40}Ar to ^{36}Ar is about 10 to 1 (cf. Hodges *et al.*, 1973; Hoffman *et al.*, 1973; and Hodges *et al.*, 1974). Thus, the contribution of the solar wind to the ^{40}Ar in the lunar atmosphere is probably negligible.

Two features of the atmospheric ^{40}Ar are of particular interest. First, the average rate of effusion of argon from the moon can be calculated on the basis of atmospheric escape. The magnitude of this loss rate is so large that it requires argon release from deep within the moon. Second, the rate of effusion of argon from the moon varies over a wide range in an apparently episodic pattern reminiscent of the fluctuations of moonquake activity reported by Latham *et al.* (1973) and by Lammlein (1974).

EXPERIMENTAL DATA

Figure 1 shows mass spectrometric measurements of gas concentration at mass 40 amu at the Apollo 17 landing site. The data are restricted mainly to lunar nights. High rates of degassing of remnant spaceflight hardware in sunlight locally obscured the lunar atmosphere in daytime.

The characteristic behavior of the mass 40 amu data in Fig. 1, i.e. the slow post sunset decrease, nighttime minimum, and a distinct pocket of gas at the sunrise terminator, was predicted by Hodges and Johnson (1968) to be the nighttime part of the diurnal variations of a condensable atmospheric gas.

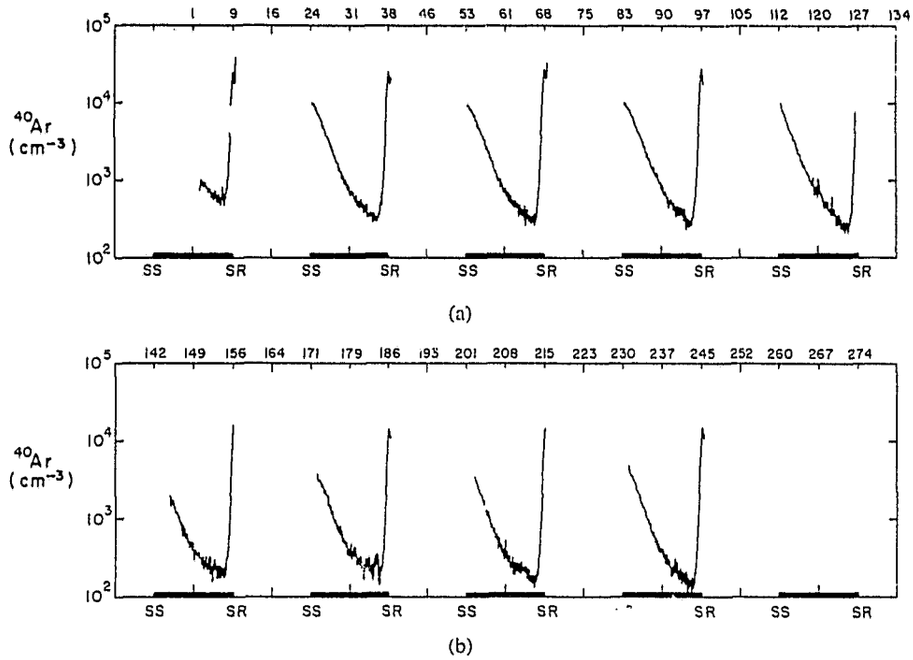

Fig. 1. Measured concentration of ^{40}Ar at the Apollo 17 site during 1973. The upper abscissa gives calendar days of quarter-phases of the sun. Sunrises (SR), sunsets (SS), and periods of darkness (dark bar) are specified on the lower scale.

The midnight minimum is due to adsorption on the cold nighttime lunar surface. Subsequent release of the adsorbed gas, mainly at the sunrise terminator, causes the presunrise increase. There is no reasonable alternative explanation of the presunrise increase in terms of an artifact gas release from spaceflight components at the site. Therefore, it is concluded that the nighttime 40 amu data represent true measurements of native ^{40}Ar.

DETERMINATION OF THE EFFUSION RATE

An important feature of the data is that the pattern of the diurnal variation of ^{40}Ar changes in amplitude from lunation to lunation. This is shown clearly in Fig. 2, where data from lunations of maximum and minimum abundances are superimposed. The theory of these diurnal variations developed in Hodges *et al.* (1974) suggests that the total rate of photoionization of argon on the moon, Ψ_I, is related to the sunrise concentration, n_{SR} by

$$\Psi_I = 4.4 \times 10^{16} \times n_{SR} \text{ (atoms/sec)} \tag{1}$$

This formula is based on an iterative fit of a Monte Carlo simulation of the lunar atmosphere to a small, preliminary sample of experimental data. Subsequent processing of all of the data suggests that the fraction of argon in sunlight was

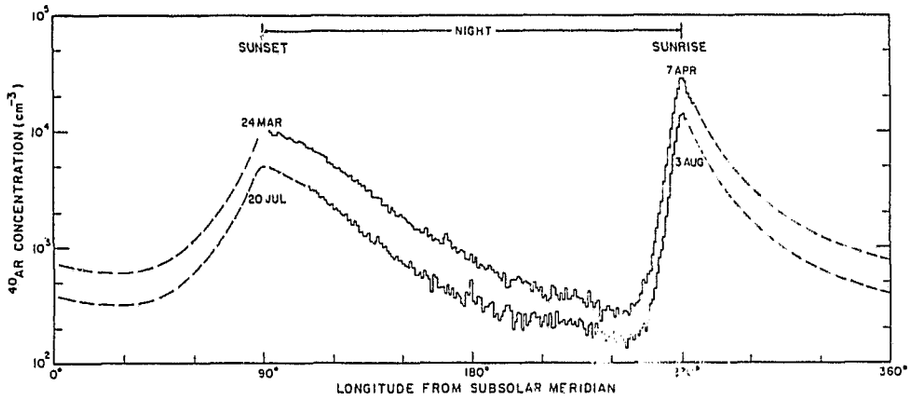

Fig. 2. Diurnal oscillations of ^{40}Ar during lunations of maximum and minimum abundances. Dashed curves are theoretical extrapolations which show expected daytime behavior.

underestimated, and, hence, the photoionization rate should have been greater. The Monte Carlo calculations have not been repeated for the full data set, but this would change the photoionization rate by 25% or less, which is undoubtedly less than the error due to the uncertainty in the photoionization time for argon, which has been estimated to be about 18 days by Manka (1972) and about 12 days by Johnson *et al.* (1972).

Application of expression (1) to the extrema of n_{SR} indicated in Fig. 2 gives maximum and minimum ionization rates of about 1.2×10^{21} atoms/sec and 6×10^{20} atoms/sec, respectively. If half the photoions escape while the rest are driven into the moon by solar wind $\mathbf{v} \times \mathbf{B}$ acceleration and subsequently become recycled into the atmosphere, the average rate of supply of new atoms must be in the range of 3×10^{20} to 6×10^{20} atoms/sec.

If the present relative isotopic abundance of ^{40}K is assumed to be 119 ppm, and the total lunar abundance of potassium is 300 ppm, then the total rate of production of ^{40}Ar is 7.3×10^{22} atoms/sec. Comparison of this rate with that needed to supply average atmospheric losses suggests that about 0.6% of the argon produced throughout the moon manages to escape. If potassium is uniformly distributed through the moon, the rate of loss is equivalent to the total rate of production in the upper 3.5 km of the lunar crust. As was noted previously by Hodges *et al.* (1974), there is no presently active gardening or weathering process that could produce this effect, even in the upper few millimeters of the soil.

The rate of supply of argon in the lunar atmosphere is assumed to be the sum of Ψ_0, the rate of effusion of new atoms into the atmosphere, and Ψ_R, the rate of release of recycled atoms, i.e. former atmospheric particles which have been imbedded in soil grains as atmospheric ions and which subsequently reemerge into the atmosphere. This rate of supply must be balanced by a loss rate, consisting of

the static model photoionization rate Ψ_i with a correction for finite residence time. Thus, the equation of continuity for atmospheric argon is approximately

$$\Psi_0 + \Psi_R = \Psi_i + \tau_L \frac{d\Psi_i}{dt} \tag{2}$$

The time constant for escape of the atmosphere is τ_L, which was estimated by Hodges *et al.* (1974) to be about 100 days. Subsequent discussion will show that the true value of τ_L is probably only about 50 days.

Over a long time period it is necessary that the average value of Ψ_R equal the fraction of Ψ_i which is reimplanted in the lunar soil. Hodges and Hoffman (1974) have shown that there is a detailed, essentially instantaneous, balance of influx of solar wind alpha particles and outflow of helium atoms from the soil. Presumably a similar balance could exist in the recycling of atmospheric ^{40}Ar. Thus, it is assumed that

$$\Psi_R = K\Psi_i \tag{3}$$

where K is the fraction of argon photoions which return to the moon.

Figure 3 shows the time history of the total rate of photoionization of ^{40}Ar during the period of 1973 when mass spectrometer data was obtained. Data points are based on application of relation 1 to measured sunrise concentrations. The actual rate of effusion of ^{40}Ar from the interior of the moon can be inferred from Fig. 3 by application of Eq. (2). However, this requires knowledge of the parameters K and τ_L.

In Fig. 3 a rapid decrease of the argon loss rate can be noted in April and May. The exponential time constant for this decrease of Ψ_i is about 100 days. Since it is

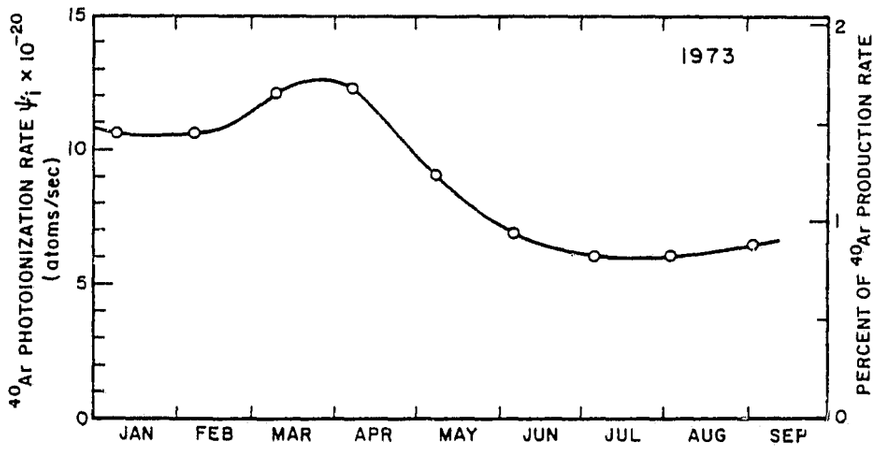

Fig. 3. Rate of photoionization of ^{40}Ar in the lunar atmosphere during 1973, derived by application of Eq. (1) to sunrise data (circles). The right-hand ordinate is based on an average lunar potassium abundance of 300 ppm.

REPRODUCIBILITY OF THE ORIGINAL PAGE IS POOR

necessary that $\Psi_0 \geqslant 0$, expression (2) requires

$$\tau_L \leqslant 100(1-K) \text{ days} \tag{4}$$

The work of Manka and Michel (1971) suggests that the most likely value for K is 0.5, and hence $\tau_L \leqslant 50$ days seems to be necessary. The aforementioned estimates of photoionization time in the range of 12–18 days, and the greater likelihood of an atom being on the nighttime side of the moon than on the daytime side, seem to require that τ_L be at least 50 days. Therefore, it must be presumed that the April–May decline in ^{40}Ar occurred as a result of a decrease of Ψ_0 to nearly zero.

Figure 4 shows the rate of effusion of new argon atoms from the interior of the moon for the equality condition of expression (4). These graphs are solutions to Eq. (2) with Ψ_I represented by the solid line of Fig. 3. The graph $K = 0.5$ and $\tau_L = 50$ days represents the most likely case, while those for $K = 0.3$ and 0.7 show a range of possibilities.

The notable feature of the graphs of Fig. 4 is the sharp decreases in Ψ_0 in early April 1973. This time would be essentially unchanged by any choices of τ_L and K. It corresponds to a predicted minimum of the 206-day oscillation of moonquake activity extrapolated from the 1972 seismic data reported by Latham *et al.* (1973). In addition it can be noted in Fig. 3 that Ψ_0, and hence the total argon abundance, went through two minima in 1973, which were separated in time by about 6–7 months. This phenomenon is also in agreement with a correlation of argon release with the 206-day component of moonquake activity variations.

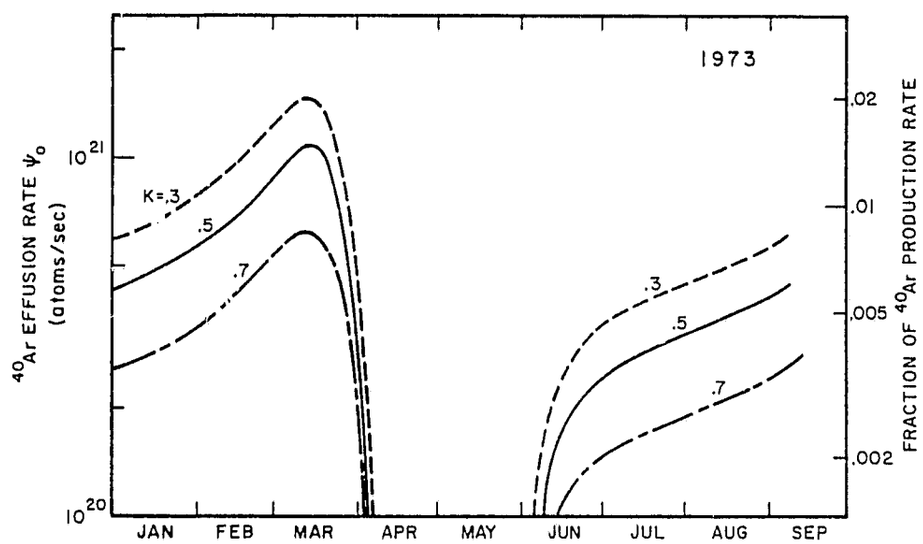

Fig. 4. Rate of effusion of argon from the interior of the moon for $K = 0.3$, 0.5, and 0.7 with $\tau_L = 100 \times (1-K)$ days.

CONCLUSIONS

Discovery of the time variation of the rate of effusion of ^{40}Ar from the moon is significant. It gives direct evidence of the existence of an active transient process which occurs within the moon. The depth of origin of the argon is uncertain, but it is surely below the regolith. At depths the order of a few tens of kilometers, the temperature may be sufficient to drive enough gas from fractured materials to account for the average atmospheric abundance, but this model cannot explain the time variation. The alternative seems to be percolation of argon from a semi-molten core into one or more voids which vent transiently to the atmosphere through deep fissures.

Whatever the origin of the atmospheric argon, its transient nature strongly suggests a release mechanism which is coupled with some form of seismic activity. This leads to two avenues of speculation: that the release of argon is due to internal movements which periodically open paths to the lunar surface, or that the pressure of the gas trapped in a cavity builds up to the point where it creates its own path of escape. It is clear that a strong argument could be made for either of these causal relationships, or for a combination of the two.

The mechanism for escape of argon from the moon should be expected to bring other gases to the surface. If so, their identification in available mass spectrometer data is complicated by artifact contributions. Preliminary analyses suggest that CO and CH_4 may be present in small amounts at night. However, these are probably of solar wind origin. If water vapor were discharged from the moon, it would probably be adsorbed at a much warmer temperature than argon, and hence would exist only in the as-yet unexplored daytime part of the atmosphere.

It is particularly unfortunate that the period of measurement of ^{40}Ar at the Apollo 17 site only lasted through 9 lunations. While that data base is sufficient to show the transient behavior and the rudiments of an episodic pattern of release, it leaves the interpretation of this phenomenon open to speculation. Whether it is caused by, or is the cause of, moonquake activity demands further study, as do the implications of the magnitude of the release rate.

Acknowledgments—Data processing efforts of Mr. H. D. Hammack are gratefully acknowledged. This research has been supported by the National Aeronautics and Space Administration under contract NAS 9-12074.

REFERENCES

Hodges R. R. and Johnson F. S. (1968) Lateral transport in planetary exospheres. *J. Geophys. Res.* **73**, 7307–7317.

Hodges R. R., Hoffman J. H., Johnson F. S., and Evans D. E. (1973) Composition and dynamics of lunar atmosphere. *Proc. Fourth Lunar Sci. Conf., Geochim. Cosmochim. Acta*, Suppl. 4, Vol. 3, pp. 2855–2864. Pergamon.

Hodges R. R., Hoffman J. H., and Johnson F. S. (1974) Lunar atmosphere. *Icarus.* **21**, pp. 415–426.

Hodges R. R. and Hoffman J. H. (1974) Measurements of solar wind helium in the lunar atmosphere. *Geophysical Research Letters*, **1**, pp. 69–71.

Hoffman J. H., Hodges R. R., Johnson F. S., and Evans D. E. (1973) Lunar atmospheric composition results from Apollo 17. *Proc. Fourth Lunar Sci. Conf., Geochim. Cosmochim. Acta.*, Suppl. 4, Vol. 3, pp. 2865–2875. Pergamon.

Lammlein D. (1974) Moonquakes and tides (abstract). In *Lunar Science—V*, p. 433. The Lunar Science Institute, Houston.

Latham G., Dorman J., Duennebier F., Ewing M., Lammlein D., and Nakamura Y. (1973) Moonquakes, meteoroids, and the state of the lunar interior. *Proc. Fourth Lunar Science Conference, Geochim. Cosmochim. Acta*, Suppl. 4, Vol. 3, pp. 2515–2527. Pergamon.

Manka R. H. (1972) Lunar atmosphere and ionosphere. Ph.D. thesis. Rice University.

Manka R. H. and Michel F. C. (1971) Lunar atmosphere as a source of lunar surface elements. *Proc. Second Lunar Sci. Conf., Geochim. Cosmochim. Acta*, Suppl. 2, Vol. 2, pp. 1717–1728. MIT Press.

MEASUREMENTS OF SOLAR WIND HELIUM IN THE LUNAR ATMOSPHERE

R. R. Hodges, Jr. and J. H. Hoffman

The University of Texas at Dallas
Richardson, Texas 75080

Abstract. Measurements of lunar atmospheric helium during 1973 from the Apollo 17 lunar surface mass spectrometer are presented. The average helium abundance is shown to be about 70% of the theoretical model value, suggesting that the solar wind helium flux in 1973, during sunspot minimum, was substantially less than the expected average flux. Large amplitude transients in the helium data indicate rapid response of the lunar atmosphere to changes in solar wind. The atmospheric helium abundance is shown to be correlated with the geomagnetic index Kp.

The concentration of helium in the lunar atmosphere has been measured by the mass spectrometer at the Apollo 17 landing site during nighttimes of the first 10 lunations of 1973. Thermal degassing of remnant spaceflight hardware in sunlight has severely limited the collection of daytime data.

Figure 1 shows theoretical and experimental average data on the diurnal oscillation of helium on the moon. The histogram gives the Monte Carlo result for the Apollo 17 latitude reported by Hodges (1973). Data points correspond to averages over 18° intervals of longitude of all available measurements obtained during 10 lunations. The error bars, which show the variance of the data, are indicative of systematic changes in the helium abundance, which are discussed below. The general features of the theoretical and average experimental distributions are similar but the amplitude of the latter is only about 70% of the former. This difference is significant, and probably is due to a lower than average flux of α-particles in the solar wind during 1973. There is other evidence of changes in the relative abundance of helium in the solar wind with the solar cycle (Robbins et. al., 1970).

Figure 2 shows the detailed history of nighttime helium concentration at the Apollo 17 site during the first 10 lunations of 1973. These plots are smoothed by averaging all raw data in 1° increments of synodic rotation. In no lunation does the helium concentration follow the smooth average behavior shown in Figure 1. Instead there are several transient events superimposed on each diurnal oscillation, which must be due to significant variations in the rate of supply of helium.

Helium is produced on the moon by neutralization of the solar wind α-particle influx. The impinging ions have energies of the order of 4000 eV, which should cause entrappment of much of their influx in surface rocks, leading to a balance of ion trapping and atomic release rates in the lunar soil. The sudden changes in atmospheric helium indicate a rapid response to solar wind variations. An almost instantaneous one-for-one replacement of trapped helium in the soil seems to be the most plausible explanation of this phenomenon. A less likely possibility is that the transient atmospheric events are caused by release of trapped helium in periods of enhanced weathering of surface rocks, perhaps caused by increased solar wind impact energy, or other solar activity. Wilcox et al. (1967) have noted that solar wind velocity is strongly correlated with Kp, and Hirshberg et al. (1972) have found that the helium fraction of the solar wind tends to increase linearly with solar wind velocity. Thus, it should be expected that the changes in helium abundance on the moon are related to variations of Kp.

The time required for an abrupt change in the solar wind to alter the nighttime atmosphere can be estimated from exospheric diffusion theory (Hodges, 1972) as roughly $R^2/H\langle v\rangle$, where R is the radius of the moon, H is the scale height for helium, and $\langle v\rangle$ is the mean atomic speed. For an average lunar temperature of 200°K this time is about 3 hours, which is convenient for comparison of the measurements with tabulated Kp data.

The total abundance of helium on the moon is proportional to n/n_o, where n is the 3 hour average of measured concentration, and n_o is the

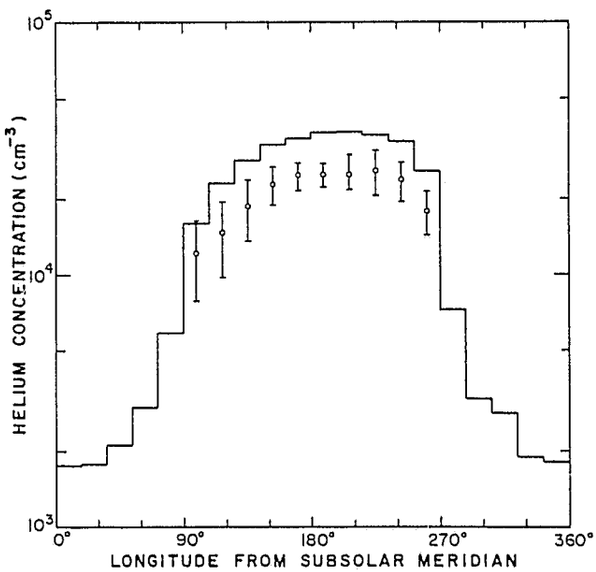

Fig. 1. Synodic variation of the average concentration of helium at the Apollo 17 site (circles) superimposed on a theoretical model (histogram). Error bars represent standard deviations for all data in each 18° increment of longitude.

Copyright 1974 by the American Geophysical Union.

corresponding static model concentration at the Apollo 17 site. The latter has been obtained by fitting a smooth curve to the calculated model of Hodges (1973). An estimate of the effective solar wind flux of helium needed to supply the lunar atmosphere can be found from the relation

$$\phi_{sw} = \phi_o \left\{ \frac{n}{n_o} + \tau \frac{d}{dt} (n/n_o) \right\} \qquad (1)$$

where ϕ_o is the average solar wind flux used in calculation of n_o (1.35×10^7 cm^{-2} sec^{-1}), and τ is the average atomic residence time for helium on the moon (about 8×10^4 sec).

Figure 3 shows the correlation of Kp with effective solar wind flux of helium given by equation 1. Circles represent average flux values and error bars indicate standard deviations of all data in each increment of Kp. Individual data points are plotted for Kp >6$^+$. The upper graph gives the total measurement time represented by the data at each value of Kp. Over the range of Kp from 0$^+$ to 5 there are more than 30 data points in each interval, while the average number

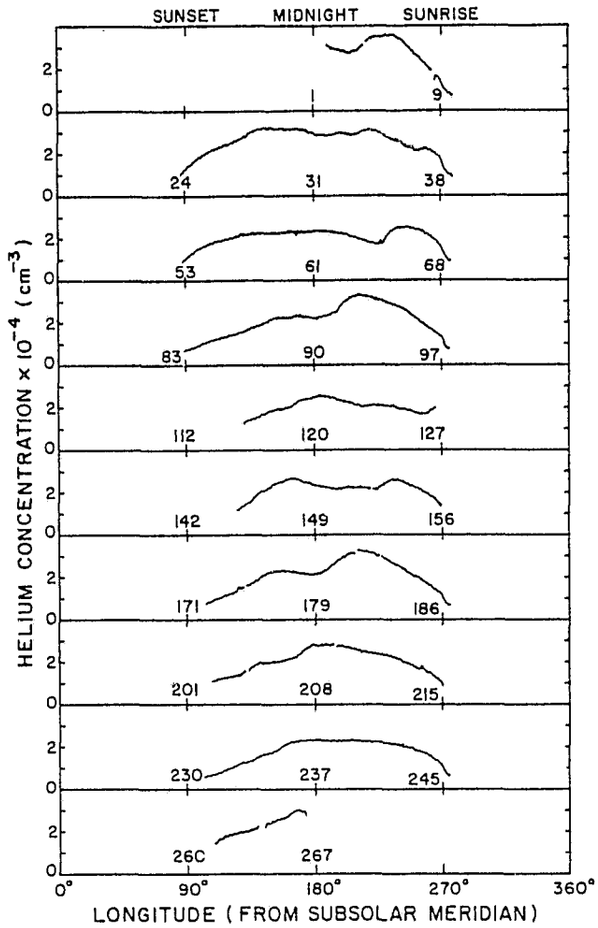

Fig. 2. Measured helium concentrations averaged over 1° increments of longitude in the first 10 lunations of 1973. Day of the year is given at 90°, 180° and 270° of solar longitude in each graph.

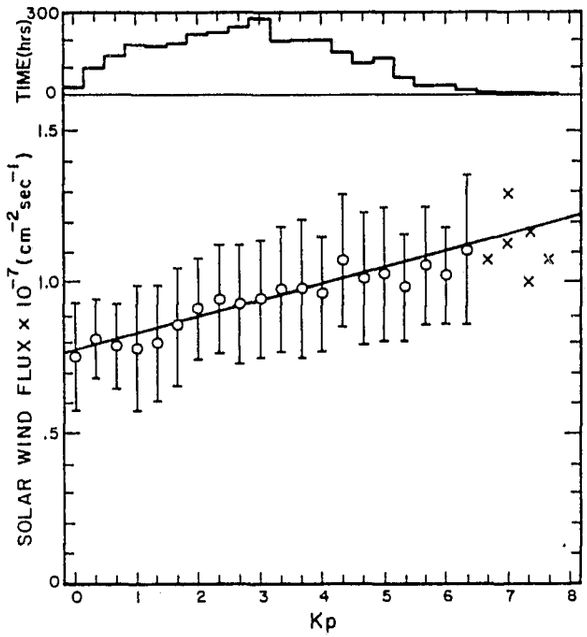

Fig. 3. The equivalent solar wind flux of helium needed to supply the lunar atmosphere (lower graph), and total time of data accumulation (upper graph) as functions of Kp. In the lower graph, circles represent flux averages, error bars give standard deviations of the data, and crosses represent individual data points at high values of Kp.

for all intervals exceeds 60 (i.e. 180 hours). The average solar wind flux of helium for the 1973 data is 9.2×10^6 cm^{-2} sec^{-1}, which is 68% of the nominal flux assumed in the model calculation shown in Figure 1.

The linear mean-square regression line in Figure 3, which is fitted to all of the available 3 hour average data points (963), clearly shows a correlation of effective solar wind flux and Kp. It can be represented by:

$$\phi_{sw} = (7.7 \pm 2.0 + 0.54 \times \mathrm{Kp}) \times 10^6 \mathrm{cm}^{-2}\mathrm{sec}^{-1}. \qquad (2)$$

The slope of this line is not as steep as might be inferred from the solar wind data of Wilcox et al. (1967) and Hirshberg et al. (1972). Perhaps this indicates that the release of trapped helium from the lunar soil involves two separate mechanisms: one which responds instantly to changes in the solar wind, and another which reflects a longer term balance with the average α-particle trapping rate. It is also possible that the correlation of the influx with Kp may be greater during large amplitude transient events than that obtained here for all of the data.

Acknowledgments. Data processing efforts of Mr. H. D. Hammack are gratefully acknowledged. This research has been supported by NASA under contract NAS9-12074.

References

Hirshberg, J., J. R. Asbridge, and D. E. Robbins, Velocity and flux dependence of the solar-wind helium abundance, J. Geophys. Res., 77, 3583, 1972.

Hodges, R. R., Helium and hydrogen in the lunar atmosphere, J. Geophys. Res., 78, 8055, 1973.

Hodges, R. R., Applicability of a diffusion model to lateral transport in the terrestrial and lunar exospheres, Planet. Space Sci., 20, 103, 1972.

Robbins, D. E., A. J. Hundhausen, and S. J. Bame, Helium in the solar wind, J. Geophys. Res., 75, 1178, 1970.

Wilcox, J. M., K. H. Schatten, and N. F. Ness, Influence of interplanetary magnetic field and plasma on geomagnetic activity during quiet-sun conditions, J. Geophys. Res., 72, 19, 1967.

(Received April 1, 1974;
revised May 17, 1974;
accepted May 22, 1974.)

Model Atmospheres for Mercury Based on a Lunar Analogy

R. R. HODGES, JR.

University of Texas at Dallas, Dallas, Texas 75230

Similarities in daytime spectral reflectivities and nighttime infrared emissions from Mercury and the moon are shown to imply that the atmosphere of Mercury must be tenuous, like that of the moon. The theory of formation, transport, and loss in the lunar atmosphere is applied to Mercury. Models of the Hermian atmosphere at perihelion and aphelion are presented, based on the solar wind as the dominant source of gases. Only the noncondensable species, hydrogen, helium, and neon, are considered. Of these, helium is the most abundant atmospheric gas, with maximum concentration of about 4×10^7 cm^{-3} at the nighttime surface. The maximum concentration of H_2 is 6×10^6 cm^{-3}, and that of neon is 7×10^5 cm^{-3}.

Evidence of atmospheric gases on Mercury is apparently nonexistent. *Belton et al.* [1967] have determined from spectroscopic observations that the surface pressure of CO_2 is less than 0.35 mbar. They have further proposed that the atmosphere of Mercury may be entirely a collisionless exosphere, similar to that of the moon. Probably, the most important reason to accept a lunar analogy is the similarly cold nighttime surface temperatures of these planets. The surface of the moon falls below 100°K at night, adsorption of all gases except hydrogen, helium, and neon [*Hodges et al.*, 1974] thus being caused. Infrared emission measurements of Mercury by *Murdock and Ney* [1970] give an average dark side temperature of 111 ± 3°K, which suggests adsorptive removal of all but the noncondensable species at night, as on the moon.

Adsorption of condensable gases on the dark side of Mercury does not prohibit the formation of an atmosphere. The only constraint is that the surface pressure of any species at night is probably less than its vapor pressure at 111°K. Thus the presence of a significant amount of condensable gas would lead to formation of important frozen deposits on the night side and a nonnegligible transport of heat, essentially from the daytime side of the sunrise terminator, where adsorbed gases are released, across the entire terminator to the dark side.

Formation of an atmosphere on Mercury is largely dependent on the rates of escape of gases. If there is little magnetization of the planet, so that the solar wind impinges directly on its daytime surface, then photoionized atmospheric gases may escape owing to acceleration of newly formed ions by fields associated with the solar wind [*Manka and Michel*, 1971]. This is the principal loss mechanism for lunar gases other than hydrogen and helium (which escape thermally).

If Mercury should have a relatively strong steady magnetic field that is capable of shielding its atmospheric gases from the solar wind, then loss rates of photoionized constituents would have been negligible, as on earth. Volcanic gases released from the planet over geologic time would either be present in the atmosphere or have reacted with surface materials to form stable compounds. In addition, all of the radiogenic ^{40}Ar released from the planet would be present in the atmosphere. The amount of ^{40}Ar is open to question, however. *Turekian* [1964] has estimated that 10% of the argon produced in the earth has been released, mainly from the crust. On the moon, where gardening of surface materials is minimal, the present rate of effusion of ^{40}Ar is about 0.4% of the total production rate [*Hodges et al.*, 1974]. If these release rates are extrapolated in proportion to planetary mass to Mercury, the terrestrial and lunar analog amounts of ^{40}Ar released over 4.5 b.y. are 2.8×10^{12} and 1.5×10^{11} tons, respectively, and the corresponding average surface pressures are 1.4 and 0.08 mbar. With the addition of less certain amounts of volcanic gases it appears that a reasonably dense atmosphere would have formed. This atmosphere would also result in appreciable heat transport to the dark hemisphere. The cold temperature of the dark surface of Mercury suggests a lack of atmospheric heat flow and hence implies a tenuous atmosphere in which escape of photoionized constituents has not been inhibited continuously by a magnetic field. A field that is presently strong but was relatively weak over a recent geologic period is not precluded by this argument, however.

The purpose of this paper is to present a hypothetical model of the atmosphere of Mercury that is based on the assumption that the moon and Mercury are similarly inactive planets. This includes a premise that the present magnetic field of Mercury is weak enough to permit the solar wind to impinge on its surface.

SOURCES OF ATMOSPHERE

If the solar wind impinges on the surface of Mercury, then it is probably the dominant source of atmospheric gases. Solar wind ions have kinetic energies of about 1 keV per amu. This is sufficient to embed each ion in the rock or soil grain that it strikes. Whether these particles reemerge as atmospheric constituents depends on the degree of saturation of solar wind gases in surface materials. If the soil on Mercury is regularly overturned to a great depth by geophysical processes, then unsaturated materials that are brought to the surface may provide a continuous sink for a large part of the solar wind influx. On the other hand, if the crust of Mercury is inactive, like that of the moon, then the soil is probably saturated with solar wind gases and a balance of influx and atmospheric supply must exist. This provides an upper bound for the rate of supply of atmospheric gases by the solar wind.

The dominant ion species of the solar wind is the proton. However, on the moon the daytime concentration of atomic hydrogen is less than 10 cm^{-3} [*Fastie et al.*, 1973], whereas the solar wind could supply an atmosphere of about 3×10^3 cm^{-3} [*Hodges et al.*, 1974; *Hodges*, 1973; *Hartle and Thomas*, 1974]. Evidently, the difference is due to formation of H_2 at the lunar surface. A similar process would be expected on Mercury, leading to atmospheric H_2 but to little atomic hydrogen.

By analogy with the moon, helium, neon, and ^{36}Ar should

Copyright © 1974 by the American Geophysical Union.

also exist on Mercury owing to the solar wind influx. Oxygen ions of the solar wind probably react with underoxidized surface materials and provide no atmosphere. Solar wind carbon probably reacts with impacting protons to form CH_4, whereas nitrogen forms NH_3, both of which must enter the atmosphere and subsequently escape from the planet if the surface materials are saturated with C and N.

Whether Mercury has a magnetic field or not, some gases must evolve from the planet itself. If Mercury is an active planet, volcanic gases such as H_2O, CO_2, CO, SO_2, or H_2S may enter the atmosphere at rates comparable to those on earth, Venus, or Mars. At the other geologic extreme, if Mercury is as inactive as the moon, its sources of gas may be limited mainly to the radiogenic species ^{4}He and ^{40}Ar.

LUNAR ANALOG OF THE HERMIAN ATMOSPHERE

For purposes of this discussion it is assumed that Mercury is geologically similar to the moon, at least at its surface. This theory implies a lack of significant gardening processes acting on the soil over the last several hundred million years. In addition, the magnetic field intensity of Mercury is presumed to be small enough that solar wind ions may impact the surface. Principal loss mechanisms for a moonlike atmosphere include thermal escape and photoionization followed by acceleration by the $\mathbf{v} \times \mathbf{B}$ fields in the solar wind. Thermal escape is important only for hydrogen and helium, whereas photoionization affects all species. Chemical removal of active gases is probably not important if there is little gardening activity to bring new materials to the surface.

As on the moon the major noncondensable gases on Mercury are likely to be H_2, ^{4}He, and ^{20}Ne, all of which arise because of the impinging solar wind. To find Hermian abundances and distributions of these gases, it is convenient to use the Monte Carlo technique described by *Hodges* [1973] and *Hodges et al.* [1974], in which the distribution of the downward flux of molecules of a given species at the surface is found by recording the impact points of a molecule as it traverses the surface of the planet in a succession of random ballistic trajectories. Maxwellian statistics are used to determine the distribution of trajectories. A molecule is lost from the atmosphere whenever its speed exceeds the escape velocity or when the time a trajectory is in sunlight exceeds a random deviate of an exponential distribution of photoionization time. Whenever a molecule is lost, the location of the point of creation of the next molecule is chosen according to a source distribution.

The present calculation scheme differs from the earlier version [*Hodges*, 1973] in that the average values of the radial component of velocity for downcoming and upgoing particles, $\langle v_D \rangle$ and $\langle v_U \rangle$, respectively, are found in addition to the relative distribution of molecular impacts per unit area I. To convert I to a particle flux, it is necessary to introduce the flux amplitude Φ_0, i.e., the flux of molecules colliding with the surface is

$$\Phi_D = \Phi_0 I \tag{1}$$

The concentration of downcoming molecules at the surface is $\Phi_D/\langle v_D \rangle$. As these particles are presumed to return to the atmosphere after a surface collision, their upgoing flux is also Φ_D and their concentration is $\Phi_D/\langle v_U \rangle$. In addition, the release of gas from the surface produces a concentration of $\Phi_S/\langle v_U \rangle$, if the average radial velocity is assumed to be $\langle v_U \rangle$ for all upgoing particles. Thus the total concentration is

$$n = (\Phi_D/\langle v_D \rangle) + [(\Phi_D + \Phi_S)/\langle v_U \rangle] \tag{2}$$

If the gas is assumed to be Maxwellian as it leaves the surface

$$\langle v_U \rangle = \langle v \rangle/2 = \tfrac{1}{2}(8kT/\pi m)^{1/2} \tag{3}$$

where k is Boltzmann's constant, T is surface temperature, and m is molecular mass. The average downcoming velocity $\langle v_D \rangle$ may differ from $\langle v_U \rangle$ because the downward velocity distribution does not include speeds greater than the speed for escape and also because this distribution corresponds to a composite effect of the varying temperature at the origins of trajectories, which end at the point of interest.

A prevalent assumption regarding the source flux Φ_S on the moon is that implanted solar wind gases are released into the atmosphere in proportion to the local solar wind influx [cf. *Hodges*, 1973; *Hodges et al.*, 1974; *Hartle and Thomas*, 1974]. It is also generally assumed that half of the photoions produced in the atmosphere are reimplanted in surface rocks [*Manka and Michel*, 1971]. Thus equilibrium of trapped solar wind gases in rocks requires that the total source flux equal the total solar wind flux plus half the total photoionization rate. If release of trapped atoms is spatially correlated with the solar wind influx, then

$$\Phi_S = \begin{cases} \left(\Phi_{SW} + \dfrac{N_S}{2\pi R^2 \tau_i}\right) \cos \chi & \chi < \pi/2 \\ 0 & \chi \geq \pi/2 \end{cases} \tag{4}$$

where χ is the solar zenith angle, Φ_{SW} is the solar wind flux of ions responsible for the gas in question, N_S is the total number of molecules in sunlight, R is the Hermocentric radius, and τ_i is the photoionization time constant.

Equilibrium of atmospheric content requires that the total source of new molecules equal the total rate of loss of atmosphere, i.e.,

$$R^2 \int d\Omega\, \Phi_S = \frac{N_S}{\tau_i} + R^2 \int d\Omega (\Phi_D + \Phi_S)(1 + E)e^{-E} \tag{5}$$

where $d\Omega$ is the differential element of the solid angle and the support of the integrand is the spherical surface of the planet. The left-hand side gives the total rate of effusion of new gas molecules from the surface. The first term on the right-hand side is the ratio of the total number of particles in sunlight to the mean lifetime, giving the total rate of photoionization, whereas the second term gives the rate of loss due to Jeans's thermal evaporation mechanism. The escape factor E is given by

$$E = GMm/kTR \tag{6}$$

where GM is the gravitational parameter for the planet.

Among the data accumulated in the Monte Carlo calculation are average molecular lifetime $\langle t_L \rangle$ and average time spent in sunlight $\langle t_S \rangle$. The ratio of these parameters is obviously

$$\langle t_S \rangle/\langle t_L \rangle = N_S/N_T \tag{7}$$

where N_T is the total atmospheric content of the species in question and is also defined by

$$N_T = \langle t_L \rangle R^2 \int d\Omega\, \Phi_S \tag{8}$$

Manipulation of expressions (5), (7), and (8) leads to

$$N_S = \pi R^2 \Phi_{SW} \langle t_S \rangle / (1 - \langle t_S \rangle / 2\tau_i) \tag{9}$$

$$\Phi_S = \Phi_{SW} \cos \chi u(\cos \chi)/(1 - \langle t_S \rangle / 2\tau_i) \tag{10}$$

where u is the unit step function. Substitution of these relations in equation (5) gives the flux amplitude

$$\Phi_0 = \frac{\pi\Phi_{SW}(1 - B - \langle t_S\rangle/\tau_i)}{A(1 - \langle t_S\rangle/2\tau_i)} \tag{11}$$

where

$$A = \int d\Omega\ I(1 + E)e^{-E} \tag{12}$$

$$B = \frac{1}{\pi}\int d\Omega \cos\chi\ u(\cos\chi)(1 + E)e^{-E} \tag{13}$$

This result is not useful for heavy gases that do not escape thermally (e.g., neon) because neither A nor $\langle t_S\rangle$ can be evaluated with sufficient accuracy.

An alternative for heavy gases is to use the barometric approximation, so that N_S can be expressed as

$$N_S = R^2 \int d\Omega\ nH\{u(\cos\chi) + u(-\cos\chi) \cdot \exp[E(1 - \csc\chi)]\} \tag{14}$$

where H is the scale height

$$H = R/E \tag{15}$$

and the altitude of cutoff of sunlight at night is approximated as the midpoint between the umbra and the penumbra (R csc χ). Combining equations (1), (2), (5), and (14) leads to

$$\Phi_0 = \frac{\pi\Phi_{SW}(1 - B - 2D)}{A + C + BC - AD} \tag{16}$$

where

$$C = \frac{1}{2\tau_i}\int d\Omega\ IH\left(\frac{1}{\langle v_D\rangle} + \frac{1}{\langle v_U\rangle}\right) \cdot \{u(\cos\chi) + u(-\cos\chi)\exp[E(1 - \csc\chi)]\} \tag{17}$$

$$D = \frac{1}{\pi\tau_i}\int d\Omega\ \frac{H}{\langle v\rangle}\cos\chi\ u(\cos\chi) \tag{18}$$

The consistency of expressions (11) and (16) has been established by the fact that both gave essentially the same result for helium in the calculations that are discussed subsequently.

Planetary and orbital parameters used in the present calculations are based on the data of *Ash et al.* [1967] and are given in the following list:

Parameters	Values
Planet radius (R)	2.42×10^3 km
GM	2.18×10^4 km^3/s^2
Surface escape speed	4.24 km/s
Orbit semimajor axis	0.3871 AU
Orbital eccentricity	0.2056
Perihelion distance	0.3075 AU
Aphelion distance	0.4667 AU

The temperature model adopted here is similar to that assumed by *Yeh and Chang* [1972] for the moon, in which the daytime temperature corresponds to radiative equilibrium with insolation, whereas the nighttime temperature is approximated by a constant. Owing to similarities of the spectral reflectivity of Mercury with various lunar regions [*McCord and Adams*, 1972] it is assumed that the ratio of subsolar temperatures of these planets is the ¼ power of the ratio of the solar radiation flux. Thus if the lunar temperature maximum is approximated as 390°K, then the daytime temperature of Mercury is given by

$$T = 390R_S^{-1/2}\cos^{1/4}\chi \tag{19}$$

where R_S is the sun-Mercury distance in astronomical units. From perihelion to aphelion the maximum daytime temperature of Mercury varies from 703° to 571°K. At night and very near the terminator in daytime the temperature is assumed to be 111°K in accordance with the infrared measurement of *Murdock and Ney* [1970].

The solar wind flux of protons at 1 AU is assumed to be 3×10^8 cm^{-2} s^{-1}, that of helium ions is 1.4×10^7 cm^{-2} s^{-1}, and that of ^{20}Ne ions is 2.4×10^4 cm^{-2} s^{-1}. The bases for these fluxes are discussed in *Hodges et al.* [1974] and *Johnson et al.* [1972]. Photoionization lifetimes at 1 AU adopted here are 10^7 s for H_2, 1.7×10^7 s for helium [*Kockarts*, 1973], and 6×10^6 s for neon [*Manka*, 1972]. Table 1 lists extrapolations of these parameters to Mercury at perihelion and aphelion. In addition, daytime values of Jeans's escape parameter E and escape probability, $(1 + E)\exp(-E)$, are given along with diurnal limits of the scale height. It can be noted that the daytime values of E for hydrogen are comparable to the lunar value for helium.

Calculated atmospheric models for a lunar analog of Mercury at perihelion and aphelion are shown in Figures 1 and 2, respectively. The H_2 graphs correspond to 2×10^5 molecular trajectories each, whereas those for helium and neon are each based on data from 2×10^6 trajectories. All gases have maximum concentration at night roughly in accordance with the $T^{-5/2}$ law of exospheric equilibrium [*Hodges and Johnson*, 1968]. Table 2 lists numerical data for the perihelion and aphelion model atmospheres. Atmospheric mass is found by application of equation (8).

DISCUSSION

A model of the helium distribution on Mercury at aphelion has been calculated by *Hartle et al.* [1973]. Scaling their normalized graphical results for a solar wind source indicates a concentration of about 1.5×10^6 cm^{-3} at the subsolar point and about 4×10^7 cm^{-3} at night. The present model gives a greater daytime concentration but essentially the same nighttime result. A difference in the daytime concentrations from these two models should be expected owing to the neglect of photoionization as a loss process in the model of Hartle et al. It may seem that the model of Hartle et al. should have given a greater daytime abundance, but the converse result is understandable because the effect of photoionization is to increase the source rate due to recycling of half of the photoionized particles, which are reimplanted in the surface of the planet.

One of the interesting facets of the present atmospheric models is that helium and hydrogen are more abundant than neon, whereas on the moon the opposite is true [*Hodges et al.*, 1974]. This situation is mainly because of a large difference in the daytime escape probability for helium between the planets, i.e., for helium at 0 solar zenith angle on Mercury

$$(1 + E)e^{-E} \cong 0.0043 \text{ to } 0.015 \tag{20a}$$

and on the moon

$$(1 + E)e^{-E} \cong 0.15 \tag{20b}$$

TABLE 1. Atmospheric Parameters for Mercury

	Perihelion			Aphelion		
	H_2	^4He	^{20}Ne	H_2	^4He	^{20}Ne
Solar wind influx, molecules/s	2.9×10^{26}	2.6×10^{25}	4.6×10^{22}	1.3×10^{26}	1.1×10^{25}	2.0×10^{22}
Photoionization time, s	9.5×10^{6}	1.6×10^{6}	5.7×10^{5}	2.2×10^{7}	3.6×10^{6}	1.3×10^{6}
Daytime escape parameters						
Escape factor E	3.1	6.2	31	3.8	7.6	38
Escape probability $(1 + E)e^{-E}$	0.19	0.015	10^{-12}	0.11	0.0043	10^{-15}
Scale height H, km						
Subsolar point	780	390	78	640	320	64
Night	124	62	12	124	62	12

Since escape of helium is considerably less likely on Mercury, its abundance there becomes more closely related to the slower process of photoionization loss. It can be noted in Table 2 that the lifetimes of neon and helium are comparable, and hence the ratio of their abundances is roughly the same as the ratio of their sources of supply.

The maximum gas concentration on Mercury is about 4.5×10^7 cm^{-3}. If a collision cross section of about 3×10^{-16} cm^2 for helium is assumed, the mean free path length at night is about 75 km, which corresponds roughly to the helium scale height (cf. Table 1). It has been shown [*Hodges*, 1972] that the transition between thermospheric and exospheric lateral transport processes occurs at about the altitude where the mean free path length is equal to twice the scale height of the transported gas. The depth of the transition region is the order of the scale height of the dominant gas, and thus the exospheric theory used above is probably applicable to helium, and certainly it applies to neon. However, there is a legitimate question regarding hydrogen. The nighttime mean free path length is twice the scale height of H_2 (i.e., 250 km) at an altitude of about 90 km. Thus the nighttime data for H_2 given in Figures 1 and 2 and in Table 2 probably refer to an exobase level at 90 km, and the nighttime surface concentrations of H_2 are likely to be about twice the indicated values.

In daytime there is no question that the exobase is the surface of the planet and that the exospheric transport theory applies. The concentrations appear to be too small to permit formation of an ionosphere with sufficient conductivity to cause a deflection of a significant fraction of the solar wind around the planet, as seems to occur on Mars and Venus.

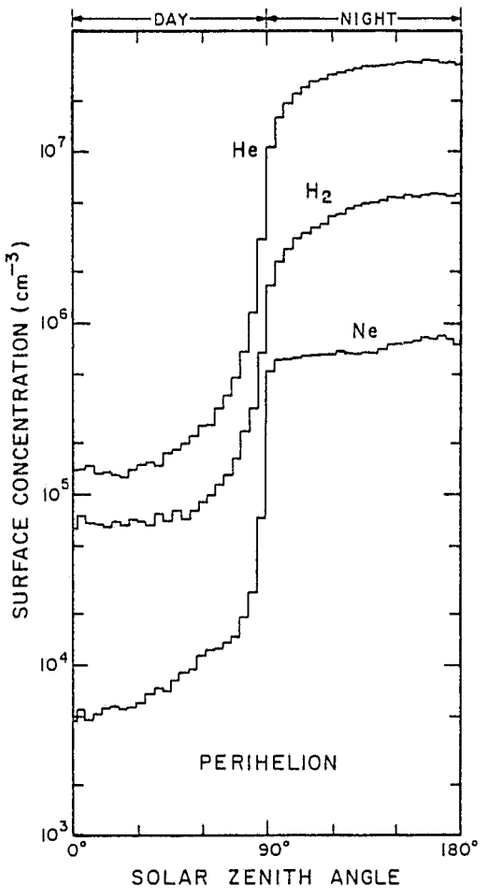

Fig. 1. Perihelion model atmosphere surface concentrations of helium, hydrogen, and neon as functions of solar zenith angle.

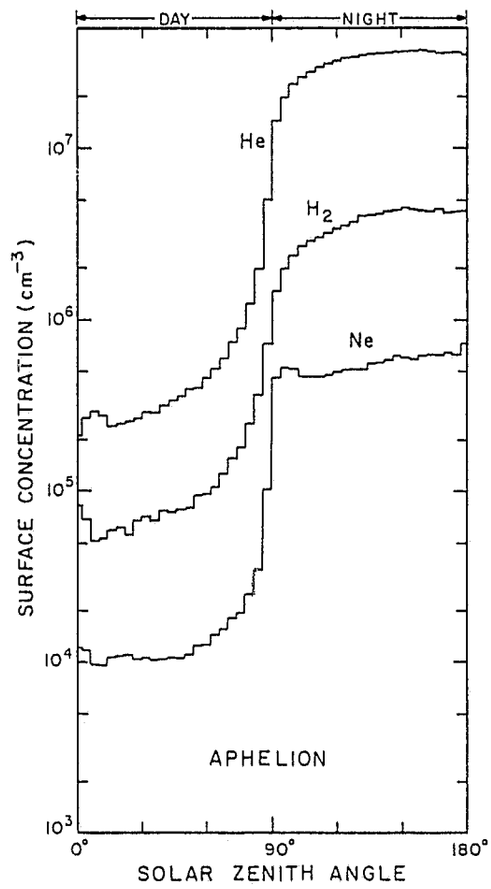

Fig. 2. Aphelion model atmosphere surface concentrations for helium, hydrogen, and neon as functions of solar zenith angle.

TABLE 2. Mercury Model Atmosphere Data (Lunar Analog)

	Perihelion			Aphelion		
	H_2	^4He	^{20}Ne	H_2	^4He	^{20}Ne
Concentration, cm^{-3}						
Day	7×10^4	1.4×10^6	6×10^5	6×10^4	2.5×10^6	1×10^4
Night	5.5×10^6	3.3×10^7	7×10^6	4.5×10^6	3.7×10^7	6×10^6
Atmospheric mass, tons	240	555	12	200	623	8
Molecular lifetime, s	2×10^5	2×10^6	4×10^6	4×10^5	6×10^6	6×10^6
Probability of escape	5.4	1.2	~0	6.2	0.8	~0
Probability of photoionization						

There are some important uncertainties associated with the foregoing model. The degree of saturation of surface materials with solar wind gases may not be great enough to cause the atmosphere to be in balance with the solar wind. Because of this possibility the present results must be regarded as upper bounds on atmospheric gas abundances. A similar argument can also be applied if Mercury has a magnetic field that limits the amount of the solar wind reaching the planet. Then the ion influx would be less, and the likelihood of trapping impinging ions would be greater. However, the probability of escape of the photoions would be less. The net result should be a decrease in the H_2 and He levels because thermal escape is not affected by a magnetic field. It could also cause an increase in the amount of neon, due to inhibition of the photoionization loss process.

This theory leaves the nagging question of what gases may constitute the atmosphere of Mercury if there is a strong magnetic field at present. It should be noted that the absence of evidence of a dense atmosphere is probably a good argument against expecting a strong steady state magnetic field because such a field would have acted to trap photoions, precluding escape of heavy volcanic and radiogenic gases, which would have formed an atmosphere. However, a fluctuating magnetic field that has been quite weak in the recent past but is presently strong is a possibility to which the present lunar analogy does not apply.

Acknowledgments. It is a pleasure to acknowledge the work of H. D. Hammack in the programming of numerical computations. This research was supported by NASA under grant NGL 44-004-026.

* * *

The Editor thanks R. E. Hartle and another referee for their assistance in evaluating this paper.

REFERENCES

Ash, M. E., I. I. Shapiro, and W. B. Smith, Astronomical constants and planetary ephemerides deduced from radar and optical observations, *Astron. J.*, *72*, 338, 1967.

Belton, M. J. S., D. M. Hunten, and M. B. McElroy, A search for an atmosphere on Mercury, *Astrophys. J.*, *150*, 1111, 1967.

Fastie, W. G., P. D. Feldman, R. C. Henry, H. W. Moos, C. A. Barth, G. E. Thomas, and T. M. Donahue, A search for ultraviolet emissions from the lunar atmosphere, *Science*, *182*, 710, 1973.

Hartle, R. E., and G. E. Thomas, Neutral and ion exosphere models for lunar hydrogen and helium, *J. Geophys. Res.*, *79*, 1519, 1974.

Hartle, R. E., K. W. Ogilvie, and C. S. Wu, Neutral and ion-exospheres in the solar wind with applications to Mercury, *Planet. Space Sci.*, *21*, 2181, 1973.

Hodges, R. R. Applicability of a diffusion model to lateral transport in the terrestrial and lunar exospheres, *Planet. Space Sci.*, *20*, 103, 1972.

Hodges, R. R., Helium and hydrogen in the lunar atmosphere, *J. Geophys. Res.*, *78*, 8055, 1973.

Hodges, R. R., and F. S. Johnson, Lateral transport in planetary exospheres, *J. Geophys. Res.*, *73*, 7307, 1968.

Hodges, R. R., J. H. Hoffman, and F. S. Johnson, Lunar atmosphere, *Icarus*, in press, 1974.

Johnson, F. S., J. M. Carroll, and D. E. Evans, Lunar atmospheric measurements, *Geochim. Cosmochim. Acta*, *36*, *Suppl. 3*, 2231, 1972.

Kockarts, G., Helium in the terrestrial atmosphere, *Space Sci. Rev.*, *14*, 723, 1973.

Manka, R. H., Lunar atmosphere and ionosphere, Ph.D. thesis, Rice Univ., Houston, Tex., 1972.

Manka, R. H., and F. C. Michel, Lunar atmosphere as a source of lunar surface elements, *Geochim. Cosmochim. Acta*, *35*, *Suppl. 2*, 1717, 1971.

McCord, T. B., and J. B. Adams, Mercury: Interpretation of optical observations, *Icarus*, *17*, 585, 1972.

Murdock, T. L., and E. P. Ney, Mercury: The dark side temperature, *Science*, *170*, 535, 1970.

Turekian, K. K., Degassing of argon and helium from the earth, in *The Origin and Evolution of Atmospheres and Oceans*, edited by P. J. Brancazio and A. G. W. Cameron, p. 74, John Wiley, New York, 1964.

Yeh, T. T. J., and G. K. Chang, Density and flux distributions of neutral gases in the lunar atmosphere, *J. Geophys. Res.*, *77*, 1720, 1972.

(Received February 4, 1974;
accepted April 22, 1974.)

Proc. Lunar Sci. Conf. 6th (1975), p. 3039–3047.
Printed in the United States of America

Implications of atmospheric ^{40}Ar escape on the interior structure of the moon

R. R. HODGES, JR. and J. H. HOFFMAN

The University of Texas at Dallas, Richardson, Texas 75080

Abstract—Radiogenic ^{40}Ar escapes from the lunar atmosphere at a rate of about 2×10^{21} atoms/sec. This amounts to 8% of the rate of argon production in the entire moon by potassium decay. A curious feature of the argon escape rate is a variability with time scale of several months. It is shown that the variation in argon loss correlates with high-frequency lunar teleseismic events. The only apparent region of the moon which could possibly supply the amount of argon needed for escape via a plausible temporal mechanism is a semimolten asthenosphere which may be entirely primitive unfractionated lunar material, or an Fe–FeS core that is enriched in potassium. A core that is devoid of potassium is not compatible with the atmospheric argon measurements.

INTRODUCTION

ONE OF THE MOST ABUNDANT GASES of the lunar atmosphere is radiogenic ^{40}Ar, which is produced within the moon as part of the decay of ^{40}K. The fact that argon is an important atmospheric species is somewhat puzzling in view of the difficulty involved in transporting an argon atom from its place of formation deep within the solid moon to the surface and then into the atmosphere. This has spurred the development of a succession of progressively more realistic models of the argon atmosphere (cf. Hodges *et al.*, 1974; Hodges and Hoffman, 1974; Hodges, 1975), with a view toward accurate determination of the relationship between atmospheric concentration measurement and the argon escape rate. Briefly, the rate of escape of ^{40}Ar from the moon appears to be variable, implying an episodic process of release of this radiogenic gas from the interior of the moon. The average rate of loss of argon from the lunar atmosphere is about 2×10^{21} atoms/sec, which is about 8% of the present argon production rate for the entire moon (2.4×10^{22} atoms/sec) if the average lunar potassium abundance is about 100 ppm as suggested by Taylor and Jakeš (1974) and by Ganapathy and Anders (1974). To put these rates in planetologic perspective, the present rate of release of ^{40}Ar needed to account for its 1% abundance in the terrestrial atmosphere should be about 1.1×10^{24} atoms/sec if the fraction of total production effusing into the atmosphere has remained constant over geologic time. For a lunar equivalent mass of earth this rate amounts to 1.4×10^{22} atoms/sec.

It is surprising that although the rates of effusion of ^{40}Ar from the moon and earth are comparable, their atmospheric abundances differ by more than 15 orders of magnitude. The answer to this puzzle lies in differing escape processes. On earth the escape of argon ions is inhibited by the geomagnetic field, so that almost all of the argon ever released is now present in the atmosphere. However, the lack of both a lunar magnetic field and an ionosphere allows the solar wind to impinge

REPRODUCIBILITY OF THE
ORIGINAL PAGE IS POOR

directly on the planet, and hence, to accelerate any ions formed near the moon. As a result the average lifetime for lunar argon is only about 80–100 days. The product of lifetime and loss rate gives the atmospheric argon content to be only about 10^6 g, most of which resides on the nighttime surface as a result of adsorption.

SUMMARY OF EXPERIMENTAL RESULTS

All available measurements of ^{40}Ar were obtained with the Apollo 17 mass spectrometer during the first nine lunations of 1973. The malfunctioning of a power supply has precluded data collection since that time. A further limitation is that only nighttime data were obtained, owing to a large artifact gas background in daytime due to degassing of remnant spaceflight hardware at the landing site. However, the nighttime data clearly show the synodic variation of ^{40}Ar.

Figure 1 shows the measured ^{40}Ar concentration inferred from the 40 a.m.u. mass spectrometric measurements during two different lunations (Hodges and Hoffman, 1974). The dashed curves are theoretical extrapolations into daytime (Hodges, 1975). An important facet of these graphs, the change in the amount of argon on the moon by about a factor of 2 in a four-month interval, is discussed in detail later.

The synodic variation of argon is characteristic of a condensible gas. The slow post-sunset decrease in concentration indicates an increasing adsorption probability with decreasing temperature, while the nearly asymptotic behavior of the nighttime minimum requires a desorption time on the order of a day. At sunrise the bulk of the adsorbed gas is released from the lunar surface, and some of it travels into the nighttime hemisphere, giving rise to the rapid pre-sunrise increase. Incidentally, it is the pre-sunrise buildup which marks this data as an actual indication of a lunar gas; there is no apparent way for an artifact release to anticipate sunrise in this manner.

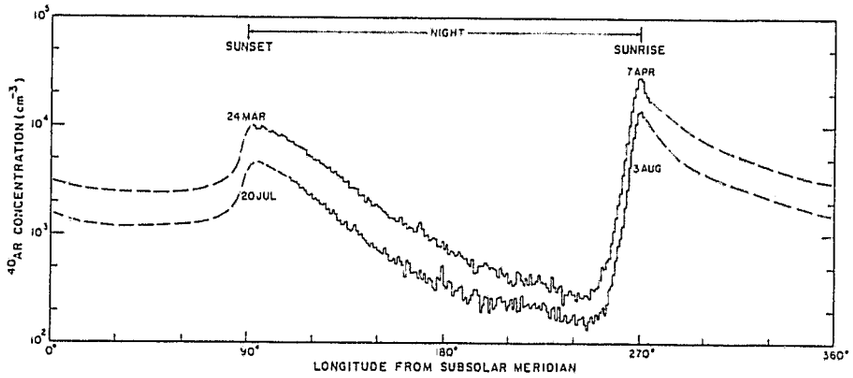

Fig. 1. Synodic variation of ^{40}Ar concentration at the Apollo 17 site during lunations of maximum and minimum argon abundances in 1973. Dashed curves are theoretical extrapolations which show predicted daytime behavior (from Hodges, 1975).

A series of Monte Carlo atmospheric simulations has been calculated for argon based on a technique first reported by Hodges (1973). Briefly, the modeling technique simulates the lunar atmosphere by following the trajectories of a succession of individual molecules over the surface of the moon, from creation to annihilation. Global variations of statistical parameters, such as the effects of temperature on the velocity distribution of atoms following surface encounters, and probabilities of adsorption, desorption, creation, and photoionization are taken into account. Particle lifetime is found by accumulating total time of flight and of adsorption. In these model calculations, surface adsorption and desorption dependencies on temperature and solar illumination were iteratively adjusted until the synodic variation at the Apollo 17 latitude (20°) of the model distribution matched the average measured variation. Two forms of desorption are needed to explain the data. The first is the spontaneous process of thermal desorption, and the second is a photon process in which qualitative laboratory tests show that certain gases, including argon, are released from a surface by the visible range of the solar spectrum. In order that the model reproduce the measured sunrise to sunset concentration ratio it is necessary to assume that the illumination of a soil grain surface causes the release of adsorbed atoms with unity probability. To account for soil texture and orography it has been assumed that the probability of illumination of an exposed soil surface increases from 0 to 0.5 as lunar rotation moves the grain through a band of $\pm 2°$ of solar zenith angle about the spherical moon–sunrise terminator, and that the probability of illumination of the remaining surface area increases linearly thereafter with increasing zenith angle. In practice about half of the atoms adsorbed at low latitude are released by the photon interaction process, while spontaneous desorption is more likely at high latitudes where the time needed for sunrise to traverse the orographic uncertainty becomes quite long.

Among the parameters to emerge from the model study are the following. Average argon lifetime on the moon is about 100 days, of which 80% of the time is spent adsorbed on the surface. The average sticking time for an adsorbed atom is 1.1 days. The rate of photoionization of argon in the lunar atmosphere (number of atoms per second) is about 9×10^{16} times the sunrise concentration at the Apollo 17 latitude (20°). Thus the loss rate corresponding to the average measured argon sunrise concentration in 1973 is about 2×10^{21} atoms/sec.

Figure 2 shows the temporal variation of the total argon photoionization rate during 1973. It should be noted that this rate is proportional to both atmospheric abundance and to escape rate. Triangles represent the most accurate determinations of the photoionization rate at sunrises where the concentration is greatest. Each circle gives the rate found by model extrapolation of a 5° longitudinal average of concentration to an equivalent sunrise concentration. High values of the circles early in the year are due to a decaying artifact contribution to the low-nighttime concentration. The large variance of the photoionization rate represented by the circles is indicative of the noise inherent in the nighttime concentration data and errors in the model.

Two important aspects of the ^{40}Ar rate show up clearly in Fig. 2. First, the time

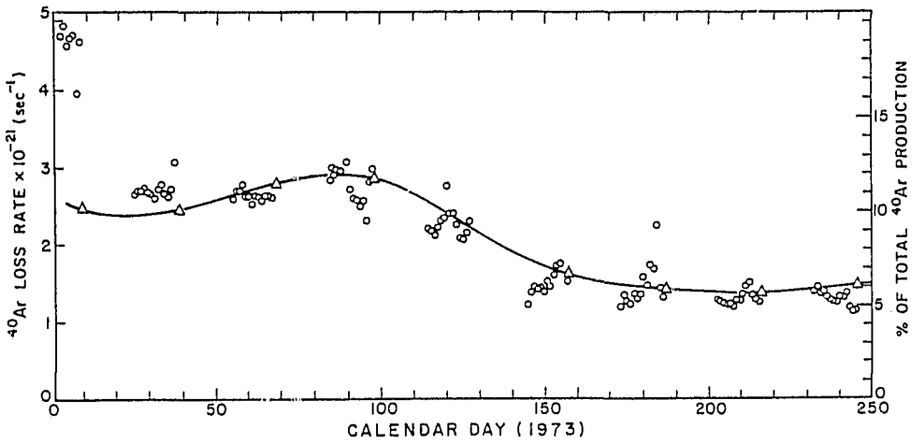

Fig. 2. Temporal variation of the rate of loss of ^{40}Ar from the lunar atmosphere due to photoionization during 1973.

average of the loss rate is roughly 2×10^{21} atoms/sec, corresponding to about 8% of the total lunar production of ^{40}Ar if the potassium abundance is 100 ppm. If a large fraction of the photoions were to impact the lunar surface and subsequently become recycled into the atmosphere, then the actual source of new atoms would be a lesser part of the production rate. However, the second obvious feature of Fig. 2, the time variation of the photoionization rate (and hence of argon abundance), argues strongly that there is very little recycling of ^{40}Ar. The clue that argon recycling is unimportant is found in the decay of the photoionization rate between about day 100 and day 150, where the decay time-constant is roughly equivalent to the average lifetime of argon atoms, i.e. about 100 days.

If ψ_s is used to denote the total rate of supply of atoms, both new and recycled, to the atmosphere and ψ_l is the photoionization rate, then continuity requires

$$\psi_s = \psi_l + \tau \frac{d\psi_l}{dt} \tag{1}$$

where τ is the average atomic lifetime. Figure 3 shows the argon source, ψ_s, required to supply the photoionization rate shown in Fig. 2 for three values of the lifetime τ.

An important feature of Eq. (1), and hence of Fig. 3, is that the total argon source must include an essentially constant contribution from recycled atoms, and that temporal variation of ψ_s must arise from internal changes in the moon which affect the rate of release of new argon atoms. Since ψ_s is a positive definite quantity, it is obvious that the lifetime which emerges from the atmospheric model calculations, 100 days, is nearly an upper bound. In addition, the 100-day lifetime allows for very little recycled argon. A decrease in the lifetime to 60 days would be consistent with a recycling rate of about 8×10^{20} atoms/sec or roughly 40% of

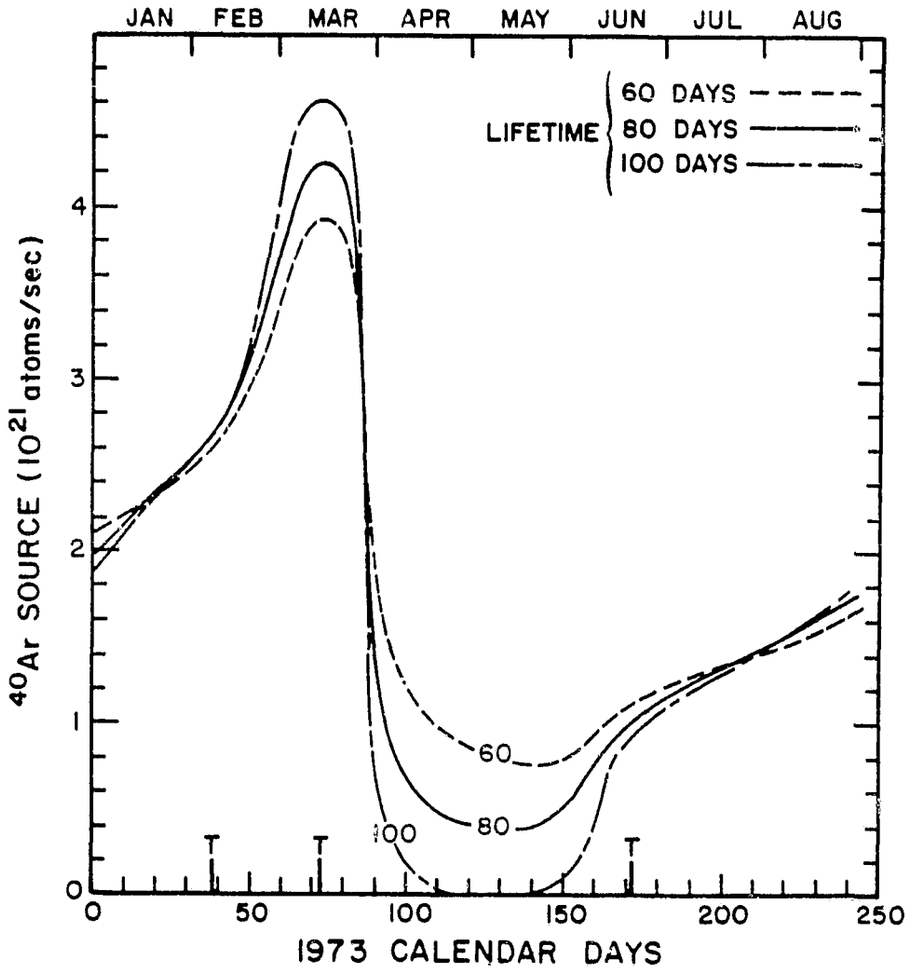

Fig. 3. Rate of supply of ^{40}Ar needed to explain the time-varying loss rate shown in Fig. 2. Marks denoted by T on the lower abscissa give the times of occurrence of high-frequency teleseismic events reported by Nakamura *et al.* (1974).

the total source. However, model calculations for a wide variety of surface parameters have consistently given a lifetime in excess of 80 days. The shortest model lifetimes occur when adsorption probability is increased near the poles, but this always produces an inconsistently large sunset concentration at the Apollo 17 latitude (20°). Thus the best judgment is that the recycling fraction of the total argon photoionization rate is quite small, and that it probably is less than 10% to be consistent with a lifetime in the 80–100-day range. This constrains the rate of release of retrapped, parentless ^{40}Ar from the regolith.

On the lower abscissa of Fig. 3 there are three events each denoted by *T*. These mark high-frequency lunar teleseismic events reported by Nakamura *et al.* (1974) during the argon measurement period. It is interesting to note that each of these events accompanies a rise in the argon source. In addition, the event on day 72, which was the largest such event recorded on the moon, coincided with the peak of the argon source. Owing to the inherent smoothing of the total atmospheric argon abundance due to its 100-day lifetime it is not possible to resolve the argon supply rate data on a finer side.

ARGON PRODUCTION IN THE MOON

The source of atmospheric ^{40}Ar is clearly potassium, but the magnitude and time variability of the argon escape rate have nontrivial implications on the internal structure of the moon. What is needed is the identification of the means by which about 8% of the lunar argon production has access to the atmosphere. In subsequent discussion various depth intervals of the moon are examined in terms of argon production and release mechanisms. It will become apparent that the seemingly obvious source regions are not capable of supplying the escaping argon.

Lunar surface

Trapped argon in the surface layer of the soil must be released by a solar-wind weathering process in a manner similar to the release of implanted solar-wind helium (Hodges and Hoffman, 1975). Typical abundances of trapped ^{40}Ar in returned soil samples are within an order of magnitude of 5×10^{-5} cc STP/g. If this number is taken as an estimate of the average abundance of argon in the entire regolith, then the release of the 2×10^{21} argon atoms/sec needed to supply the atmosphere would require a weathering process which removes about 75 cm of soil from the moon per million years. Since this erosion rate is several orders of magnitude greater than the soil escape rate determined by Fireman (1974) it is not reasonable to consider surface weathering to be an important source of atmospheric argon.

Regolith to 25 km depth

A monotonic increase in seismic velocities with depth to about 25 km has been explained by Toksöz *et al.* (1972) to indicate a pressure effect on soils and broken rocks near the surface, changing to rocks having micro and macro cracks at greater depth. Argon which has diffused from within rocks to surface or fracture boundaries should be an atmospheric source. The Apollo 15 and 16 orbital γ-ray spectrometer data reported by Metzger *et al.* (1974) suggests that the average potassium abundance of the surface lunar soil is about 1000 ppm, while geochemical models of Taylor and Jakeš (1974) indicate a crust average of 600 ppm. Accepting these as representative estimates of the potassium abundance in the

upper 25 km of the moon, the rate of argon production there is in the range of $3–5 \times 10^{21}$ atoms/sec. Release of 2×10^{21} atoms/sec (the atmospheric escape rate) would imply loss of about half of the argon production. Returned regolith samples do not generally exhibit a depletion of ^{40}Ar that would confirm this loss process. In addition, there is no time dependent phenomenon which would vary the argon release rate on the time scales observed in the Apollo 17 mass spectrometer data.

Lower crust and upper lithosphere (25–300 km)

Seismic data reveal the beginning of a competent rock layer at about 25 km depth and an apparently petrological discontinuity at about 65 km, marking the upper boundary of the mantle (Toksöz *et al.*, 1972). Nearly constant seismic velocities suggest a lack of rock fracturing. The geochemical models of the lunar interior of Taylor and Jakeš (1974) indicate that about 70% of the moon's potassium has been captured in this region by differentiation. However, the release of enough radiogenic argon from solid rock to supply escape is not a practical postulate, even if increasing temperature with depth is considered to increase the argon diffusion velocity. Again there is no practical mechanism to cause temporal changes in the release rate.

Lower lithosphere (300–1000 km)

Differentiation is thought to have depleted this region of potassium (Taylor and Jakeš, 1974) so it should not be a source of argon.

Asthenosphere (below 1000 km)

The central part of the moon is thought to be semimolten because seismic shear waves are attenuated below 1000 km (Latham *et al.*, 1973). Two viable, alternate models of this asthenosphere have been proposed by Taylor and Jakeš (1974). One is a conventional Fe–FeS core formed early in lunar evolution. If the process of formation of such a core should have fractionated the entire moon, displacing all potassium from the core, then there is no apparent explanation of the atmospheric argon. However, a core in which potassium has been concentrated is a plausible source of argon.

The alternative asthenosphere model of Taylor and Jakeš (1974) is a region of primitive unfractionated material, remnant of an early melting of the outer 100 km of the moon. The present partially molten state of the asthenosphere commenced after fractionation of the lithosphere, and is maintained by radioactive decay of K, Th, and U. About 8% of the moon's potassium should be trapped below 1000 km if the whole moon average potassium abundance is 100 ppm. This is sufficient to supply the atmosphere provided that all of the argon escapes, which in turn seems to imply that either the semimolten state is pervasive of the entire asthenosphere, or that the asthenosphere has gradually fractionated to form

pockets of material rich in K, Th, and U, which are naturally hot and from which argon can readily escape.

DISCUSSION

The only apparent, viable explanation of the lunar atmospheric argon is that it effuses from a semimolten asthenosphere. In addition, it is necessary that the potassium abundance in the asthenosphere be at least as great as the whole moon average of 100 ppm.

The mechanism of conduction of argon from the asthenosphere to the atmosphere can be conjectured to involve a percolative process in which the gas collects either in bubble-like areas near the 1000 km depth, or in voids nearer the lunar surface. Subsequent increasing pressure could force the opening of deep fissures, causing sudden release of gas to the atmosphere.

A correlation of increases in the atmospheric argon supply rate with the high-frequency lunar teleseismic events reported by Nakamura *et al.* (1974) was discussed earlier (cf. Fig. 3). Time resolution of the argon source is not sufficiently accurate to establish that this correlation is not fortuitous, but its existence substantiates the above pressure release hypothesis. In addition, the seismic correlation supports the hypothesis advanced by Hodges and Hoffman (1974) that argon release may be the cause of some moonquake activity. The amount of seismic energy available from this process has an upper bound equal to the stored energy prior to release (i.e. pressure times volume). At 300 K the average argon escape rate could supply about 2×10^{15} ergs/yr, which is of the same order of magnitude as the bound on the total rate of seismic energy release from the moon reported by Latham *et al.* (1972).

Acknowledgments—This research has been supported by the National Aeronautics and Space Administration under contract NAS 9-12074 and under grant NSG-7034.

REFERENCES

Fireman E. L. (1974) Regolith history from cosmic-ray-produced nuclides. *Proc. Lunar Sci. Conf. 5th*, p. 2075–2092.

Ganapathy R. and Anders E. (1974) Bulk compositions of the moon and earth, estimated from meteorites. *Proc. Lunar Sci. Conf. 5th*, p. 1181–1206.

Hodges R. R. (1973) Helium and hydrogen in the lunar atmosphere. *J. Geophys. Res.* 78, 8055–8064.

Hodges R. R. (1975) Formation of the lunar atmosphere. *The Moon*. In press.

Hodges R. R. and Hoffman J. H. (1974) Episodic release of ^{40}Ar from the interior of the moon. *Proc. Lunar Sci. Conf. 5th*, p. 2955–2961.

Hodges R. R. and Hoffman J. H. (1975) Nonthermal escape of helium from the moon (abstract). In *Lunar Science VI*, p. 379–380. The Lunar Science Institute, Houston.

Hodges R. R., Hoffman J. H., and Johnson F. S. (1974) The lunar atmosphere. *Icarus* 21, 415–426.

Latham G., Ewing M., Dorman J., Lammlein D., Press F., Toksöz N., Sutton G., Duennebier F., and Nakamura Y. (1972) Moonquakes and lunar tectonism results from the Apollo passive seismic experiment. *Proc. Lunar Sci. Conf. 3rd*, p. 2519–2526.

Latham G., Dorman J., Duennebier F., Ewing M., Lammlein D., and Nakamura Y. (1973) Moonquakes, meteoroids, and the state of the lunar interior. *Proc. Lunar Sci. Conf. 4th*, p. 2515–2527.

Metzger A. E., Trombka J. I., Reedy R. C., and Arnold J. R. (1974) Element concentrations from lunar orbital gamma-ray measurements. *Proc. Lunar Sci. Conf. 5th*, p. 1067–1078.

Nakamura Y., Dorman J., Duennebier F., Ewing M., Lammlein D., and Latham G. (1974) High frequency lunar teleseismic events. *Proc. Lunar Sci. Conf. 5th*, p. 2883–2890.

Taylor S. R. and Jakeš P. (1974) The geochemical evolution of the moon. *Proc. Lunar Sci. Conf. 5th*, p.1287–1305.

Toksöz M. N., Press F., Dainty A., Anderson K., Latham G., Ewing M., Dorman J., Lammlein D., Sutton G., and Duennebier F. (1972) Structure, composition, and properties of lunar crust. *Proc. Lunar Sci. Conf. 3rd*, p. 2527–2544.

MOLECULAR GAS SPECIES IN THE LUNAR ATMOSPHERE*

J. H. HOFFMAN and R. R. HODGES, JR.
The University of Texas at Dallas, Richardson, Tex., U.S.A.

Abstract. There is good evidence for the existence of very small amounts of methane, ammonia and carbon dioxide in the very tenuous lunar atmosphere which consists primarily of the rare gases helium, neon and argon. All of these gases, except ^{40}Ar, originate from solar wind particles which impinge on the lunar surface and are imbedded in the surface material. Here they may form molecules before being released into the atmosphere, or may be released directly, as is the case for rare gases. Evidence for the existence of the molecular gas species is based on the pre-dawn enhancement of the mass peaks attributable to these compounds in the data from the Apollo 17 Lunar Mass Spectrometer. Methane is the most abundant molecular gas but its concentration is exceedingly low, 1×10^3 mol cm^{-3}, slightly less than ^{36}Ar, whereas the solar wind flux of carbon is approximately 2000 times that of ^{36}Ar. Several reasons are advanced for the very low concentration of methane in the lunar atmosphere.

1. Introduction

The lunar atmosphere is known to be extremely tenuous consisting principally of the rare gases helium, neon and argon. The origin of these gases, except for ^{40}Ar, is from the solar wind which impinges upon the lunar surface and is imbedded in the surface, material. If the surface is saturated with a gas of a particular solar wind constituent, this gas is released into the atmosphere at the same rate as it is accreted from the solar wind. Those gases which do not condense at the low nighttime lunar surface temperatures are distributed roughly as $T^{-5/2}$ throughout the lunar atmosphere (Hodges and Johnson, 1968). Since the daytime surface temperature is a factor of 4 higher than the nighttime surface temperature, there is roughly 30 times the gas concentration on the night side as on the day side. Furthermore, the concentrations of these noncondensable gases tend to be a minimum at the subsolar point and show a maximum late in the lunar night where the surface temperature is the lowest.

A condensable gas, that is one which is adsorbed on the surface at nighttime temperatures, will have minima in its distribution in both the daytime and nighttime with maxima at the terminators. Because such a gas is released quickly at the sunrise terminator by photon desorption or the rapid heating of the surface, this gas will have its maximum concentration at this location. An example of such a condensable gas is ^{40}Ar, whereas ^{4}He behaves as a noncondensable gas.

Since condensable gases exhibit their maximum concentrations at the sunrise terminator it is at this region that a search of the Apollo 17 Lunar Mass Spectrometer data has been made for other condensable gases in the lunar atmosphere. Most molecular gas species, such as CH_4 and NH_3, are expected to behave as condensable gases since argon behaves that way and their freezing points are above that of argon.

* Paper presented at the Conference on 'Interactions of the Interplanetary Plasma with the Modern and Ancient Moon', sponsored by the Lunar Science Institute, Houston, Texas and held at the Lake Geneva Campus of George Williams College, Wisconsin, between September 30 and October 4, 1974.

The Moon **14** (1975) 159–167. *All Rights Reserved*
Copyright © 1975 by D. Reidel Publishing Company, Dordrecht-Holland

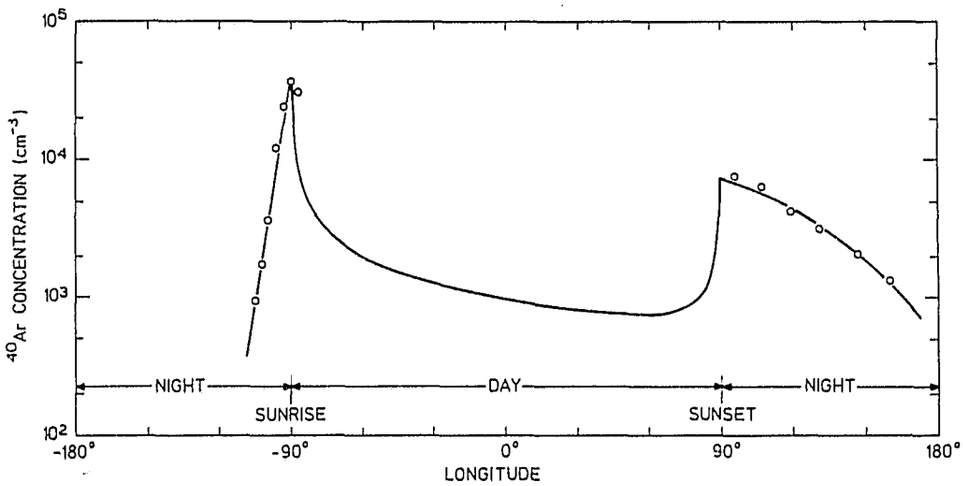

Fig. 1. Model for the distribution of ^{40}Ar as a function of longitude (with the sub-solar point at 0°) fitted to the data from the Apollo 17 Lunar Mass Spectrometer.

The reason for searching the sunrise region for such gases is that just prior to sunrise the lunar surface temperature and the temperature of the instruments on the lunar surface are at a minimum and therefore the contamination level of artifact gases is at a minimum, whereas a condensable gas shows a marked pre-dawn enhancement. That is, prior to the terminator crossing of a given point, gases which have been released from the approaching terminator region will travel in ballistic trajectories (as do all gas molecules as they move across the lunar surface) into the nighttime region a distance of between 1 and 2 scale heights. This phenomenon is manifested as an increase in concentration of such condensable gas species beginning some 10° before the terminator reaches the point in question and increasing steadily until shortly after the terminator has passed the point. Therefore, in order to determine whether a given gas species is truly a lunar gas rather than an artifact, it must exhibit a pre-dawn enhancement. To illustrate the behavior of a condensable gas, Figure 1 shows a model calculation (Hodges *et al.*, 1973) for the distribution of ^{40}Ar. The concentration of argon is plotted against the solar elevation angle, where 0° is the subsolar point, 90° is sunset and 270° is sunrise. This model curve has been fitted to argon data obtained from the Apollo 17 Lunar Mass Spectrometer. It shows clearly the pre-dawn enhancement starting some 10° before sunrise, the maximum just after sunrise, the minimum throughout the daytime with a lesser maximum at sunset and finally the nighttime minimum.

2. Instrumentation

The Apollo 17 carried amongst its ALSEP experiments a neutral magnetic sector field mass spectrometer designed to measure the composition of the lunar atmosphere. This instrument was deployed at the Taurus-Littrow landing site and operated

REPRODUCIBILITY OF THE ORIGINAL PAGE IS POOR

This article has been published originally in:

The Moon

An International Journal of Lunar Studies

Editors: H. ALFVÉN, *Royal Institute of Technology, Stockholm, Sweden;* Z. KOPAL, *University of Manchester, England;* H. C. UREY, *University of California, La Jolla, Calif., U.S.A.*

Editorial Office:
Managing Editor: Z. Kopal, *University of Manchester, England*;
Assoc. Man. Editor: M. D. Moutsoulas, *University of Athens, Greece*;
Editorial Assistant: Mrs. E. B. Carling-Finlay, *University of Manchester, England.*

Editorial Board: J. R. Arnold, J. A. Bastin, A. G. W. Cameron, D. H. Eckhardt, D. E. Gault, C. L. Goudas, Sh. T. Habibullin, T. Hagfors, B. W. Hapke, J. W. Head, L. D. Jaffe, Wm. M. Kaula, R. L. Kovach; K. Koziel, D. Lal, G. V. Latham, F. Link, E. J. Öpik, G. H. Pettengill, A. E. Ringwood, L. B. Ronca, J. W. Salisbury, R. W. Shorthill, C. P. Sonett, D. W. Strangway, M. N. Toksoz, V. S. Troitski, F. B. Waranius, D. F. Winter.

The aim of this journal is to provide an inter-disciplinary but monothematic medium for publication of the results of original investigations in all fields of lunar studies – including astronomy (both optical and radio-astronomy), astronautics, chemistry, geology, space physics, and all other aspects of the scientific study of our satellite by spacecraft as well as by the more traditional approaches of groundbased astronomy.

Subscription Information:
One volume of 500 pages in 4 issues. Price per volume Dfl. 155,– / US $62.00, plus postage and handling.
Private price per volume Dfl. 48,– / US $19.50, plus postage and handling.

Back Volumes:
Vols. 1–8 (1969–1973) Dfl. 165,– / US $66.00, per volume
Vols. 9–11 (1974) Dfl. 155,– / US $62.00 per volume

Indexed or abstracted by:
American Mathematical Monthly, Astrophysical Abstracts, Bulletins du BRGM, Chemical Abstracts, Geotitles Weekly, G.S.A. Bibliography Project, Geophysical Abstracts, IEEE Transactions, International Geology Review, Journal of Abstracts, Nuclear Science Abstracts, Office National d'Etudes et de Recherches Aerospatiales, Physikalische Berichte, Science Abstracts, Weltraumfahrt, Zentralblatt für Mathematik.

D. REIDEL PUBLISHING COMPANY
Dordrecht - Holland / Boston - U.S.A.

successfully for approximately 10 months from December 27, 1972, until mid October 1973. Data obtained from this instrument on the concentrations of the lunar atmosphere rare gases as well as upper limits on the concentrations of hydrogen and several other gases have been published (Hoffman *et al.*, 1974; Hodges *et al.*, 1974; Hodges and Hoffman, 1974a, b). The instrument was operated mainly during the nighttime as the daytime gas concentrations were extraordinarily high (10^7 cm^{-3} range), which precluded the operation of the instrument for long periods of time at these concentration levels. These daytime gases are considered to be artifact, coming from the landing site, the lunar module, the instruments of the ALSEP series and the lunar mass spectrometer itself. The concentrations of these gases did decay with time, albeit, at a relatively slow rate.

The instrument consisted of a magnetic sector field mass spectrometer which scanned the mass range from 1 to 110 amu with a sensitivity of approximately 1 count s^{-1} equals 200 mol cm^{-3} (Hoffman *et al.*, 1973). The scan of the mass spectrum was accomplished in 13.5 min and the data were telemetered back to earth through the ALSEP central station. The mass spectrum was divided into three channels which were scanned simultaneously covering the mass ranges from 1 through 4, 12 through 48, and 27 through 110 amu. An artifact ramp-like background of counts appeared on the mid mass channels starting at approximately mass 26 and extending through the end of the sweep at mass 12. Likewise, it appeared at mass 2 and extended through mass 1 on the low mass channel. The presence of this background ramp, which rose to a level of the order of 100 counts s^{-1} at the end of the mass sweep (low mass end) generally made the mid mass channel somewhat unusuable for the search for very low amplitude peaks from mass 26 through mass 12. This range of the spectrum of course covers that region where water vapor, methane and ammonia would be found. However, during the sixth and seventh lunations the ramp was compressed by thermal cycling of the electronics, until it reached a sufficiently low level that the mass 18 through 12 range was completely free of background counts. It is at this time that a search has been made for the existence of molecular gas species on the Moon.

3. Results

The counting rates for 10 different gas species shown in Figures 2 and 3 are plotted as a function of normal elevation of the Sun from 340° to 10°. The point at which the terminator crosses the Apollo 17 site corresponds to a normal elevation of 360° (or 0°). Since the Taurus-Littrow site is essentially a valley surrounded by hills on most sides, the Sun must rise to between 4 and 5 degrees above the horizontal before the valley floor where the instrument is located is illuminated and localized heating begins. At this time the terminator has moved 4 or 5° to the west of the site and the hills themselves surrounding the valley are illuminated and are being heated. The sunrise point at the site is noted in the figures.

The sharp upswing of the data in a number of the graphs at sunrise is due to the rapid heating of the instrument and its surrounding area at sunrise causing a rapid boil

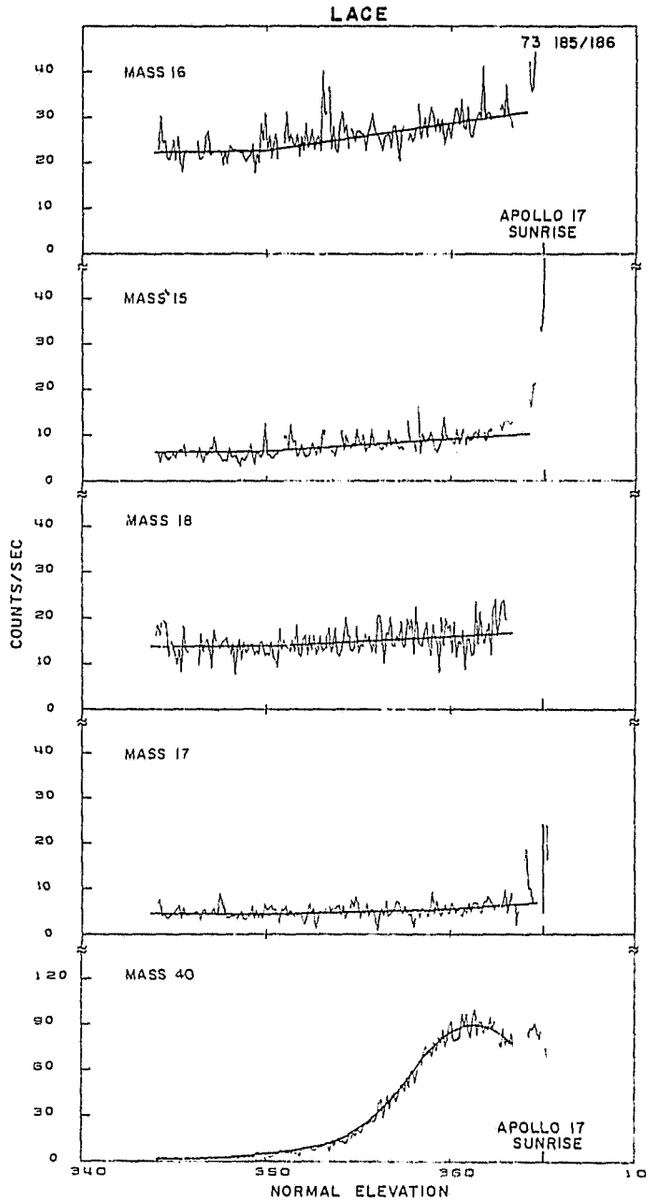

Fig. 2. Counting rate of 5 gas species as a function of normal elevation of the Sun where 0° is at the terminator crossing of the Apollo 17 landing site. Sunrise occurs nearly 5° after terminator crossing. Pre-dawn enhancement (see text) is indicated by positive slope of lines fitted to data.

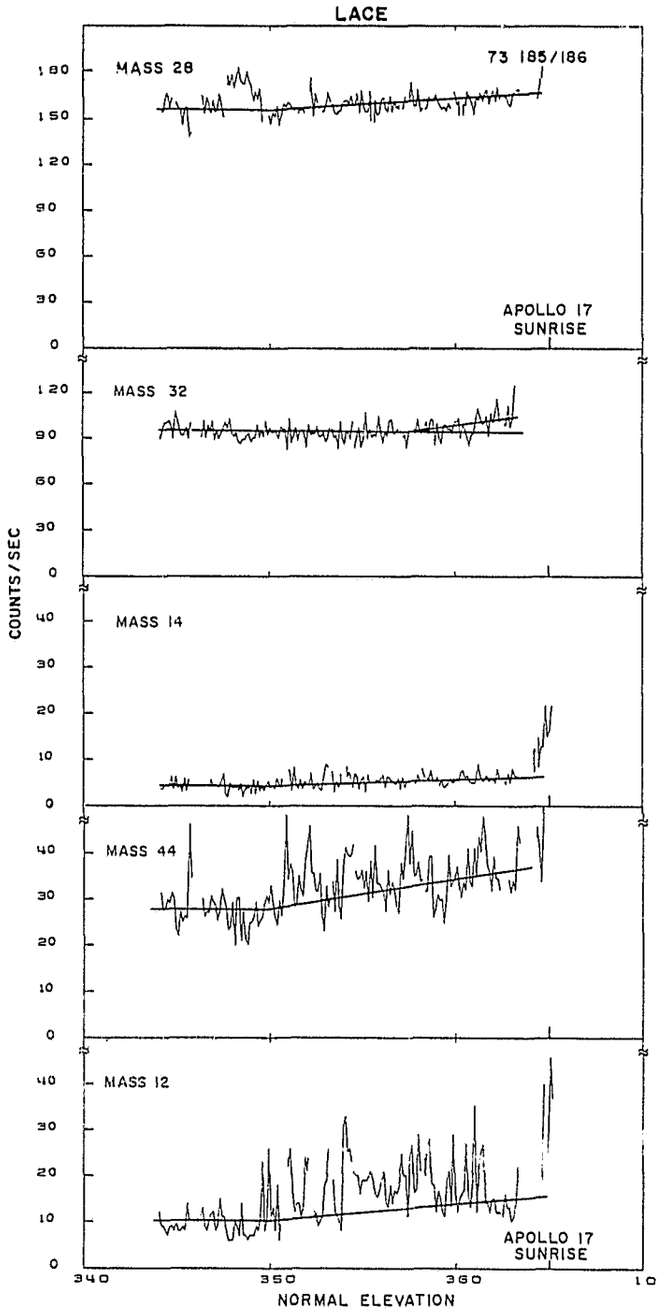

Fig. 3. Similar to Figure 2 except for 5 different gas species.

off of artifact gases which override any quantity of ambient lunar gases that may exist at this time. Therefore, data have not been taken beyond this point.

The data shown in each graph are the actual counting rates for each mass peak in the spectrum plotted every 13.5 min, the instrument scan time, and connected by straight lines. Linear fits to these data are shown having in most cases a positive slope beginning at 350° and extending on to sunrise. The difference between this fitted line and the base level between 340 and 350° is taken to be the pre-dawn enhancement at sunrise.

The mass 16 and 15 plots show a definite pre-dawn enhancement whereas the 18 and 17 show only a very small pre-dawn enhancement, the equivalent of a few counts. The mass 40 curve being ^{40}Ar, is shown for comparison as it exhibits a very marked pre-dawn enhancement which peaks at slightly past the terminator crossing, at 1 or 2 degrees normal elevation, whereas the 16 curve continues to increase to sunrise. This indicates that possibly the argon is loosely bound at the lunar nighttime temperature and is readily released at the terminator, probably by a photon process, and therefore exhibits the maximum concentration at this location. Methane, on the other hand, if this is what the mass 16 peak enhancement is indeed due to, is more tightly bound in the adsorption process than argon and requires heating of the lunar surface after the terminator crossing before the gas is released. This could cause the maximum in the concentration of methane to occur a number of degrees beyond the terminator into the daylight side of the Moon in a region where the mass spectrometer data is masked by the artifact gases being released from the Apollo 17 site.

The mass 28 and 32 peaks exhibit a pre-dawn enhancement that commences with the terminator crossing at 360° and continues on to sunrise. In these cases either the pre-dawn enhancement prior to terminator crossing is masked by the rather high background level of these peaks or there is no pre-dawn enhancement and the increase after terminator crossing is due to the heating of the hills around the site and a warming of portions of the instrumentation at the site by infrared radiation from the warm hillside. The mass spectrometer ion source temperature sensor, however, does not show any increase in temperature at this time. The heating and consequent outgassing would then have to come from some other instrument at the site or from the lunar module which is some 300 m away. The mass 44 and 12 data are relatively noisy compared to that of say mass 14 which is a peak of lower amplitude than even mass 12. The noise in these data is not explained at this time. However, there does appear to be a bona-fide pre-dawn enhancement of the 44 data and a very slight one of the mass 12 data. 44, of course, is due to CO_2 and 12 is probably formed in the mass spectrometer ion source from all of the gases containing carbon, such as CH_4, CO and CO_2.

Table I is a summary of the data extracted from Figures 2 and 3. In the first column is a list of the 12 mass peaks whose data were shown in Figures 2 and 3. The second column is the pre-dawn enhanced counting rate, that is, the increase in counts at sunrise over the background level between 340 and 350° normal elevation. The error bar is a best estimate of the range of slopes of lines that could reasonably be fitted to the data. Masses 18, 28, and 32 have a lower limit of 0 counts. The next several

TABLE I

Pre-Dawn Enhancement

Mass (amu)	Counts[a]	Parent molecule							Total
		CH_4	NH_3	H_2O	N_2	CO	O_2	CO_2	
12	2±2	0.2	–	–	–	0	–	0.3	0.5
14	2±1	0.5	0.02	–	0.3	0	–	–	0.8
15	5±2	5	0.07	–	–	–	–	–	5
16	8±2	6	0.8	0.3	–	0	0.4	0.5	8
17	2+2 −1	–	1	1	–	–	–	–	2
18	3±3	–	–	3	–	–	–	–	3
28	4±4	–	–	–	4	0	–	0.6	4.6
32	5±5	–	–	–	–	–	5	0	5
40	90±10	–	–	–	–	–	–	–	90
44	7±5	–	–	–	–	–	–	7	7

[a] Counting rate increase at sunrise.

columns show possible parent molecules which could account for the mass peaks listed in column 1. CH_4, methane, has a parent peak mass number of 16 amu but an ion source using 70 volt electrons as the ionization mechanism produces a peak at mass 15 which is 80% of the 16 peak amplitude. It is deemed that the mass 15 peak can have no source other than CH_3 from methane since the 30, 41 and 43 peaks are zero. This precludes CH_3 being formed in the ion source from other compounds, such as CH_3CO or CH_3CN or C_2H_6. Since this peak is most likely entirely due to methane, the corresponding methane abundance is taken to be equivalent to 6 counts.

In a similar manner water vapor is a parent peak at mass 18 with fragment peaks at 17 and 16 of 30 and 10% of the 18 peak respectively. The 3 counts of water vapor at mass 18 is considered a tentative value since, from the slope of the curve of Figure 2, a 0 count is allowed. Since the water vapor gives a 1 count contribution to the 17 peak the remainder of 1 count is very likely due to ammonia which has fragmentary peaks at 16 of .8 counts and traces at mass 15 and 14.

Since there are possibly 2 counts at mass 14 and the entire peak amplitude is not accounted for from methane and ammonia, the 28 peak, if it is finite, is attributed to nitrogen rather than CO, since nitrogen produces a fragmentary peak at mass 14 of either N^+ or N_2^{++} of approximately 7.5% of the 28 peak. This would leave the most probable value of the CO peak at 0 count. The oxygen peak at mass 32 could be 5 counts although again a 0 lower limit is an allowable value. It appears likely that there is some CO_2 with a most probable value of 7 counts and a minimum value of 2 counts. CO_2 gives rise to small fragmentary peaks at mass 28, 16 and 12.

The last column of Table I is the total accumulated counts from the parent and fragmentary peaks listed in the previous column. It may be observed that in all cases except for mass 12 and 14 the entire peak is accounted for from the molecules listed in the table. However, the total counts of the last column are all within the error bars attributed to the counts of the second column of the table. This shows that there is

REPRODUCIBILITY OF THE ORIGINAL PAGE IS POOR

rather positive evidence for the existence of methane, argon, possibly a small amount of ammonia and a small amount of CO_2 at the terminator.

Table II contains a listing of the gas concentrations for each species that appeared in Table I. The sensitivity of the mass spectrometer to all of these gases is approximately 2×10^2 mol cm^{-3} for each count. The certainties listed are roughly equivalent to the variances in the data given in Table I. ^{36}Ar is shown in the table for comparison. On the right hand side of the table are listed the solar wind fluxes for carbon, nitrogen and ^{36}Ar based upon the elemental abundances of Cameron (1968) and assuming that

TABLE II

Gas concentrations and solar wind fluxes

Parent substance	Sunrise concentration	Element	Solar wind flux[a] (cm^{-2} s^{-1})
CH_4	$(1.2 \pm 0.4) \times 10^3$	C	1.6×10^6
NH_3	$\binom{4+4}{-2} \times 10^2$	N	2.8×10^5
H_2O	$(6 \pm 6) \times 10^2$	^{36}Ar	8×10^2
N_2	$(8 \pm 8) \times 10^2$		
CO	$\binom{0+16}{-0} \times 10^2$		
O_2	$(1 \pm 1) \times 10^3$		
CO_2	$(1.4 \pm 1.0) \times 10^3$		
^{36}Ar	$(1.6 \pm 0.4) \times 10^3$		

Instrument sensitivity; 1 count = 200 mol cm^{-3}

[a] Based on H flux of 3×10^8 cm^{-2} s^{-1}.

the hydrogen flux is 3×10^8 cm^{-2} s^{-1}. The argon flux is derived from the ratios of the rare gas species as measured by Geiss *et al.* (1972) using and H^+/He^+ ratio of 0.045, a ^{4}He/^{20}Ne ratio of 560 and a ^{20}Ne/^{36}Ar ratio of 30. Since the ^{36}Ar solar wind flux is several orders of magnitude less than the nitrogen or carbon fluxes, it is striking to note that the abundance of any of the carbon or nitrogen compounds is equivalent to or less than that of ^{36}Ar.

Several possible reasons are advanced for these very low abundances. First of all, molecular gas species tend to have higher adsorption affinities than argon, a phenomenon which is the basis of gas chromatography. Thus, it is possible that the maximum rates of release of molecular gases will be farther into the dayside, where the temperature is higher, and they will not be transported as readily into the nightside region. This hypothesis is supported by the fact that all of the pre-dawn enhancement curves for the molecular gas species continue to rise all the way to sunrise whereas the ^{40}argon has turned over and already started its decrease at this time. Therefore, the maximum concentration of the molecular gas species may occur some 10 or more degrees beyond the terminator region. This could account for a factor of perhaps 5 lower abundance of the molecular species at sunrise. Second, since these gases may be affected by the surface temperature differently than is argon, the distribution of the

molecular species may be somewhat modified over the argon distribution shown in Figure 1. That is, the abundance of the molecular species could be much higher in the polar regions of the Moon than at the Apollo 17 latitude (20°). The cold polar regions, being a good pump or sink for these gases, could reduce their abundances in the terminator regions at mid latitudes or near the equator. This mechanism, which tends to concentrate these gases in the polar regions and thereby enhances their photo-ionization loss rate could help in accounting for the large solar wind influx of carbon and nitrogen. Third, it is possible that the majority of the solar wind carbon and nitrogen atoms form compounds which are fixed in the lunar surface materials and are not released into the lunar atmosphere. If none were released, the depth of mixing of carbon and nitrogen in the soil would have to be sufficient to account for the total influx of these elements over geologic time (Bibring *et al.*, 1974; Moore *et al.*, 1970).

4. Conclusion

It has been shown that there is indeed some evidence for the existence of methane and perhaps a very small amount of ammonia and carbon dioxide in the lunar atmosphere from the data taken by the Apollo 17 Lunar Mass Spectrometer experiment. This conclusion is based upon the pre-dawn enhancement of the concentrations of the mass peaks at the parent position for these molecular gas compounds. Methane is the most abundant of these species but its concentration is surprisingly only 1×10^3 mol cm^{-3}, slightly less than ^{36}Ar, whereas the solar wind flux of carbon is approximately 2000 times that of ^{36}Ar. Several reasons are advanced for the very low concentration of methane in the lunar atmosphere.

References

Bibring, J. P., Burlingame, A. L., Chaumont, J., Langevin, Y., Maurette, M., and Wszolek, P. C.: 1974, *Proc. Fifth Lunar Science Conf., Geochim. Cosmochim. Acta, Suppl. 5*, **2**, 1747–1762.

Cameron, A. G. W.: 1968, *Origin and Distribution of the Elements*, Pergamon Press, p. 124.

Geiss, J., Buehler, F., Ceruth, H., Eberhardt, P., and Filleux, Ch.: 1972, *Apollo 16 Preliminary Science Report*, NASA SP-315, 14-1 to 14-10.

Hodges, R. R., Jr. and Johnson, F. S.: 1968, *J. Geophys. Res.* **73**, 7307–7317.

Hodges, R. R., Jr. and Hoffman, J. H.: 1974a, *Geophys. Res. Letters* **1**, 69–71.

Hodges, R. R., Jr. and Hoffman, J. H.: 1974b, *Proc. Fifth Lunar Sci. Conf., Geochim. Cosmochim. Acta, Suppl. 5*, **3**, 2955–2961.

Hodges, R. R., Jr., Hoffman, J. H., and Johnson, F. S.: 1974, *Icarus* **21**, 415–426.

Hodges, R. R., Jr., Hoffman, J. H., Johnson, F. S., and Evans, D. E.: 1973, *Proc. Fourth Lunar Sci. Conf., Geochim. Cosmochim. Acta, Suppl. 4*, **3**, 2855–2864.

Hoffman, J. H., Hodges, R. R., Jr., Johnson, F. S., and Evans, D. E.: 1974, *Space Research* XIV, 607–614.

Hoffman, J. H., Hodges, R. R., Jr., Johnson, F. S., and Evans, D. E.: 1973, *Proc. Fourth Lunar Sci. Conf., Geochim. Cosmochim. Acta, Suppl. 4*, **3**, 2865–2875.

Moore, C. B., Gibson, E. K., Larimer, J. W., Lewis, C. F., and Nichiporuk, W.: 1970, *Proc. Apollo 11 Lunar Sci. Conf., Geochim. Cosmochim. Acta, Suppl. 1*, **2**, 1375–1382.

FORMATION OF THE LUNAR ATMOSPHERE*

R. R. HODGES, Jr.
The University of Texas at Dallas, Richardson, Tex., U.S.A.

Abstract. Measurements of ^{40}Ar and helium made by the Apollo 17 lunar surface mass-spectrometer are used in the synthesis of atmospheric supply and loss mechanisms. The argon data indicate that about 8% of the ^{40}Ar produced in the Moon due to decay of ^{40}K is released to the atmosphere and subsequently lost. Variability of the atmospheric abundance of argon requires that the source be localized, probably in an unfractionated, partially molten core. If so, the radiogenic helium released with the argon amounts to 10% of the atmospheric helium supply. The total rate of helium escape from the Moon accounts for only 60% of the solar wind α particle influx. This seems to require a nonthermal escape mechanism for trapped solar-wind gases, probably involving weathering of exposed soil grain surfaces by solar wind protons.

1. Introduction

Gas pressure on the Moon is so low that there is essentially no meteorological influence either on lateral heat flow or orographic weathering. The main function of the lunar atmosphere is to act as a reservoir for temporary storage of free atoms and molecules, providing a pathway for escape of certain elements from the Moon. It also has acted over geologic time as a flow channel for lateral dispersal of volatile elements which have condensed on soil grain surfaces, and as a source of some of the ions which have been implanted in these grains.

The most significant aspect of the modern lunar atmosphere is its relationship to escape. Hydrogen and helium are lost from the Moon due to Jeans's classical mechanism of thermal evaporation. Heavier particles escape as ions which are formed mainly by photon impact and less frequently by charge exchange with solar wind protons. These ions are accelerated by the induced $\mathbf{v} \times \mathbf{B}$ force in the solar wind. Most escape the Moon, but some impact it and become implanted in soil grains. Manka and Michel (1971) suggest this mechanism to be responsible for the parentless ^{40}Ar found in returned soil samples.

The importance of the problem of atmospheric escape can be demonstrated by quoting some results which are subsequently discussed more fully in this paper. Specifically, the rate of escape of ^{40}Ar from the Moon appears to be variable, implying an episodic process of release of this radiogenic gas from the interior of the Moon. The average rate of loss of argon from the lunar atmosphere is about 2×10^{21} atoms s^{-1}, which is about 8% of the present argon production rate for the entire moon (2.4×10^{22} atoms s^{-1}) if the average lunar potassium abundance is about 100 ppm as suggested by Taylor and Jakeš (1974) and by Ganapathy and Anders (1974). To put these rates in planetologic perspective, the present rate of release of ^{40}Ar to the

* Paper presented at the Conference on 'Interactions of the Interplanetary Plasma with the Modern and Ancient Moon', sponsored by the Lunar Science Institute, Houston, Texas and held at the Lake Geneva Campus of George Williams College, Wisconsin, between September 30 and October 4, 1974.

The Moon **14** (1975) 139–157. *All Rights Reserved*
Copyright © 1975 by D. Reidel Publishing Company, Dordrecht-Holland

terrestrial atmosphere from one lunar mass of Earth is about 1.4×10^{22} atoms s^{-1} if the fraction of total production effusing into the atmosphere has remained constant over geologic time.

It is surprising that the rates of effusion of ^{40}Ar from the Moon and Earth are comparable when their atmospheric abundances differ by more than 15 orders of magnitude. The answer to this puzzle lies in differing escape processes. On Earth the escape of ions is inhibited by the geomagnetic field, so that almost all of the argon ever released is now present in the atmosphere. However, the lack of both a lunar magnetic field and an ionosphere allows the solar wind to impinge directly on the planet; and, hence, to accelerate any ions formed near the Moon. As a result, the average lifetime for lunar argon is only about 80 to 100 days. The product of lifetime and loss rate gives atmospheric abundance, which amounts to the minuscule lunar atmosphere having about 10^6 gm of argon.

In essence, the lunar atmosphere serves as a pipeline for escape, not only of argon, but of virtually all atmospheric gases. Viewed in another way, the atmospheric abundance of a gas specifies its escape rate, which in turn specifies a loss parameter for the entire Moon. The importance of the argon loss is obvious in modeling the lunar interior. Another example is that only 60% of the solar wind influx of helium is currently escaping from the lunar atmosphere, which implies the existence of a second, nonthermal loss mechanism for helium and, hence, for other solar wind gases as well.

The key to understanding present lunar atmospheric escape, and the past influence of the atmosphere on the distribution of volatile elements in the regolith as well, lies in the tedious process of atmospheric modeling. Collisions between particles are so infrequent that the lunar atmosphere is usually considered to be entirely an exosphere, with the regolith serving as a classical exobase. Atoms and molecules travel in ballistic trajectories between encounters with the regolith. Upgoing velocities at the surface have thermal distribution, resulting in the average lateral extent of a trajectory being proportional to temperature and inversely proportional to mass. The light gases, hydrogen and helium, have significant fractions of hyperbolic orbits to account for most of their escape rates, whereas this thermal evaporation is virtually nonexistent for heavier species.

Owing to the temperature dependence of the average lateral extent of ballistic trajectories a particle moves down a temperature gradient in larger steps than it moves up. In the absence of surface adsorption this results in a statistical preference of an exospheric particle to spend more time in the cold nighttime region than in daytime. The cumulative statistical effect of many atoms is a nighttime concentration maximum. Hodges and Johnson (1968) have shown that ballistic transport causes an exospheric lateral flow pattern which approximately tends to equalize $nT^{5/2}$ over the exobase (where n is concentration and T is temperature.) Thus, the nearly 4 to 1 day to night surface temperature ratio on the Moon should result in about a 30 to 1 night to day ratio of concentration. This condition is nearly attained by helium, but many other gases seem to be adsorbed at night, creating a nighttime minimum and a maximum at sunrise where desorption tends to occur.

Surface processes of adsorption and desorption are species dependent as well as being functions of temperature and solar illumination (for desorption). As a result it is necessary to synthesize these parameters from experimental data. The only extensive, artifact-free data on condensible gas are the Apollo 17 mass spectrometer measurements of ^{40}Ar. Some limited data, reported in a separate paper by Hoffman and Hodges (1975), show qualitative evidence for the existence of other condensible gases on the Moon.

To pursue the subject of the formation of the lunar atmosphere it is necessary to be specific regarding species. Therefore, subsequent discussion will concentrate on the two best understood lunar gases: ^{40}Ar and helium. It is fortunate that these represent extremes of lunar atmospheric physics. The argon is radiogenic and entirely of lunar origin, reflecting the degassing of the interior of the Moon. In contrast most of the helium comes from solar wind α particles which have impacted the Moon. Another important difference is that argon is adsorbed at night while helium is not. In addition the sticking time of argon is short enough that desorption has a noticeable effect at night. Following the sections on argon and helium is a less quantitative discussion of other atmospheric processes and constituents.

In subsequent analysis all atmospheric modeling is based on a Monte Carlo technique which was first reported in Hodges (1973) and modified as noted in Hodges *et al.* (1974) and Hodges (1974). Briefly, the modeling technique simulates the lunar atmosphere by following the trajectories of a succession of individual molecules over the surface of the Moon, from creation to annihilation. Global variations of statistical parameters, such as the effects of temperature on the velocity distribution of atoms following surface encounters, and probabilities of adsorption, desorption, creation, and photoionization are taken into account. Particle lifetime is found by accumulating total time of flight and of adsorption. The influence of the perturbation of the lunar gravitational potential by the Earth is approximated by assuming that particles with greater energy than is required to reach the inner Lagrangian collinear point (0.956 times lunar escape energy; cf. Kopal, 1966) are lost from the Moon. This seemingly slight difference in the definition of escape has the surprisingly large effect of halving the average lifetime of helium atoms.

2. ^{40}Ar

The ^{40}Ar data from the Apollo 17 lunar surface mass spectrometer have been presented in Hodges and Hoffman (1974a). Figure 1 shows the entire data set available from that experiment, which consists of lunar nightime measurements through the first 9 lunations of 1973. Daytime measurements were precluded by high rates of degassing of remnant spaceflight hardware in sunlight.

Figure 2 shows the nature of the synodic variation of argon by superposition of data from the two lunations in which the maximum and minimum abundances of argon occurred. It is immediately apparent that the amount of argon on the Moon dropped by about a factor of 2 in a four month period. The history of the 1973 argon variation and its implications are discussed later.

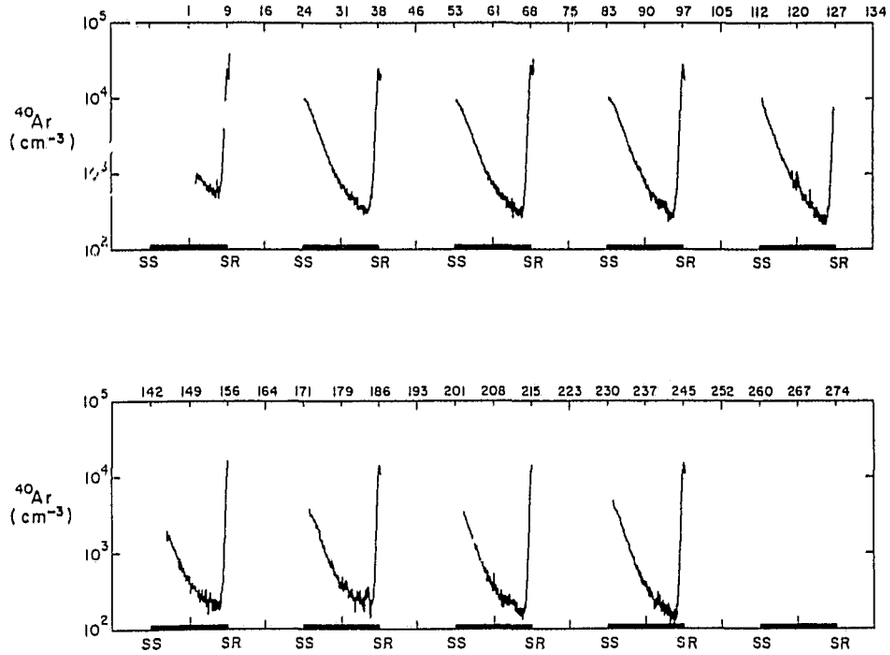

Fig. 1. Measured concentration of ^{40}Ar at the Apollo 17 site during 1973. The upper abscissa gives calendar days of quarterphases of the Sun. Sunrises (SR), sunsets (SS), and periods of darkness (dark bar) are specified on the lower scale.

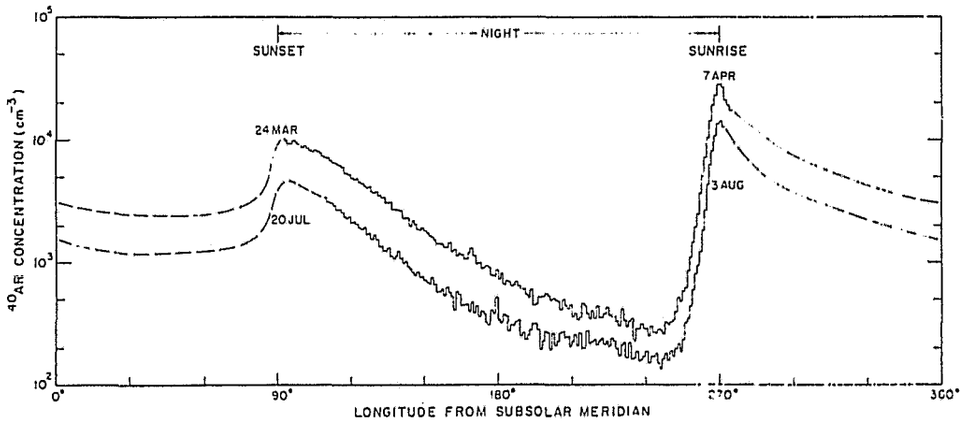

Fig. 2. Synodic variations of ^{40}Ar during lunations of maximum and minimum abundances. Dashed curves are theoretical extrapolations which show expected daytime behavior.

REPRODUCIBILITY OF THE ORIGINAL PAGE IS POOR

The synodic variation of argon is characteristic of a condensible gas. The slow post sunset decrease in concentration indicates an increasing adsorption probability with decreasing temperature, while the nearly asymptotic behavior of the nighttime minimum requires an appreciable amount of desorption. At sunrise the bulk of the adsorbed gas is released from the lunar surface, and some of it travels into the nighttime hemisphere, giving rise to the rapid presunrise increase. Incidentally, it is the presunrise buildup which marks this data as an actual indication of a lunar gas; there is no apparent way for an artifact release to anticipate sunrise in this manner.

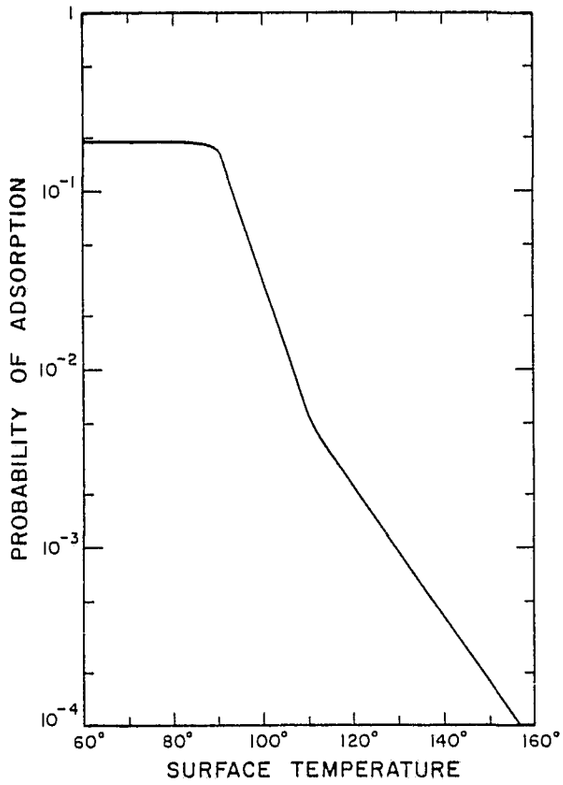

Fig. 3. Probability of adsorption of atmospheric argon on the lunar surface as a function of temperature.

A series of Monte Carlo simulated argon atmospheres were calculated, in which adsorption and desorption dependencies on temperature and solar illumination were iteratively adjusted until the synodic variation at 20° latitude of the model distribution matched the average measured variation. The best fit of model and experiment seems to occur for the adsorption probability function shown in Figure 3. Two forms of desorption are needed to explain the data. The first is the spontaneous process of thermal desorption, which apparently depends on temperature in a manner similar to

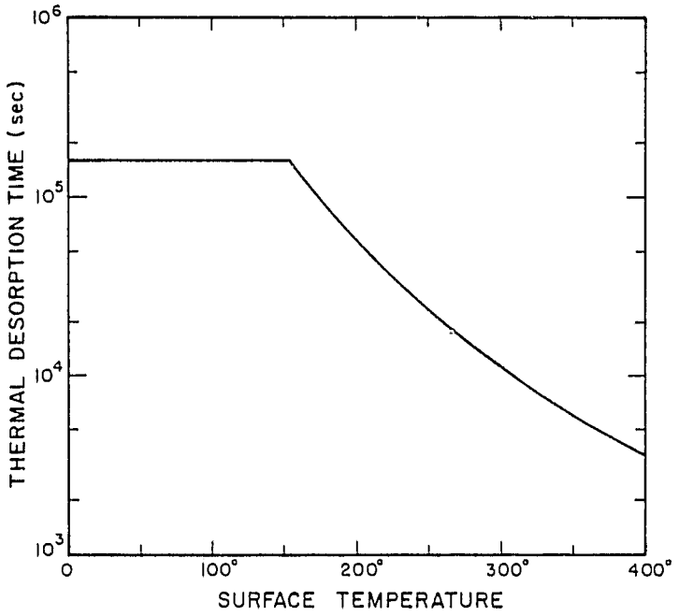

Fig. 4. Mean thermal desorption time for argon on the lunar surface as a function of temperature.

the graph of Figure 4. (The break in the curve near 150 K is an artifact introduced for analytical simplicity.) The second desorption mechanism is a photon process in which qualitative laboratory tests show that certain gases, including argon, are released from a surface by the visible range of the solar spectrum. In order that the model reproduce the measured sunrise to sunset concentration ratio it is necessary that the illumination of a soil grain surface release an atom with unity probability. To account for soil texture and orography it is assumed that the probability of illumination of an exposed soil surface increases from 0 to 0.5 as lunar rotation moves the grain through a band of $\pm 2°$ of solar zenith angle about the spherical moon sunrise terminator, and that the probability of illumination of the remaining surface area increases linearly thereafter with increasing zenith angle. In practice about half of the atoms adsorbed at low latitude are released by the photon interaction process, while spontaneous desorption is more likely at high latitudes where the time needed for sunrise to traverse the orographic uncertainty becomes quite long.

The adsorption and desorption characteristics discussed above are the result of synthesis; and, hence, are not unique answers to the problem. However, the sensitivity of model atmospheres to small changes in these parameters suggests that the present results are likely to closely approximate the true lunar conditions. One nagging question is that the soil near the Apollo 17 site may not reflect average lunar characteristics. A possible way to proceed with this problem would be to construct a gas chromatographic column with lunar soil from various Apollo landing sites used as the buffer material to make direct measurements of adsorption and desorption characteristics.

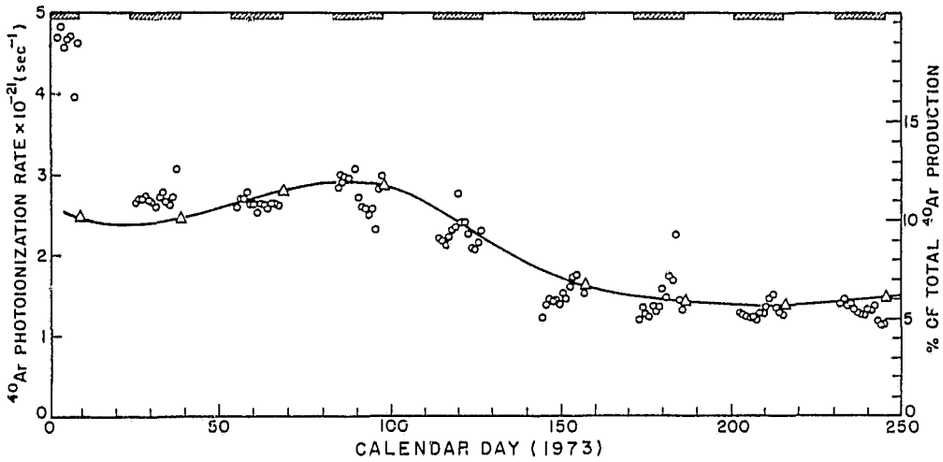

Fig. 5. Temporal variation in the rate of photoionization of ^{40}Ar in the lunar atmosphere during 1973. Triangles give sunrise values, while circles represent less accurate rates inferred from nighttime measurements.

Among the parameters to emerge from the model study are the following. Average argon lifetime on the Moon is about 100 days, of which 80% of the time is spent adsorbed on the surface. The average sticking time for an adsorbed atom is 1.1 days. The rate of photoionization of argon in the lunar atmosphere (number of atoms per second) is about 9×10^{16} times the sunrise concentration at the Apollo 17 latitude (20°). Thus the loss rate corresponding to the average argon sunrise concentration ($\sim 2 \times 10^4$ cm^{-3}) is about 2×10^{21} atoms s^{-1}.

Figure 5 shows the temporal variation of the total argon photoionization rate during 1973. It should be noted that this rate is proportional to both atmospheric abundance and to escape rate. Triangles represent the most accurate determinations of the photoionization rate at sunrises where the concentration is greatest. Each circle gives the rate found by model extrapolation of a 5° longitudinal average of concentration to an equivalent sunrise concentration. High values of the circles early in the year are due to a decaying artifact contribution to the low nighttime concentration. The large variance of the photoionization rate represented by the circles is indicative of the noise inherent in the nighttime concentration data and errors in the model.

As mentioned earlier there are two important aspects of the ^{40}Ar photoionization rate, which show up clearly in Figure 5. First, the time average of the rate is roughly 2×10^{21} atoms s^{-1}, corresponding to about 8% of the total lunar production of ^{40}Ar if the potassium abundance is 100 ppm. If a large fraction of the photoions were to impact the lunar surface and subsequently become recycled into the atmosphere, then the actual source of new atoms would be a lesser part of the production rate. However, the second obvious feature of Figure 5, the time variation of the photoionization rate (and hence of argon abundance), argues strongly that there is very little recycling of ^{40}Ar.

The clue that argon recycling is unimportant is found in the decay of the photoionization rate between about day 100 and day 150, where the decay time constant is roughly equivalent to the average lifetime of argon atoms – i.e., about 100 days. If ψ_0 is used to denote the total supply of atoms, both new and recycled, to the atmosphere, and ψ_l is the photoionization rate, then continuity requires that

$$\psi_s = \psi_l + \tau \frac{d\psi_l}{dt}, \tag{1}$$

where τ is the average atomic lifetime. Figure 6 shows the aron source, ψ_s, required to supply the photoionization rate shown in Figure 5 for three values of the lifetime τ.

An important feature of Equation (1), and hence of Figure 6, is that the total argon source must include an essentially constant contribution from recycled atoms, and that temporal variation of ψ_s must arise from internal changes in the Moon which affect the rate of release of new argon atoms. Since ψ_s is a positive definite quantity, it is obvious that the lifetime which emerges from the atmospheric model calculations, 100 days, is nearly an upper bound. In addition, the 100-day lifetime allows for very little recycled argon. A decrease in the lifetime to 60 days would be consistent with a

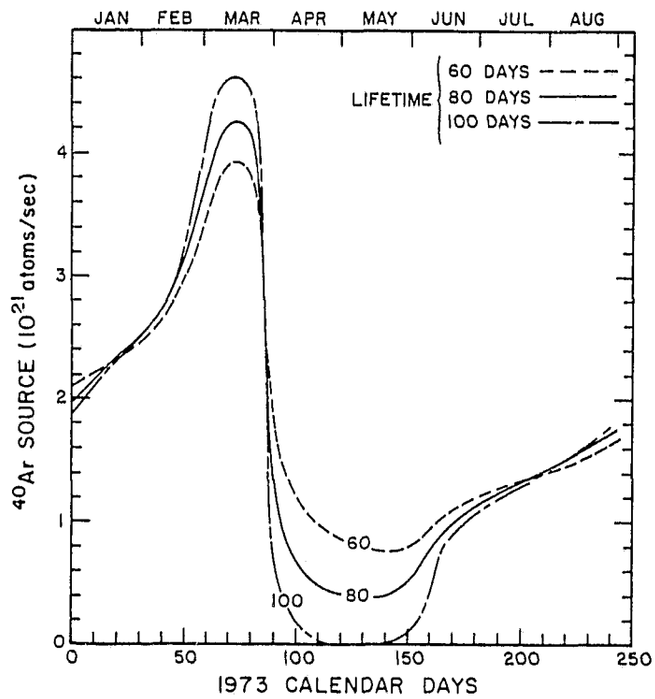

Fig. 6. The total source of ^{40}Ar needed to explain the measured atmospheric argon during 1973 for several values of the mean atomic lifetime.

recycling rate of about 8×10^{20} atoms s^{-1} or roughly 40% of the total source. However, model calculations for a wide variety of surface parameters have consistently given a lifetime in excess of 80 days. The shortest model lifetimes occur when adsorption probability is increased near the poles, but this always produces an inconsistently large sunset concentration at the Apollo 17 latitude (20°). Thus the best judgment is that the recycling fraction of the total argon photoionization rate is quite small, and that it probably is less than 10% to be consistent with a lifetime in the 80–100 day range. This places some constraints on the rate of release of retrapped, parentless ^{40}Ar from the regolith.

The most puzzling aspects of the ^{40}Ar source are its large average amplitude and its episodic nature. To put the average release rate in perspective, the release of 2×10^{21} atoms s^{-1} would correspond to release of each argon atom as it is created in the upper 8 km of the Moon if the average crustal potassium abundance is the highlands average of 600 ppm suggested by Taylor and Jakeš (1974). However, the release of these atoms

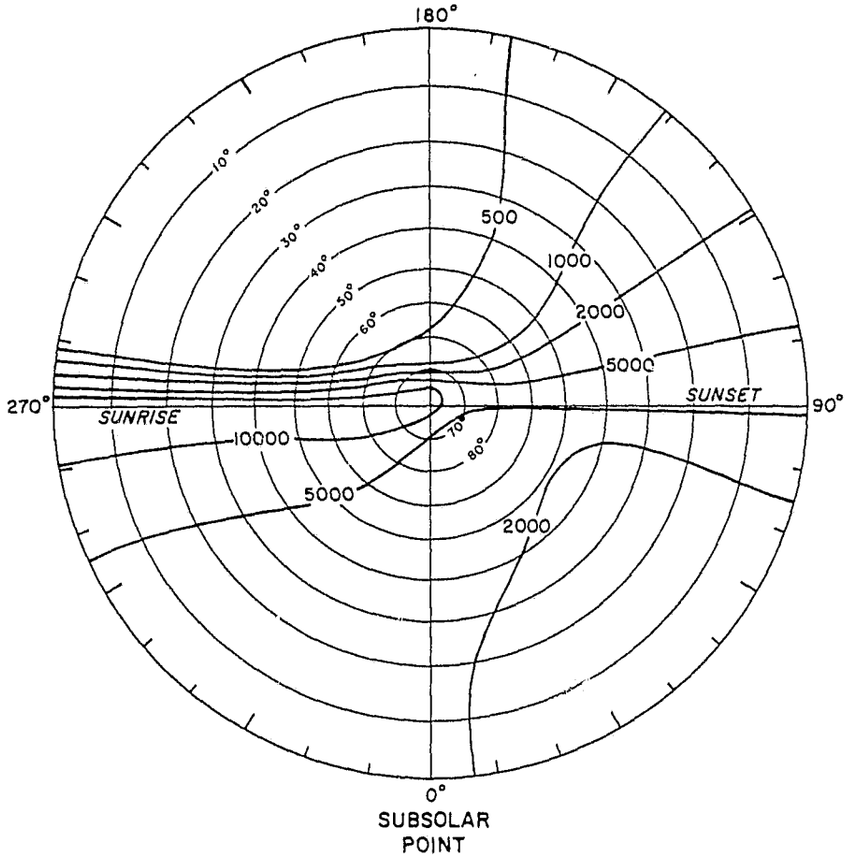

Fig. 7. The hemispheric distribution of ^{40}Ar on the lunar surface.

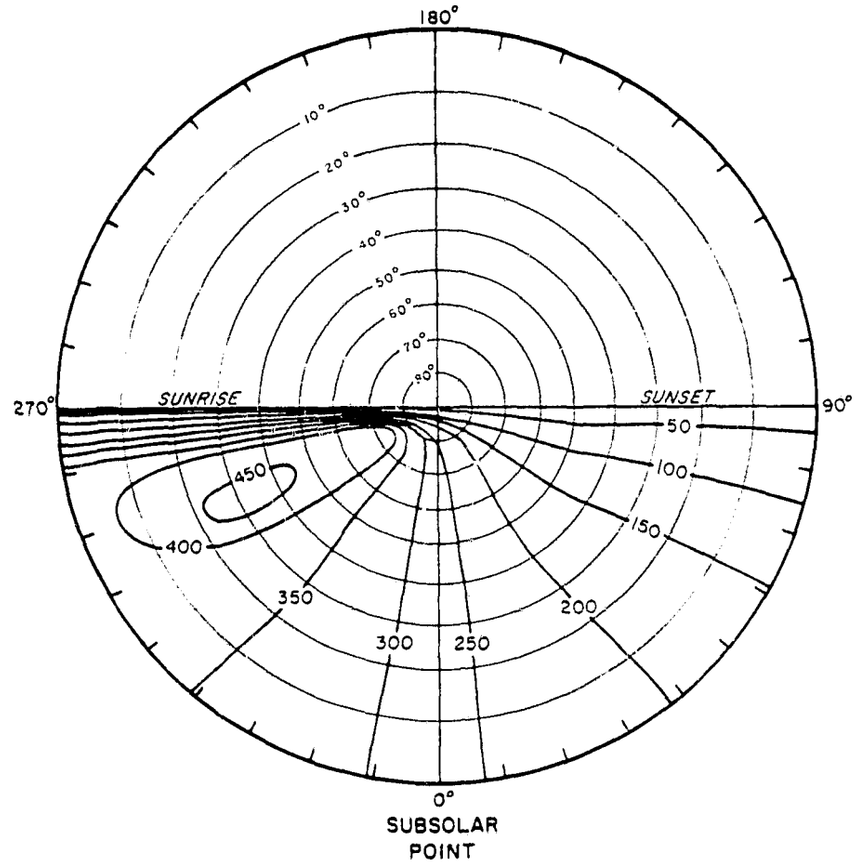

Fig. 8. The hemispheric distribution of ^{40}Ar at an altitude of 100 km above the lunar surface.

is incompatible with known weathering mechanisms. This requires consideration of a deeper source region. If the argon were postulated to come from greater depths where radioactive heating enhances diffusion of the argon atoms out of rocks and into fractured areas, the time variation would still be difficult to explain.

The only remaining source of the atmospheric argon is a semi-molten core with radius of about 750 km if the potassium abundance there is 100 ppm. This size fortuitously corresponds to one of the models proposed by Taylor and Jakeš (1974), in which a partially molten zone of primitive unfractionated lunar material occupies a core of about 750 km radius. It is also consistent with analyses of seismic data which suggest partial melting in this region (Latham *et al.*, 1973). The problem of explaining the time variation remains. Hodges and Hoffman (1974a) have suggested that there may be a correlation with seismic processes, and that either the release of argon is due to internal movements which periodically open paths to the lunar surface, or the

pressure of gas trapped in voids of the core periodically builds up to a point where the gas opens its own vent to the surface, possibly creating a seismic signal.

The rate of release of lunar radiogenic argon is so strongly tied to the interior structure of the Moon that long term measurements of atmospheric argon must eventually be made. Interpretation of such measurements will involve extrapolation of total abundance from local data. Figure 7 shows the presently most realistic model of the distribution of ^{40}Ar at the lunar surface as a topographic map in sterographic projection of the northern hemisphere. It can be noted that the sunrise and sunset maxima extend to the polar region. What is, unfortunately, not practical to show is that the maximum concentration occurs in the polar region, and is about 4×10^4 atoms cc^{-1}, or about twice the equatorial sunrise level.

Figure 8 shows the distribution of ^{40}Ar expected to be encountered by an orbiter at 100 km altitude. At night the concentration becomes too small to measure, but experience with the Apollo 17 lunar surface mass spectrometer suggests that the daytime concentrations above 50 atoms cc^{-1} could be measured by a mass spectrograph dedicated to integration of the argon peak, and designed to operate with a cold inlet system (<270 K) to suppress artifact background gases.

3. Helium

The sources of helium in the lunar atmosphere are the α particles supplied by solar wind implantation in the regolith and by decay of ^{232}Th and ^{238}U within the Moon. Johnson *et al.* (1972) have reviewed the available solar wind data and concluded that the average α particle flux is about 1.35×10^7 cm^{-2} s^{-1}, corresponding to 4.5% of the proton flux. This should result in a helium supply of 1.3×10^{24} atoms s^{-1} on the Moon. The rate of production of radiogenic helium in the Moon can be estimated by assuming the bulk Moon abundance of Th to be 0.23 ppm and U to be 0.06 ppm (cf. Taylor and Jakeš, 1974). Decay of these elements to stable lead results in a total helium source of 1.2×10^{24} atoms s^{-1}. If K, U and Th distributions in the Moon are similar then the mechanism for release of helium should be the same as that of ^{40}Ar, and, hence, the rate of supply of radiogenic helium to the lunar atmosphere should be about 10^{23} atoms s^{-1}. Thus the total available source of lunar atmospheric helium is about 1.4×10^{24} atoms s^{-1}.

Figure 9 shows theoretical and average experimental data on the synodic variation of helium at the Apollo 17 site (20° latitude). The solid line represents a numerically smoothed model obtained from a Monte Carlo calculation in which 180 impact zones were distributed longitudinally in the 20° latitude region. Amplitude of the model distribution is based on a source equivalent to the average solar wind influx of 1.3×10^{24} atoms s^{-1}.

The experimental data points in Figure 9 are from Hodges and Hoffman (1974b). Each point corresponds to an average of all available measurements which occurred during the first 10 lunations of 1973) in an 18° increment of longitude. Error bars represent the variances of these blocks of data, but they indicate systematic temporal

changes in helium abundance rather than a useful parameter of the statistical distribution of the data. The measurements were confined to lunar nighttime because of instrument operational constraints, but they suggest a good correspondence of the actual atmosphere with the theoretical model.

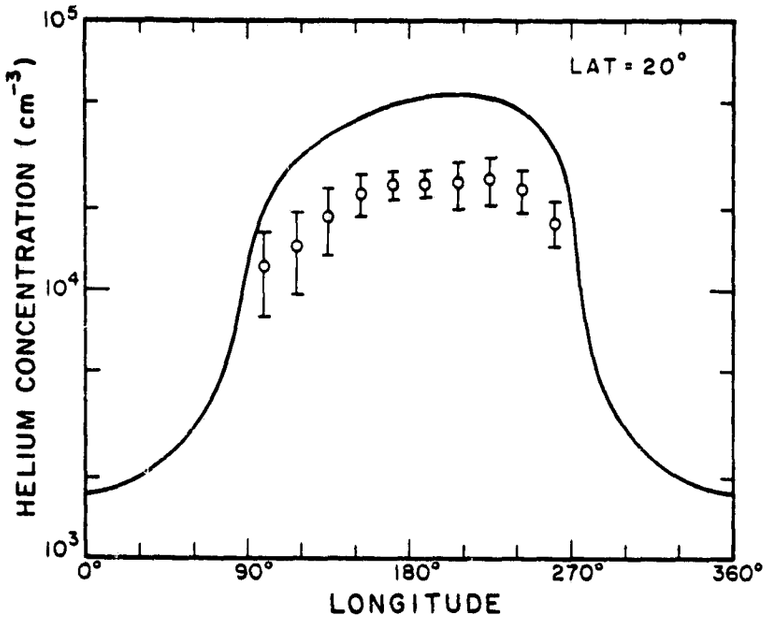

Fig. 9. Synodic variation of helium on the Moon. The solid line gives the model distribution for a solar wind source of 1.35×10^7 α particles cm^{-2} s^{-1}. Data points represent averages of all Apollo 17 mass spectrometer measurements in 18° bands of longitude.

In Figure 9 it is evident that the actual helium abundance is only about 70% of the model value and, hence, the average helium source in 1973 was probably about 9×10^{23} atoms s^{-1}. Subtracting the radiogenic source, the solar wind must have supplied about 8×10^{23} atoms s^{-1}, or about 60% of the average solar wind α particle influx. An explanation of the apparently low atmospheric supply rate is presented later.

A detailed history of the helium data, shown in Figure 10, reveals numerous deviations from the smooth model of the synodic variation. In these graphs the data has been subjected to 3 hr averaging, corresponding roughly to the atmospheric equilibration time, so that the ratio of the measured concentration to the model value at the same longitude is proportional to total atmospheric abundance at any time. The obvious deviations from the model distribution could only have occurred as responses of the atmosphere to sudden increases in the total amount of helium on the Moon. Their amplitudes appear to be too great to be accounted for by variations in the rate of effusion of radiogenic helium from the interior of the Moon.

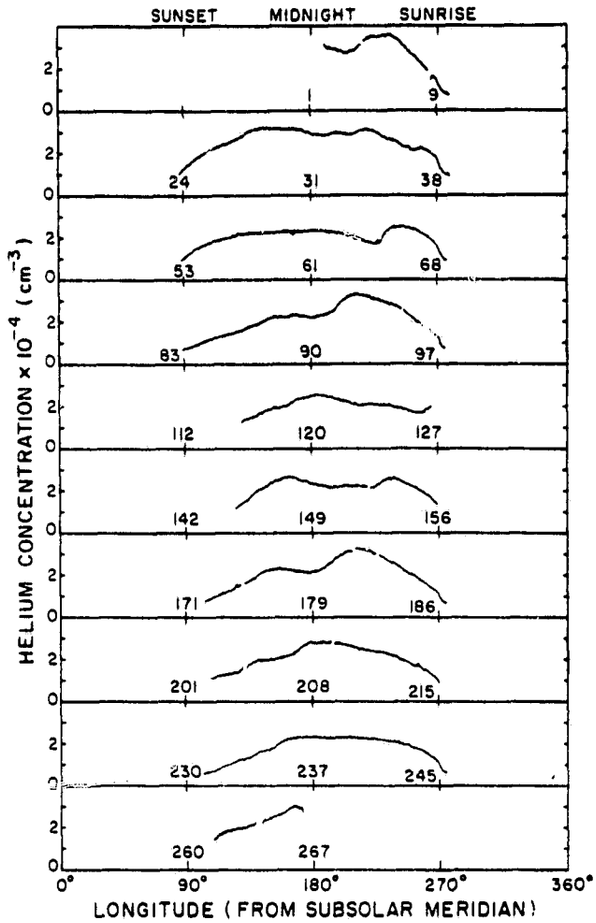

Fig. 10. Measured helium concentrations in the first 10 lunations of 1973.

The analysis of Hodges and Hoffman (1974b) showed a correlation of the variability of lunar atmospheric helium with the geomagnetic index Kp, and hence with the solar wind. This analysis was based on the equation of continuity

$$\phi_s = \phi_0 \left\{ \frac{n}{n_0} + \tau \frac{\mathrm{d}}{\mathrm{d}t} \left(\frac{n}{n_0} \right) \right\}, \tag{2}$$

where ϕ_s is the equivalent solar wind source flux of α particles necessary to supply atmospheric escape; ϕ_0, the flux used in the model calculation (1.35×10^7 cm^{-2} s^{-1}); n, the three hour average of the measured concentration; n_0, model concentration at the corresponding longitude; and τ is the average atomic lifetime for helium on the Moon. Note that the instantaneous escape rate is $\phi_0 n/n_0$.

Recent improvements in the Monte Carlo atmospheric modeling technique have included direct calculation of atomic lifetimes by summing the times of flight for all trajectories. This has resulted in a longer lifetime for helium than 8×10^4 s calculated in Hodges (1973) where lifetime was inferred from a barometric estimation of total helium abundance. The newly calculated lifetime is 2×10^5 s.

Figure 11 shows the correlation of ϕ_s, the equivalent solar wind α particle flux, with the geomagnetic index Kp for the 2×10^5 s lifetime. Circles represent average flux values in each increment of Kp, while error bars give the standard deviation of these fluxes. The upper graph gives the number of hours of data available at each value of Kp. Individual flux values are plotted for the infrequent condition $Kp > 6^+$.

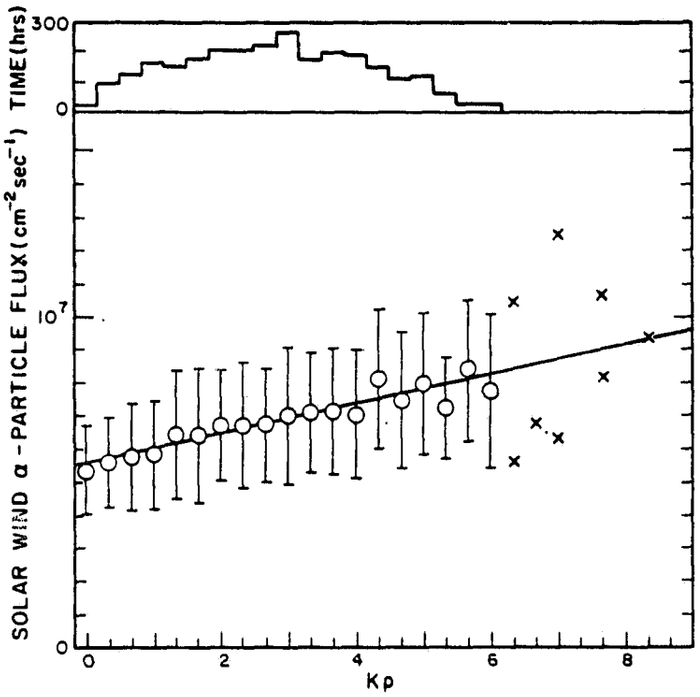

Fig. 11. The equivalent solar wind flux of helium needed to supply lunar atmospheric escape (lower graph) and total data accumulation time (upper graph) as functions of Kp. The straight line shows the linear regression of all of the data.

The straight line shown in Figure 11 gives the linear mean-square regression of all of the flux vs. Kp data. It shows that the equivalent solar wind α particle flux needed to supply the lunar atmosphere has the approximate relationship

$$\phi_s = (5.6 \pm 1.9 + 0.44 \times \mathrm{Kp}) \times 10^6 \ \mathrm{cm}^{-2}\ \mathrm{s}^{-1}. \tag{3}$$

This expression, and Figure 11 as well, differ from the results presented in Hodges

and Hoffman (1974b) because of the improved value of average lifetime used here.

The slope of the regression line in Figure 11 is not as steep as might be expected from the data on Kp correlations with the solar wind reported by Wilcox *et al.* (1967) and the results of Hirshberg *et al.* (1972). However, the apparent relationship of the equivalent lunar atmospheric source flux data and Kp has been numerically confirmed to have a correlation coefficient of 0.31. Therefore, it can be concluded that while the lunar atmosphere may depend on several helium source mechanisms, one of these is clearly related to Kp and hence to the solar wind. Since α particles impact the Moon with energies of about 4 keV, the solar wind mechanism probably does not involve the immediate neutralization of impacting α particles, but rather a process of release of previously trapped solar wind helium from soil grains.

Presumably the average rate of accretion of α particles by the lunar regolith nearly equals the average rate of release of previously trapped helium from the soil, with the slight unbalance due to the absorption of helium by previously unexposed material which has recently been brought to the lunar surface by meteor impacts. Diffusion must account for part of the release of trapped helium from the soil, but the solar wind related component is probably of greater importance.

A weathering process due to the solar wind could account for the solar wind correlated part of the helium source. One possibility is that the proton influx causes sputtering of soil grain surface material, resulting in volatilization of many elements, including trapped helium. This mechanism has been proposed by Housley (1974) as an important means of both lateral transport and escape. The fact that the present data seem to show a deficit of atmospheric helium, based on the average solar wind source, suggests that some helium is lost from the Moon as sputtered ions or as superthermal atoms which would not have been detected by the Apollo 17 mass spectrometer because its field of view was limited to nonescaping, downcoming atoms. The low energy fraction of sputtered helium could be the solar wind correlated source of lunar atmosphere.

If the hypothesis of release of trapped solar wind helium from the lunar soil by sputtering is correct, then the α particle fraction of the solar wind is not related to the unexpectedly low helium abundance in the lunar atmosphere in the 1973 measurements. The sputtered helium effusion rate must represent a very long term average of the solar wind helium implantation rate, modulated by variations in the weathering agent: the instantaneous influx of solar wind momentum.

In summary it appears that the average rate of escape of helium from the thermalized lunar atmosphere is about 9×10^{23} atoms s^{-1}, of which 10% is probably supplied by radioactive decay of Th and U in the Moon. The remaining atmospheric helium escape amounts to 60% of the solar wind inflow of α particles. The correlation of atmospheric helium with the geomagnetic index Kp suggests solar wind weathering of the soil to be an important mechanism for release of previously implanted solar wind helium. A superthermal or ionized component of the helium released by the surface weathering process seems to be needed to account for escape of the 40% of the solar wind helium which does not participate in the formation of the lunar atmosphere.

4. Other Atmospheric Processes

The foregoing atmospheric results have important implications on the physics of other volatiles on the Moon. For example, the measurements made by the Apollo 15 and 16 orbital α-particle spectrometers indicate the emanation of radon from the lunar interior to the atmosphere, a process which must be related to the release of ^{40}Ar.

What is important in the α-particle data is the rate of decay of ^{210}Po at the lunar surface, because this gives an average for the rate of diffusion of the gaseous progenator of the polonium, ^{222}Rn, to the surface region of the regolith over the last several decades. From the data reported by Bjorkholm *et al.* (1973) it appears that the average rate of ^{210}Po decay is in the range of 0.018 ± 0.01 dis cm^{-2} s^{-1}, which translates to a global average effusion rate for radon of about $7 \pm 4 \times 10^{15}$ atoms s^{-1}.

If we assume the bulk Moon average abundance of uranium to be 0.06 ppm as suggested by Taylor and Jakeš (1974), the total lunar rate of production of ^{222}Rn is 8×10^{22} atoms s^{-1}. If the radon and ^{40}Ar source regions are the same, then about 8% of the radon or 6×10^{21} atoms/sec are available for transport to the lunar surface Owing to the 3.8 day half life of radon, the large difference between the available supply and the surface effusion rate implies an average transit time of 70 to 80 days.

The argument for correlation of the argon and radon source regions suggests further preference for the model of the lunar interior proposed by Taylor and Jakeš (1974) in which the Moon has an unfractionated, partially molten core with radius of about 750 km, in which K and U are present in roughly their bulk Moon average abundances. Surface measurements of argon and radon are compatible with a release process in which radiogenic gases collect in bubble-like regions of the core. The collecting gases are vented to the lunar surface whenever the pressure reaches some critical level. To maintain the measured ^{210}Po level at the lunar surface the storage time for these pockets of gas must be on the order of 80 days, but the paucity of both argon and radon data allows for a large deviation of this time and of its average value.

Gorenstein *et al.* (1973) report spatial variations in the distribution of ^{210}Po on the Moon, which indicate localized emissions of radon followed by limited atmospheric transport prior to decay to polonium. Localized venting is in agreement with the idea of transient release of radiogenic ^{40}Ar and radon from the lunar core. However, Gorenstein *et al.* go on to suggest an episodic variability of the rate of radon emanation on a time scale of 10 to 60 yr to explain present excesses of polonium over radon on some regions of the lunar surface. This would suggest an implausible change in venting of the gas from the core over a geologically short time. One possible way out of this dilemma is to postulate that the excess part of the polonium now decaying on the lunar surface has been brought there by upward transport through the soil, perhaps via the mechanism of electrostatic levitation of dust, a process which has been discussed as the cause of horizon glow in post sunset Surveyor 7 photography by Criswell (1972). The influence of orography on the production of electric fields at the lunar surface is a possible cause of spatial differences in electrostatic regolith overturning and, hence, in the rate of migration of polonium to the surface.

The apparent evidence for regolith weathering in the present interpretation of the Apollo 17 mass spectrometric helium measurements implies that the sputtering process must affect other elements as well. This mechanism has been discussed by Housley (1974); its quantitative influence on expected lunar atmospheric gases is presented here.

Attempts at detection of the solar wind gases in the lunar atmosphere have generally been unproductive. Fastie *et al.* (1973) give an upper bound on H which is orders of magnitude below model abundances calculated by Hartle and Thomas (1974) and by Hodges *et al.* (1974). The later authors also report tentative interpretations of ^{20}Ne and ^{36}Ar measurements, which may also be considered to be upper bounds.

The pre-sunrise mass spectrometer data discussed by Hoffman and Hodges (1975) shows evidence of only slight amounts of some gases which are copiously supplied by the solar wind. Of particular interest is methane, which has about 2% the sunrise concentration of ^{40}Ar, despite a solar wind influx of carbon that is nearly 2 orders of magnitude greater than the average ^{40}Ar source. It is tempting to ascribe the atmospheric deficit of carbon to continuing implantation of solar wind ions in the soil. However, there are some serious problems with this argument. At the Apollo landing sites, where the lunar surface is shielded from the solar wind about 4 days per lunation by the geomagnetic tail, the net carbon influx is roughly 10^{13} ion cm^{-2} s^{-1}. If the soil has been steadily assimilating this carbon, then the present surface abundance of about 100 ppm translates to a mixing scale depth of 10 m b.y.$^{-1}$. However, the intensity of turbulence produced by meteor impacts must diminish with increasing depth, making uniform mixing implausible, and hence forcing the needed depth of mixing far beyond 10 m b.y.$^{-1}$. In contrast, the neutron capture data of Burnett and Woolum (1974) suggests that in the last 0.5 b.y.$^{-1}$ soil accretion rather than mixing of the regolith has occurred at the sites of the Apollo 15 and 16 deep core samples. The lack of an adequate global soil mixing mechanism indicates that an important fraction of the solar wind carbon must escape from the Moon. Thus the low levels of methane and other carbon gases in the atmosphere are difficult to explain.

Attempts to devise adsorption and desorption parameters for a methane atmospheric model which has a low terminator concentration at the Apollo 17 latitude have not been fruitful. The problem is a need for a large amount of the gas in sunlight if photoionization is the dominant cause of loss. It is possible that the adsorption probability for methane approaches unity at high latitudes, even in daytime, leading to the formation of a localized surface monolayer of methane in each polar region. Desorption from these deposits could supply virtually all photoionization losses of methane while precluding atmospheric formation at low latitudes.

Proof of the feasibility of the above model depends on further attempts at modeling. The alternative is that almost all of the solar wind carbon implanted in the soil eventually escapes due to sputtering. This seems to be contrary to the helium data discussed above, since at most only about 40% of the solar wind α particle influx is not accounted for by atmospheric escape. In addition the noticeable changes in atmospheric helium due to solar wind fluctuations suggest that an important fraction of the

helium released by proton impact has thermal energy. Thus, the nonthermal escape of a large fraction of trapped solar wind carbon from the regolith would require a mechanism which imparts orders of magnitude more kinetic energy to carbon than to helium. In a word, the escape of solar wind elements other than helium remains an enigma.

5. Conclusions

The dominant gases of the lunar atmosphere seem to be ^{40}Ar and helium. Owing to a lack of atomic collisions, each gas forms an independent atmospheric distribution. Argon is adsorbed on lunar surface soil grains at night, causing a nighttime concentration minimum. In contrast helium is virtually noncondensible, and hence has a nighttime maximum of concentration in accordance with the classical law of exospheric equilibrium.

Essentially all of the ^{40}Ar on the Moon comes from the decay of ^{40}K in the lunar interior. Variability of the amount of atmospheric argon suggests a localized source region. The magnitude of the average escape rate, about 8% of the total lunar argon production rate, indicates that the source may be a partially molten core with radius of about 750 km, from which all argon is released.

Most of the helium in the lunar atmosphere is of solar wind origin, although about 10% may be due to effusion of radiogenic helium from the lunar interior. The atmospheric helium abundance changes in response to solar wind fluctuations, suggesting surface weathering by the solar wind as a release mechanism for trapped helium. Atmospheric escape accounts for the radiogenic helium and about 60% of the solar wind α particle influx. The mode of loss of the remaining solar wind helium is probably nonthermal sputtering from soil grain surfaces.

Acknowledgment

This research was supported by NASA Grant NSG-7034.

References

Bjorkholm, P. J., Golub, L., and Gorenstein, P.: 1973, *Proc. Fourth Lunar Science Conf., Geochim. Cosmochim. Acta, Suppl. 4*, **3**, 2793–2802.

Burnett, D. S. and Woolum, D. S.: 1974, *Proc. Fifth Lunar Science Conf., Geochim. Cosmochim. Acta, Suppl. 5*, **2**, 2061–2074.

Criswell, D. R.: 1972, *Proc. Third Lunar Science Conf., Geochim. Cosmochim. Acta, Suppl. 3*, **3**, 2671–2680.

Fastie, W. G., Feldman, P. D., Henry, R. C., Moos, H. W., Barth, C. A., Thomas, G. E., and Donahue, T. M.: 1973, *Science* **182**, 710–711.

Ganapathy, R. and Anders, E.: 1974, *Proc. Fifth Lunar Science Conf., Geochim. Cosmochim. Acta, Suppl. 5*, **2**, 1181–1206.

Gorenstein, P., Golub, L., and Bjorkholm, P. J.: 1973, *Proc. Fourth Lunar Science Conf., Geochim. Cosmochim. Acta, Suppl. 4*, **3**, 2803–2810.

Hartle, R. E., and Thomas, G. E.: 1974, *J. Geophys. Res.* **79**, 1519–1526.

Hirshberg, J., Asbridge, J. R., and Robbins, D. E.: 1972, *J. Geophys. Res.* **77**, 3583–3588.

Hodges, R. R.: 1973, *J. Geophys. Res.* **78**, 8055–8064.

Hodges, R. R.: 1974, *J. Geophys. Res.* **79**, 2881–2885.
Hodges, R. R. and Hoffman, J. H.: 1974a, *Proc. Fifth Lunar Science Conf., Geochim. Cosmochim. Acta, Suppl. 5*, **3**, 2955–2961.
Hodges, R. R., and Hoffman, J. H.: 1974b, *Geophys. Res. Letters* **1**, 69–71.
Hodges, R. R. and Johnson, F. S.: 1968, *J. Geophys. Res.* **73**, 7307–7317.
Hodges, R. R., Hoffman, J. H., and Johnson, F. S.: 1974, *Icarus*, **21**, 415–426.
Hoffman, J. H. and Hodges, R. R.: 1975, The Moon, **14**, 159–167.
Housley, R. M.: 1974, 'Ion Sputtering and Volatile Transport', paper presented at Conference on Origin and Evolution of the Lunar Regolith, Houston.
Johnson, F. S., Carroll, J. M., and Evans, D. E.: 1972, *Proc. Third Lunar Science Conf., Geochim. Cosmochim. Acta, Suppl. 3*, **3**, 2231–2242.
Kopal, Z.: 1966, *An Introduction to the Study of the Moon*, (Chapter 6), Gordon and Breach, New York.
Latham, G., Dorman, J., Duennebier, F., Ewing, M., Lammlein, D., and Nakamura, Y.: 1973, *Proc. Fourth Lunar Science Conf., Geochim. Cosmochim. Acta, Suppl. 4*, **3**, 2515–2528.
Manka, R. H. and Michel, F. C.: 1971, *Proc. Second Lunar Science Conf., Geochim. Cosmochim. Acta, Suppl. 2*, **2**, 1717–1728.
Taylor, S. R. and Jakeš, P.: 1974, *Proc. Fifth Lunar Science Conf., Geochim. Cosmochim. Acta, Suppl. 3*, **2**, 1287–1305.
Wilcox, J. M., Schatten, K. H., and Ness, N. F.: 1967, *J. Geophys. Res.* **72**, 19–26.

UTD

THE UNIVERSITY OF TEXAS AT DALLAS

November 13, 1974
UTD File: LACE-4L-856
UTD Account: E1347-01

Dr. John B. Hanley, Code SM
Lunar Data Analysis & Synthesis
NASA/Headquarters
Washington, D. C. 20546

Subject: Semi-Annual Status Report for Grant NSG-7034

Dear Dr. Hanley:

Herewith are submitted three copies of the first Semi-Annual Status Report for the Investigation of the Daytime Lunar Atmosphere for Lunar Synthesis Program in accordance with the requirements of NASA Grant NSG-7034.

Your favorable review and acceptance of this report is anticipated.

Sincerely,

R. R. Hodges, Jr.
Principal Investigator

J. W. Vanderford
Executive Officer

DRY:rr
Enclosure: Status Report

cc + encl.:
NASA Scientific & Technical Information Facility (2)
F. M. Lucas, ONRRR/Austin (1)
D. A. Douvarjo, NASA/Headquarters (1)

THIS COPY FOR

cc: D. Canham
J. Hoffman
D. York

FIRST SEMI-ANNUAL STATUS REPORT

FOR

INVESTIGATION OF THE DAYTIME LUNAR ATMOSPHERE

FOR

LUNAR SYNTHESIS PROGRAM

COVERING THE PERIOD OF

1 APRIL 1974 THROUGH 30 SEPTEMBER 1974

NASA Grant NSG-7034

13 November 1974

Prepared by: R. R. Hodges, Jr.
Principal Investigator

THE UNIVERSITY OF TEXAS AT DALLAS
P. O. Box 688
Richardson, Texas 75080

1.0 PREFACE

The NASA Grant NSG-7034 was received by the University of Texas at Dallas on April 24, 1974, for scientific investigations of the daytime lunar atmosphere under the direction of Dr. R. R. Hodges, Jr. in the Institute for Physical Sciences.

2.0 INTRODUCTION

The role of the atmosphere of the moon has two important facets. First, it provides a medium for escape of some volatile elements from the planet, and second it is responsible for the implantation of certain elements in soil grains. In the ongoing study of the daytime lunar atmosphere, present effort is being directed toward understanding the atmospheric dynamics of ^{40}Ar and methane.

Emphasis has been placed on ^{40}Ar because its atmospheric abundance has been measured by the Apollo 17 Lunar Atmosphere Composition Experiment (LACE). The available data is from lunar nights only, owing to operational limitations with the LACE instrument in sunlight. However, the lunar atmospheric modeling techniques now developing at the University of Texas at Dallas permit extrapolation of soil adsorption and desorption parameters as functions of temperature from the nighttime data.

The study of ^{40}Ar on the moon is significant because this gas is radiogenic, arising from the decay of ^{40}K within the moon. Subsequent discussion will show that the rate of escape of argon from the moon is surprisingly high, and even more curious, its rate of release varies episodically on a time scale of several months.

Methane is thought to be formed in soil grains due to implantation of the solar wind protons and carbon ions. Methane escape must be at about the rate of accretion of carbon from the solar wind, but its abundance in the lunar atmosphere at night is quite low. The implications of this fact are discussed in the section on methane.

3.0 ARGON MODEL

A preliminary model of the distribution of argon in the lunar atmosphere was presented at the Fourth Lunar Science Conference (Hodges et al., 1973). Further refinement of the model has been published in Hodges et al. (1974), and some ramifications of the correspondence of that model and the ^{40}Ar data was discussed at the Fifth Lunar Science Conference (Hodges and Hoffman, 1974b) and the Lunar Interaction Conference (Hodges, 1974). The most notable result to come from the early argon modeling work is that the rate of release of ^{40}Ar from the interior of the moon is a significant fraction of the total rate of the argon production mechanism, via the decay of ^{40}K, within the moon. In addition, the rate of release, over the nine lunation life of the Apollo 17 mass spectrometer, was quite variable.

The large amplitude and episodic nature of the rate of release of argon from the moon suggest that its study as an atmospheric gas is important to understanding the physical structure of the lunar interior. In the ongoing study a great deal of progress has been made in the synthesis of the temperature dependence of the processes of argon adsorption and desorption in lunar soil, which in turn, has

influenced the model of the daytime atmospheric distribution of argon, and hence the global escape rate.

The average rate of escape of argon from the moon during the Apollo 17 mass spectrometer data collection period has been established for various models of the global argon distribution. There has been some variability in published values of this rate, but the evolution of the modeling process shows a trend toward settling on an average loss rate of about 2×10^{21} atoms/sec. This loss must be supplied by effusion from the lunar interior where ^{40}K decay occurs. If the average lunar potassium abundance is 100 ppm, the total production of ^{40}Ar is 2.4×10^{22} atoms/sec, implying that about 8% of the argon produced in the moon is released as a gas.

To put the lunar argon escape rate in planetological perspective, the rate of release of argon from earth is probably about 1.2×10^{24} atoms/sec if the release fraction of its production has remained nearly constant over geologic time. This rate is equivalent to about 1.4×10^{22} atoms/sec/lunar mass. Thus the rate of release of ^{40}Ar from the moon is only about an order of magnitude less than that from an equivalent mass of earth. This contrasts sharply with the vast difference ($\sim$ 12 orders of magnitude) in atmospheric argon abundances for the two planets. The key difference is that argon photoions escape from the moon whereas on earth they are trapped by the geomagnetic field. What is important is the fact that the rate of loss of radiogenic argon, and hence of other native gases, from the moon is significant.

Another facet of argon escape from the moon is the episodic nature of the release rate. Figure 1 shows a summary of Apollo 17 mass spectrometer data on the argon photoionization rate, which is proportional to both atmospheric abundance and loss rate. Triangles represent sunrise measurements, which are regarded as the most reliable data. Each circle corresponds to a 5° (longitude) average. High values of the circles in the early data are due to an artifact contribution which disappeared with age. The dispersal of circles about the graph is due to randomness in the low amplitude nighttime concentration.

The important aspect of Figure 1 is the fact that the rate of loss of argon from the moon varied in amplitude by almost a factor of 2 in 1973. While the variation appears to be gradual, it is misleading to infer similarly slow changes in the release rate because the lifetime of atmospheric argon is in the range of 80-100 days. This is also approximately the decay time of the data shown in Figure 1 beginning at about day 100. Thus, the rate of release of argon from the lunar interior must have dropped to nearly zero for about 50 days, beginning at about day 100.

Figure 2 shows quantitative graphs of the total ^{40}Ar source in 1973 for several values of the argon lifetime. The most likely lifetime, based on model atmosphere calculations, seems to be near 100 days. Regardless of the lifetime, it is apparent that the rate of release of argon from the moon changed drastically in 1973. There is a subtle hint that if the process is episodic, the repetition time is not less than 200 days. A correlation with the 206 day periodicity of moonquake activity remains a distinct possibility.

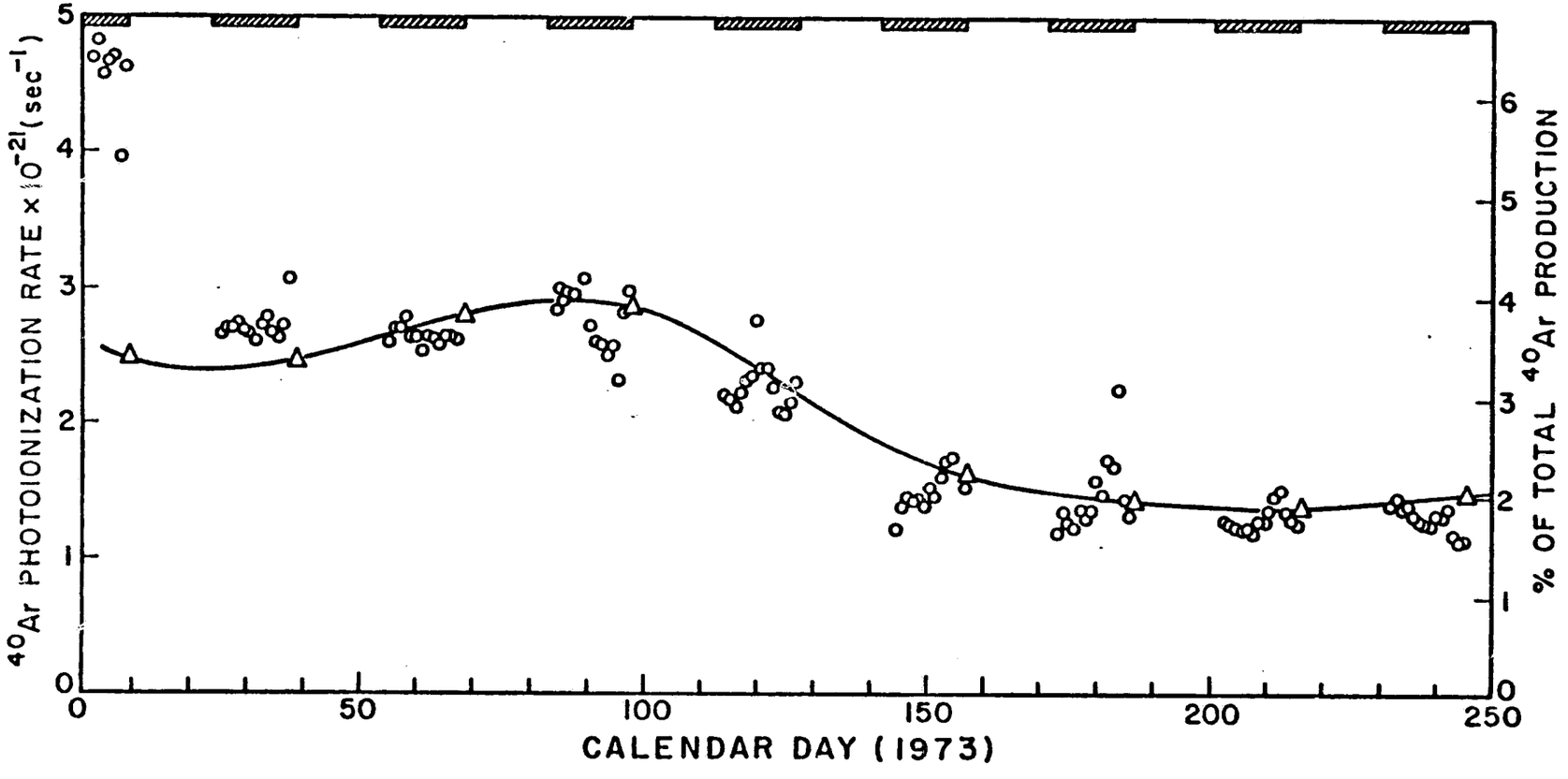

FIGURE 1

Total rate of photoionization of ^{40}Ar in the lunar atmosphere. Triangles show the high accuracy sunrise measurements, while circles give less reliable nighttime results, which are clearly influenced by contamination in the early part of the data period.

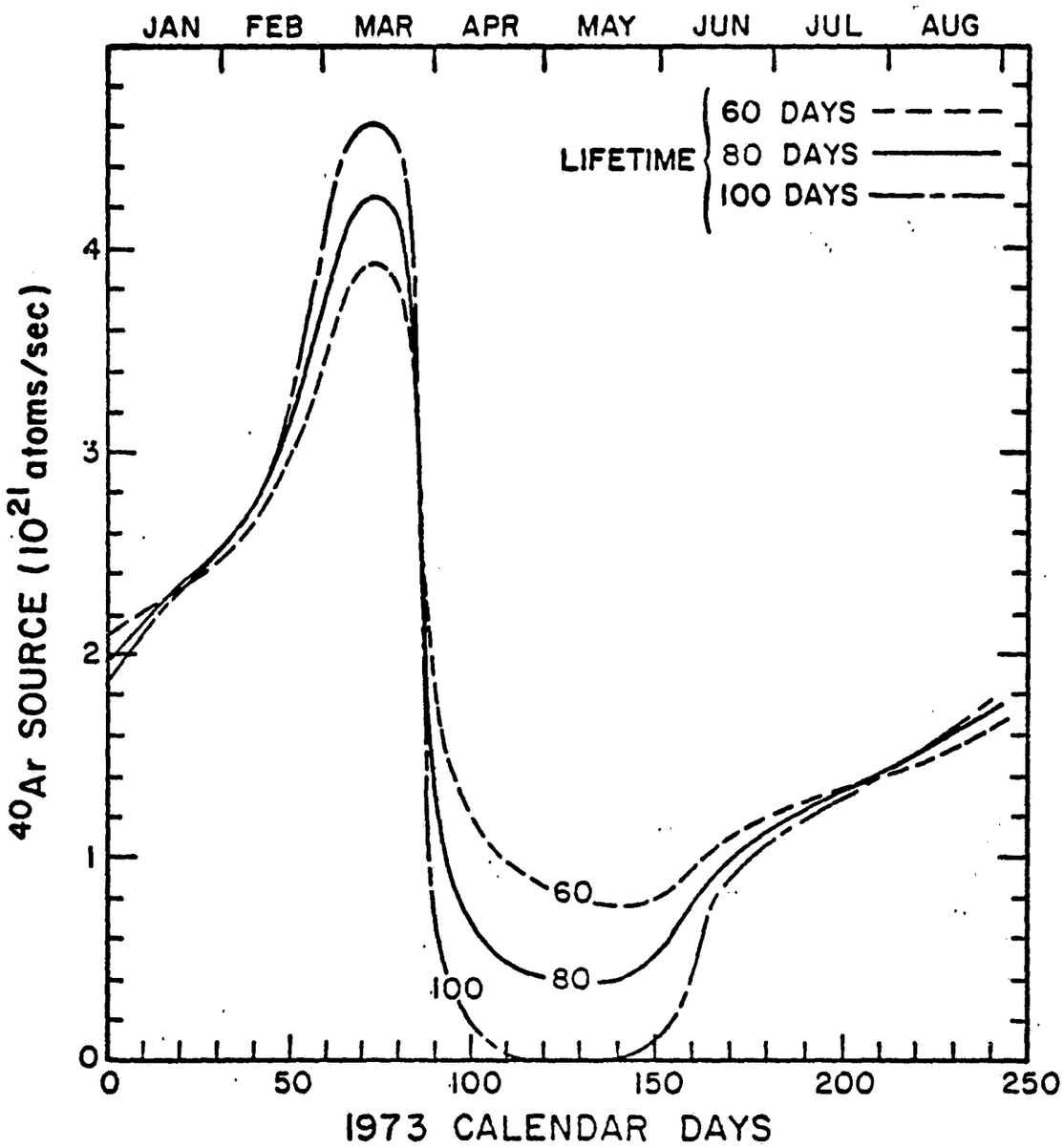

FIGURE 2

Time variations of the rate of release of argon from the moon in 1973. Model lifetimes range from 80 to 100 days.

There are some interesting ramifications of the amplitude and time variation of the release of argon from the moon. Both seem to rule out any important role for the regolith in the supply of either primary or retrapped argon to the atmosphere. If the crustal abundance of potassium were as great as 1000 ppm, the escape rate would require loss of all of the argon produced in the upper 5 km of the moon. It is doubtful that this could occur, and even more unlikely that it could be a time varying process. Substantial loss of argon from solid rock deep in the moon also seems unlikely. One good possibility is that argon diffuses from a semimolten core which has somehow managed to retain its potassium. The mechanism for episodic venting may include the formation of pockets of gas in subsurface voids, which release gas through deep fissures in response to a pressure buildup.

Whatever the cause of the argon venting from the moon, the amount vented is so great a fraction of the total rate of production of argon in the moon that it cannot be ignored in formulation of models of the lunar interior. The argon result is much more certain than the longer term episodic release pattern which has been suggested for ^{222}Rn on the basis of a present imbalance of the polonium-radon ratio shown in alpha particle spectra. This imbalance can more believably be explained by vertical transport of polonium in the soil than by time variation of the release of radon from a sufficiently shallow depth that would allow its diffusion to the lunar surface and into the atmosphere within its 3.8 day lifetime.

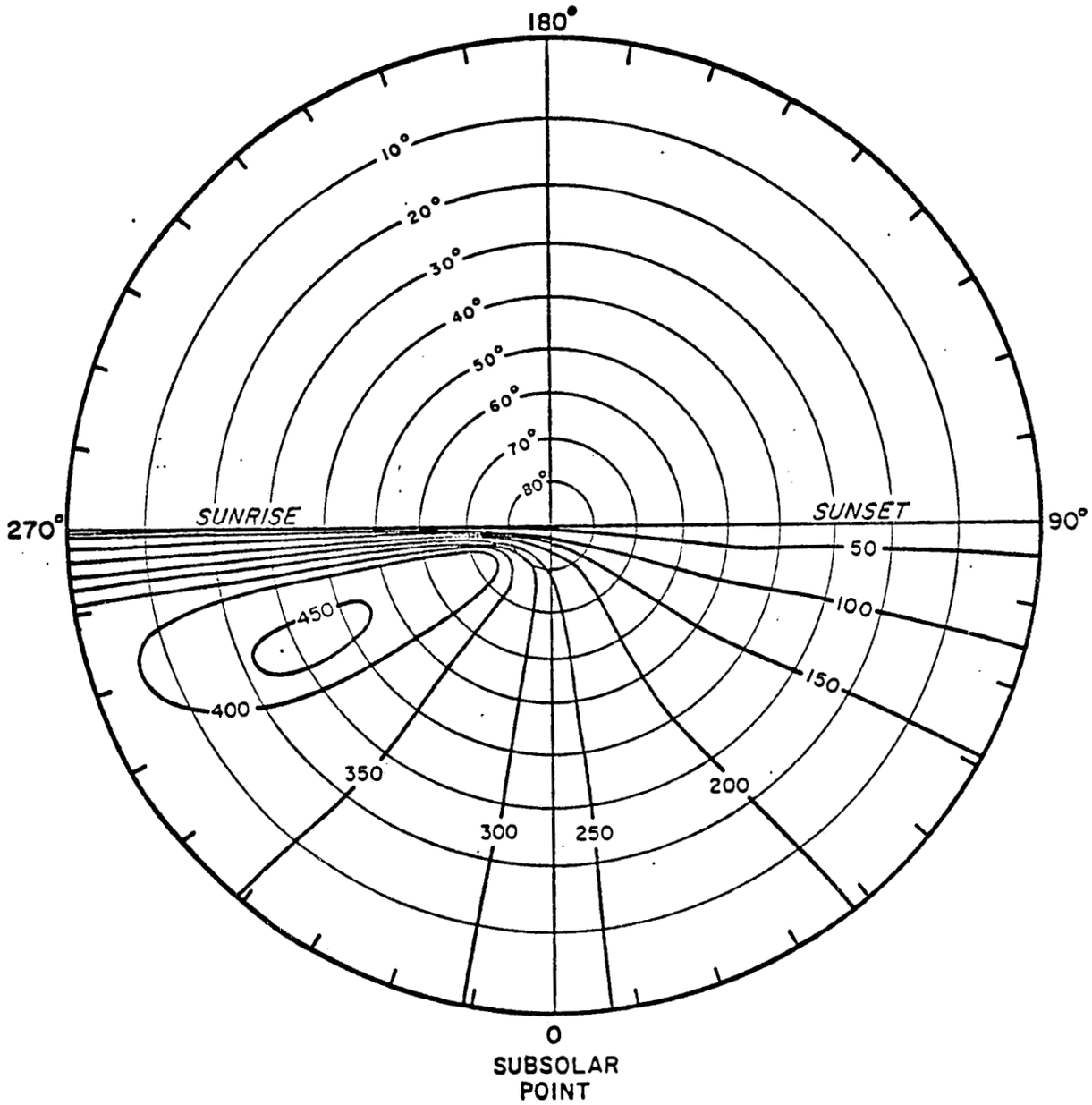

FIGURE 3

Distribution of ^{40}Ar at 100 km altitude.

Thus the study of active processes within the lunar interior must include further measurements of the time variation of the rate of release of argon from the moon. To this end it would be useful if the lunar polar orbiter were to carry a mass spectrometer dedicated to the detection of ^{40}Argon. Based on what has been learned about high-vacuum mass spectrometry in the Apollo program, it is reasonable to expect to be able to measure argon at the 20 atom/cc level in lunar orbit. Figure 3 shows a contour map of the argon model atmosphere concentration at 100 km altitude over the northern hemisphere of the moon. It can be noted that near the pole, the concentration is always about 50/cc. The maximum concentration occurs in daytime, about 25° east of the sunrise terminator and at a latitude of about 35°. The shift of the maximum from the equator is a result of the migration of the condensable gas to the poles where adsorption, residence, and hence ionization, are most likely.

4.0 METHANE

The existence of methane in the lunar atmosphere is mainly hypothesis. There is an indication of a presunrise increase at 16 amu in the Apollo 17 mass spectrometer data, which could imply a terminator concentration of about 10^3/cc, and a nighttime level <100/cc.

Carbon ions of the solar wind impinge on the moon at an average rate of 1.5×10^{23} atoms/sec, which is about an order of magnitude less than the solar wind helium influx, but an order of magnitude greater than the ^{40}Ar supply rate. Since helium escape appears to be in balance with solar wind inflow (Hodges and Hoffman, 1974 a), it seems reasonable to expect a similar equilibrium situation for carbon. The

escape of carbon from the moon requires formation of gaseous molecules, such as CH_4, CO or CO_2. The solar wind provides large amounts of both H^+ and O^+, but it seems likely that the oxygen ions should react with the abundant reduced minerals which form the lunar soil. Thus methane is expected to be the dominant carbon gas formed on the moon.

Escape of the total carbon influx is not an obvious requirement. Perhaps the best positive argument is that the occurence of soil grains with volume correlated carbon content may imply that a carbon saturation level has been reached. It is instructive to note that the length of exposure needed for trapped solar wind carbon to reach the commonly found 200 ppm level is about 100 years times the particle diameter in microns. Thus a 10μ grain requires 1000 years while a 100μ grain requires 10,000 years in the solar wind to reach 200 ppm of carbon. These times are probably near the exposure ages of particles of these sizes.

If a carbon saturation condition exists in the lunar soil, then the escape of a carbon gas at its accretion rate (about 10 times the ^{40}Ar source rate) requires a daytime atmosphere that greatly exceeds the argon abundance. The carbon gas must be adsorbed readily at night, and preliminary calculations show that its desorption time must be the order of 10-15 days. Apparently the adsorbed molecules are not released by a photon process, because there is no large sunrise pocket of CH_4, CO or CO_2. The average daytime surface concentration required to provide the carbon escape as CH_4 is about 2×10^5/cc, which corresponds to a total atmospheric mass of about 7 tons.

There are several questions which require further study regarding methane on the moon. The high probability of adsorption at near-terminator daytime temperatures and the long desorption time may produce a significant layer of adsorbed gas near the poles, which may in turn result in a vapor-pressure equilibrium in cold regions. If so, the amount of gas at low latitudes could be quite small. Another possibility is that the bulk of the solar wind influx of carbon is still being implanted in the soil, Even if this were true, it is reasonable to expect escape of 10% of the influx, which should contribute significantly to the daytime lunar atmosphere.

5.0 BIBLIOGRAPHIC REFERENCES

Hodges, R. R., J, H, Hoffman, F. S. Johnson, and D. E. Evans, Composition and Dynamics of Lunar Atmosphere, Proc. Fourth Lunar Science Conf., Geochim. Cosmochim. Acta., Suppl. 4, 3, 2855, 1973.

Hodges, R. R., Formation of the Lunar Atmosphere, Lunar Interactions Conference Abstracts, Lunar Science Institute, 1974.

Hodges, R. R., J. H. Hoffman, and F. S. Johnson, The Lunar Atmosphere, Icarus, 21, 415, 1974.

Hodges, R. R., and J. H. Hoffman, Measurement of Solar Wind Helium in the Lunar Atmosphere, Geophys, Res. Letters, 1, 69, 1974a.

Hodges, R. R., and J. H. Hoffman, Episodic Release of ^{40}Ar from the Interior of the Moon, Proc. Fifth Lunar Science Conf., Geochim. Cosmochim. Acta., (in press) 1974b.